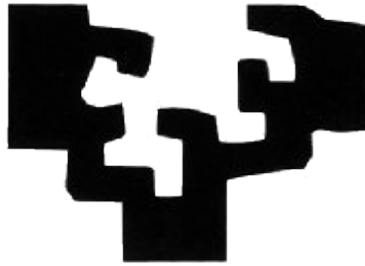eman ta zabal zazu

Universidad del País Vasco
Euskal Herriko Unibertsitatea
The University of the Basque Country

Early Medial Temporal Atrophy Scale
(EMTA)

INTERNATIONAL DOCTORAL THESIS

Jorge Alberto Villanúa Bernués

Neuroscience Department EHU-UPV.

Memory presented to obtain the degree of International Doctor in

Medicine and Surgery at the University of the Basque Country

Donostia-San Sebastián 2015

_____

To Lola, my life partner, my twin soul.

To my dearest sons Jaime & Pablo, the main reason of my life.

To my father Feliciano & mother Loreto–Mª Angeles who have passed away always in my heart & my mind.

To my sister Mª Angeles and to my brothers Lorenzo, Carlos (passed away) & Alfredo.

To my nieces & nephews, uncle, aunt, cousins & all my in-law family

_____

Scientific papers related with this Thesis

1. **Impact of APOE-Ɛ4 and family history of dementia on grey matter atrophy in cognitively healthy middle-aged adults.**

    M. Ten Kate, E.J. Sanz-Arigita, B.M. Tijms, A.M. Wink, M. Clerigue, M. Garcia-Sebastian, A. Izagirre, M. Ecay-Torres, A. Estanga, J. Villanua, H. Vrenken, P.J. Visser, P. Martinez-Lage and F. Barkhof.·

    Accepted for publication in Neurobiology of Aging

2. **Grey matter network disruptions and Alzheimer's disease pathology in non-demented elderly.**

    B.M. Tijms, M. Ten Kate, A.M. Wink, P.J. Visser, M. Ecay-Torres, M. Clerigue, A. Estanga, M. Garcia-Sebastian, A. Izagirre, J. Villanua, P. Martinez-Lage, W.M. van der Flier, P. Scheltens, E. Sanz-Arigita and F. Barkhof.

    Accepted for publication in Neurobiology of Aging

Scientific papers derived from this Thesis

1. **Early Medial Temporal Atrophy Scale (EMTA).**

    J. Villanua, M. Ten Kate, M. Garcia-Sebastian, P. Martinez-Lage, M. Ecay-Torres, A. Estanga, A. Izagirre, M. Clerigue , J.I. Emparanza , J.F. Martí Massó, F. Barkhof, E.J. Sanz-Arigita. To be submitted to the American Journal of Neuroradiology.

_____

Patent derived from this Thesis (on viability analysis process)

1. **Early (Goiz) Medial Temporal Atrophy Scale (EMTA).**

    Pattern recognition software for MR imaging of hippocampus structures to automate the application of EMTA) (particularly its stadium S4 - subjects last stage of the preclinical phase of Alzheimer´s disease).

    Bioef-Biodonostia-Osatek SA, Cita-Alzheimer Foundation.

ACADEMIA...

ACTA DE GRADO DE DOCTOR O DOCTORA
ACTA DE DEFENSA DE TESIS DOCTORAL

DOCTORANDO **DON JORGE VILLANÚA BERNUÉS**

TITULO DE LA TESIS: **Early Medial Temporal Atrophy Scale (EMTA)**

El Tribunal designado por la Comisión de Postgrado de la UPV/EHU para calificar la Tesis Doctoral arriba indicada y reunido en el día de la fecha, una vez efectuada la defensa por el/la doctorando/a y contestadas las objeciones y/o sugerencias que se le han formulado, ha otorgado por_____la calificación de:

unanimidad ó mayoría

SOBRESALIENTE / NOTABLE / APROBADO / NO APTO

Idioma/s de defensa (en caso de más de un idioma, especificar porcentaje defendido en cada idioma):

Castellano _____

Euskera _____

Otros Idiomas (especificar cuál/cuales y porcentaje) _____

En _____ a _____ de _____ de _____

EL/LA PRESIDENTE/A,   EL/LA SECRETARIO/A,

Fdo.:   Fdo.:

Dr/a: _____   Dr/a: _____

VOCAL 1º,   VOCAL 2º,   VOCAL 3º,

Fdo.:   Fdo.:   Fdo.:

Dr/a: _____   Dr/a:_____   Dr/a:_____

EL/LA DOCTORANDO/A,

Fdo.: Jorge Villanúa Bernués

NAZIOARTEKO
BIKAINTASUN
CAMPUSA

CAMPUS DE
EXCELENCIA
INTERNACIONAL

Universidad   Euskal Herriko
del Pais Vasco Unibertsitatea

AUTORIZACIÓN DEL DEPARTAMENTO

El Consejo del Departamento de Neurociencias, en reunión celebrada el día 11 de noviembre de 2015 ha acordado dar la conformidad a la admisión a trámite de presentación de la Tesis Doctoral titulada:

Early Medial Temporal Atrophy Scale (EMTA)

dirigida por los Dres. José Félix Martí Massó y Ernesto Sanz-Arigita y presentada por Don Jorge Villanúa Bernués, ante este Departamento.

En Leioa (Bizkaia) a, 11 de noviembre de 2015

VºBº DIRECTOR DEL DEPARTAMENTO   SECRETARIA DEL DEPARTAMENTO

Fdo.: Rafael Sarria Aróstegui   Fdo.: Izaskun Elezgarai Gabantxo

AUTORIZACIÓN DE LA COMISIÓN ACADÉMICA DEL PROGRAMA DE DOCTORADO

La Comisión Académica del Programa de Doctorado en Neurociencias en reunión celebrada el día 11 de noviembre de 2015, ha acordado dar la conformidad a la presentación de la Tesis Doctoral titulada:

Early Medial Temporal Atrophy Scale (EMTA)

dirigida por el Dr. José Félix Martí Massó y por el Dr. Ernesto Sanz-Arigita

y presentada por Don Jorge Villanúa Bernués

adscrito o adscrita al Departamento de Neurociencias

En Leioa, a 11 de noviembre de 2015

EL MIEMBRO DE LA COMISIÓN ACADÉMICA RESPONSABLE DEL PROGRAMA DE DOCTORADO

Fdo.: Inmaculada Gerrikagoitia Marina

Universidad Euskal Herriko NAZIOARTEKO
del País Vasco Unibertsitatea BIKAINTASUN
CAMPUSA
CAMPUS DE
EXCELENCIA
INTERNACIONAL

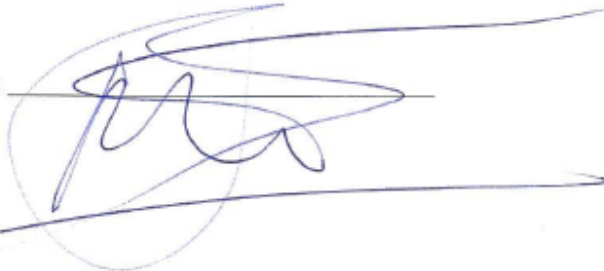> **AUTORIZACION DEL/LA DIRECTOR/A DE TESIS**
> **PARA SU PRESENTACION**

El Dr. JOSÉ FÉLIX MARTÍ MASSO con N.I.F. 39628956W y el Dr. ERNESTO SANZ ARIGITA con N.I.F 33421301R como Directores de la Tesis Doctoral: Early Medial Temporal Atrophy Scale (EMTA). realizada en el Programa de Doctorado en Neurociencia por el Doctorando Don. JORGE ALBERTO VILLANÚA BERNUÉS, autorizan la presentación de la citada Tesis Doctoral, dado que reúne las condiciones necesarias para su defensa.

En Donostia-San Sebastian a 5 de Noviembre del 2015

EL/LA DIRECTOR/A DE LA TESIS

Dr. ERNESTO J. SNZ - ARIGITA

Fdo.: _____

Jf MARTÍ MASO

_____

Thesis Directors

José Félix Martí Masso MD, PhD

Head of Neurology service

Donostia University Hospital.

UPV-EHU Titular Professor

Osakidetza

DONOSTIA UNIBERTSITATE OSPITALEA
HOSPITAL UNIVERSITARIO DONOSTIA

eman ta zabal zazu

Universidad del País Vasco
Euskal Herriko Unibertsitatea
The University of the Basque Country

Ernesto Sanz Arigita PhD

Radiology and Image

Analysis Center – VUmc.

The Netherlands

Department Science &

Technology. University of

Bordeaux

VUmc

université de BORDEAUX

_____

In appreciation

To the altruist contribution of

the Guipuzcoa Alzheimer´s Project (GAP) Volunteers

To the sponsorship to this thesis project

15

Cristina Gervás MD

Radiologist. Osatek SA

Head of Guipuzkoa Territory

Head of Donostia Unit

Other Osatek SA Direction Board members

Julio Arrizabalaga MD, PhD

Scientific Director

Biodonostia research Institute

Frederik Barkhof MD, PhD

Radiology and Image

Analysis Center – VUmc.

The Netherlands

(3 month VUmc stage)

_____

To the distinguished scientific contribution to the development of the (EMTA)

Ernesto Sanz-Arigita PhD

Radiology and Image

Analysis Center – VUmc.

The Netherlands

Mara Ten Kate MD, PhDc

Radiology and Image

Analysis Center – VUmc.

The Netherlands

Pablo Martínez-Lage MD, PhD

Head of Neurology department

Cita-Alzheimer Foundation

Frederik Barkhof MD, PhD

Radiology and Image

Analysis Center – VUmc.

The Netherlands

Maite Sebastián-García PhD

Neuroimaging department

Cita-Alzheimer Foundation

Miriam Ecay-Torres MsC, PhDc

Neurology department

Cita-Alzheimer Foundation

_____

To the distinguished scientific contribution to the correction of this Thesis

Adolfo López de Munain MD, PhD

Head of Neuroscience department

Biodonostia research Institute

Ander Matheu PhD

Head of Neuro-oncology department

Biodonostia research Institute

José María Alustiza MD, PhD

Radiologist. Osatek SA

Scientist member Hepatolgy department

Biodonostia research Institute

Begoña Indakoetxea MD

Neurologist. Neurology service

Donostia University Hospital

Emma Salvador MD

Scientist assitant & data manager.

Osatek SA

Scientist member Hepatolgy department

Biodonostia research Institute

Jose I. Emparanza MD, PhD

Head of Clinical Epidemiology

UnitCASPe, CIBER-ESP,

BioDonostia

Hospital Universitario Donostia

Mirian Barandiaran MsC, PhDc

Neuropsycologist.

Neurology service

Donostia University Hospital

ElleMarije Altena MsC, PhD

Department science & technology

University of Bordeaux

Abreviation

3D MPRAGE- Three Dimensional Magnetization Prepared Rapid Acquisition GRE (3D Inversion Recovery)

AChE-Acetylcholinesterase

AD- Alzheimer's disease

ADEM- Acute disseminated encephalomyelitis

ADNI- Alzheimer's disease neuroimaging initiative

API- Alzheimer's prevention initiative

ASL-Arterial spin labeling

BET-Brain extraction tool

CDR-Conversion dementia risk

CSA-AD- Cortical sign areas of Alzheimer's disease

CSF- Cerebro spinal fluid

DESCRIPA- Development of screening guidelines and criteria for predemetia Alzheimer's disease

DIAN- Dominantly inherited Alzheimer network

DMN- Default mode network

EMTA $_4$-Early Medial Temporal Lobe Atrophy in preclinical Alzheimer's disease -4 stages.

EMTA $_5$-Early Medial Temporal Lobe Atrophy in preclinical Alzheimer's disease -5 stages.

EMTA $_6$-Early Medial Temporal Lobe Atrophy in preclinical Alzheimer's disease -6 stages.

ENTA- Early medial temporal lobe atrophy scale

EO-Early onset Alzheimer disease

FDG- Fluoro-2-deoxy-D-glucose

FIRST- Subcortical structure segmentation

FLIRT- FMRIB's Linear Image Registration Tool

FSL- FMRIB Software Library v5.0

FSL-View- Imaging visor facility used with FSL.

GM-Grey matter

Hipp-Hippocampus

HR-High risk

HV-Hippocampal volume

ILV-Inferior lateral ventricle

IMI- European innovative medicines initiative

IWG- International working group

LO-Late onset Alzheimer Disease

LR-Low risk

MCI- Mild cognitive impairment

MMSE-Mini mental state examination.

MNI512-Reference brain space of Monteal Neurological Insitute built on 512 normal representative subjects.

MRI-Magnetic resonance imaging

MTA-MTLA scale- Medial temporal lobe atrophy scale (Sheltens).

MTL- Medial temporal lobe

NFTs- Neurofibrillary tangles

NIA-AA-National institute on aging-Alzheimer's association.

NINCDS-ADRDA- National institute of neurological and communicate disorders and stroke-Alzheimer's disease and related disorders association

OR-Odds ratio

PAR-Parietal

PcAD- Preclinical Alzheimer disease.

PCC- Posterior cingulate cortex

PET- Positron emission tomography

PIB- Pittsburgh compound B

PRCC- Precuneus

SBP- Swedish brain power

SPM-Statistical parametric map

TOP- Posterior parietal-occipital cortex

VBM-Voxel Based Morphometry

VERTEX- Statistic analysis performed using FIRST utils to investigate localised shape differences

WMH-white matter hyperintensities

Tables and figures index

21

Figures index

THESIS SUMMARY IN SPANISH

ESCALA DE ATROFIA TEMPRANA DEL LOBULO TEMPORAL MEDIAL (EMTA).

1) INTRODUCCIóN

El concepto y definición de la Enfermedad de Alzheimer (EA) preclínica (EAPc) ha sido posible gracias a la aparición y desarrollo de un modelo de biomarcadores específicos para la misma (1, 2). Sin embargo, en los modelos de biomarcadores desarrollados por el grupo de trabajo internacional (GTI) y la asociación del instituto internacional en envejecimiento y EA (AIIE-EA), la resonancia magnética (RM) estructural (1, 3-5) se utiliza bien como un biomarcador tardío en la fisiopatología de la EAPc (4, 5) o se ha excluido en las versiones mas recientes de los mismos (4, 6). Los biomarcadores preclínicos y clínicos actualmente aceptados para la EA son los derivados del análisis del liquido cefalorraquídeo (LCR) (Aß -42, T-tau o P-tau) o de las técnicas de tomografía por emisión de positrones (TEP) de amiloide (1). Sin embargo, estos biomarcadores en la práctica clínica no son lo suficientemente sensibles por sí mismos para detectar las primeras fases del proceso neurodegenerativo.

La escala radiológica para el estudio de la atrofia del lóbulo temporal medial (MTA) de Sheltens _et al._ fue desarrollada en 1992 (5) y dado que las técnicas de morfometría basada en voxeles no son una herramienta incorporada a la práctica clínica, la escala de Sheltens _et al._ está todavía en uso. Fue desarrollada en plano coronal (7, 8) y consta de cinco grados (0-4) definidos por la magnitud del ancho de la fisura coroidea , del ancho del asta temporal del ventrículo lateral y por la altura de hipocampo.

Esta escala ha sido validada mediante estudios volumétricos y neuropsicológicos a lo largo de los últimos 20 años como una herramienta diagnóstica útil para clasificar los grados de atrofia del lóbulo temporal en enfermos con demencia por EA moderada o severa frente a controles sanos con unos rendimientos diagnósticos representados por una sensibilidad del 70-100% y una especificidad del 67-96% (9).

Así pues está justificado tener en cuenta el grado de atrofia registrado en la escala de Sheltens _et al._ combinada con información clínica en el diagnóstico clínico de pacientes de EA.

La propuesta original de Scheltens et al. (MTA) recomienda en un punto de corte ajustado por edad consistente en valores de puntuación de su escala ≥2 en cualquiera de los dos hemisferios que serán considerados anormales para personas menores de 75 años de edad, y valores de puntuación de su escala ≥3 serán considerados anormales para personas por encima de 75 años de edad (5). Estos puntos de corte han mostrado, no obstante, una baja especificidad (67%) (10). También se ha propuesto un punto de corte de esta escala ≥1.5 basado en la puntuación media de ambos hemisferios (11). Este punto de corte muestra una alta especificidad (94%), pero una baja sensibilidad (46%). Se ha descrito mas recientemente, un nuevo punto de corte ≥2 basado también en la puntuación media de ambos hemisferios con una alta sensibilidad en pacientes mayores de 75 años (12), y finalmente que una puntuación de 3 podría considerarse normal en individuos mayores de 80 años de edad (13). Entre 45 y 65 años de edad se ha propuesto un punto de corte ≥1 basado también en la puntuación media de ambos hemisferios (11, 14). El área bajo la curva ROC que muestra el mayor rendimiento ajustado por décadas de edad es 78.5 (14). Así pues para el estudio de la EAPc la escala de Scheltens et al. tiene un valor limitado, habida cuenta que solamente se ha propuesto un punto de corte de ≥1.5 como media de la puntuación de ambos hemisferios, así pues existe la necesidad de describir una nueva escala mas específica y sensible para juzgar la atrofia del lóbulo temporal medial en sujetos entre 40 y 60 años (EAPc).

2) HIPOTESIS y OBJETIVOS

a) Hipótesis

La hipótesis de esta tesis es que existe una atrofia hipocampal de bajo grado (AHBG) previa al diagnóstico de la aparición de la demencia en la EA. Basándose en esta hipótesis nuestro objetivo es desarrollar una nueva escala de atrofia del lóbulo temporal medial por RM (EMTA) en los sujetos en etapas finales de la EAPc, definida por los criterios AIIE-EA (presencia de una disminución de Aß1-42 junto con el aumento de T-tau o P-tau en el LCR, pero sin déficit

cognitivo, mostrando únicamente un rendimiento bajo en la prueba de memoria verbal-TAVEC - versión en español de la prueba CVLT) (1, 2, 15, 16). La aplicación de esta nueva escala sólo requiere la experiencia de un neurorradiológo entrenado, resultando un método rápido y de bajo coste para identificar a los sujetos que podrían beneficiarse de las nuevas terapias ahora en fases II y III de ensayos clínicos (17, 18).

Nuestra hipótesis está basada en los siguientes hechos:

i) Hay AHBG antes de que sea detectable en el rango descrito por las escalas radiológicas de atrofia disponibles actualmente y utilizadas para el diagnóstico.

ii) Esta atrofia AHBG es diferente en términos de magnitud de los efectos del envejecimiento y podría corresponder a las primeras etapas de la EA antes de que aparezcan los déficits cognitivos que conducen al diagnóstico clínico de la misma.

iii) Es posible detectar esta AHBG por medio de una nueva escala de atrofia radiológica basada en criterios anatómicos bien definidos: EMTA

iv). Esta nueva escala tiene una alta concordancia cuando es leída por diferentes especialistas

iv) La AHBG puede medirse cuantitativamente y los cambios volumétricos medidos corresponden a los cambios anatómicos definidos y a las etapas de atrofia radiológica propuestas.

v) Junto con otros biomarcadores tempranos de la EA, la EMTA. puede resultar de gran utilidad para detectar las primeras fases del proceso neurodegenerativo previas a la aparición de la demencia.

b) Objetivos

i) Definir y validar una nueva escala de AHBG basada en la RM estructural (EMTA), para identificar las fases preclínicas de los sujetos con EA (EAPc).

ii) Probar la reproducibilidad por radiólogos y neurólogos independientes cualificados de la aplicación de la EMTA.

iii) Cuantificar volumétricamente la AHBG y comparar los resultados obtenidos con los criterios de atrofia de base anatómica previamente identificados en la EMTA.

iv) Comparar el rendimiento de la EMTA con los resultados de otros biomarcadores de EA (LCR y biomarcadores cognitivos) en la misma población a estudio.

3) MATERIAL y METODOS

a) Cohorte PGA

i) Diseño

Este estudio tiene un diseño transversal y está realizado en una cohorte de adultos cognitivamente sanos que participaron en el Proyecto Guipúzcoa Alzheimer (PGA) . El protocolo de adquisición de imagen por RM de esta cohorte esta basado en los proyectos de Redes en Riesgo y Conectad diseñados por el Dr. Ernesto J. Sanz-Arigita.

El Comité de Ética local aprobó el protocolo del estudio y todos los sujetos dieron su consentimiento informado por escrito para el mismo: para la recogida, el almacenamiento de las muestras biológicas y genéticas; así como para la realización del estudio de RM.

ii) Sujetos a estudio

(1) Criterios de inclusión

Se incluyeron en el estudio voluntarios adultos mayores de 35 años y menores de 80. A todos los participantes se les invito a realizarse una punción lumbar para la obtención de una muestra de LCR y su posterior envío al Biobanco. Los voluntarios que no otorgaron su consentimiento para la realización de la punción lumbar no fueron excluidos. Un 50% de las muestra eran personas con antecedentes familiares de demencia por EA en primer grado (padre, madre o hermano) y el otro 50% de la muestras no tenía antecedentes de EA. Se contó con el testimonio de acompañantes de los voluntarios para contrastar la información obtenida en las entrevistas clínicas.

(2) Criterios de exclusión

Se excluyeron:

- Los individuos que tenían criterios de demencia leve, moderada o grave según los criterios del DSM-IV y del estadio de CDR ≥ 1.
- Los que sujetos con antecedentes de enfermedad neurológica que pudieran causar demencia o deterioro cognitivo.

- Los individuos con historia de accidente cerebrovascular sintomático que dejó secuelas cognitivas significativas (por ejemplo, afasia).
- Los voluntarios con antecedentes de enfermedad psiquiátrica diagnosticada que pudiera causar demencia o deterioro cognitivo. No se excluyen aquellas personas con síntomas psiquiátricos leves (ansiedad, depresión).
- Los pacientes con enfermedad sistémica grave o no controlada que pudiera causar deterioro cognitivo o demencia o que pudiera restringir la participación en el estudio.
- Los sujetos que sufrían una limitación sensorial como ceguera o sordera o cualquier limitación significativa (afasia severa, ansiedad excesiva, falta de fluidez o comprensión suficiente en castellano o euskera) para la realización de las pruebas cognitivas.
- Los voluntarios que presentaban una contraindicación absoluta para la realización de RM a intensidad de campo de 3 Tesla: marcapasos, stents metálicos contraindicados, metralla, claustrofobia, y extensos tatuajes.
Los candidatos que se negaron a firmar el consentimiento informado.

b) Estudios de RM craneal

A todos los individuos se les practicó una RM craneal con el siguiente protocolo de adquisición y análisis:

i) Protocolo de adquisición

Se obtuvieron exploraciones de RM cerebral utilizando un equipo de 3 Tesla (Siemens Magnetom Tim Trío ®) y una bobina de la cabeza de 32 canales. Se adquirieron secuencias volumétricas estructurales de voxel cuadrado de 1,25mm potenciadas en T1 (imagen anatómica) que se utilizaron para el posterior análisis de las mismas mediante técnicas de morfometría basada en voxeles (MBV).

ii) Realización de las máscaras de los patrones – estadios de la nueva escala.

(1) FSL-view

Se utilizó FSL-view ® para realizar las mascaras – moldes de los patrones o estadios de la nueva escala sobre las imágenes anatómicas T1 de RM a las que

previamente se les había sometido al proceso de extracción del parénquima cerebral respecto del resto de las estructuras que lo rodean (BET®), seguido de uno de registro (FLIRT®) según el espacio de referencia del cerebro del instituto neurológico de Montreal (MNI 512 a 1mm). En estos moldes o máscaras se aplicó un código de color distinto para caracterizar a:

     (a) la cisura coroidea (medial a la fimbria) –amarillo oscuro.

     (b) la porción medial del asta temporal del ventrículo lateral (lateral a la fimbria) y localizada sobre el cuerpo del hipocampo- amarillo claro

     (c) la porción inferior y lateral del asta temporal del ventrículo lateral (lateral al cuerpo del hipocampo)-amarillo claro

     (d) La cisura transversa peritroncular-naranja

     (e) el cuerpo del hipocampo-rojo

iii) Post-procesado MBV

(1) Vertex-FIRST ®

Se utilizó FIRST® (segmentación de estructuras subcorticales) para segmentar la amígdala y el hipocampo a partir de la imagen T1 (imagen anatómica) y estimar las diferencias de la forma de los contornos de estas estructuras entre los grupos propuestos a estudio.

(2)   SPM 8 ®

Las imágenes T1 (imagen anatómica) fueron segmentadas para el estudio del volumen de la sustancia gris de la totalidad del lóbulo temporal utilizando la herramienta MBV8 ® para la obtención del mapa paramétrico estadístico SPM8 ® que se ejecuta en MATLAB ® 2011

(3) Free-Surfer ®

La reconstrucción volumétrica de la cortical y la segmentación volumétrica de las estructuras cisternales y ventriculares de la totalidad del lóbulo temporal se realizó con el paquete gratuito de análisis de imagen FreeSurfer ® (http://surfer.nmr.mgh.harvard.edu/).

iv) Lectura de las RM aplicando la nueva escala

(1)   Un equipo compuesto de neurorradiólogos

Un equipo compuesto por un neurorradiólogo (NR) y un residente de neurorradiologia (rNR), se entrenaron en la aplicación de la nueva escala, sirviendo su trabajo de base para el cálculo de los índices de variabilidad intra e interobservador sobre un grupo de imágenes correspondientes a 60 sujetos de la cohorte de PGA elegidos al azar incluyendo individuos clasificados en todos los estadios de la nueva escala.

c) Pruebas cognitivas

Todos los participantes fueron estudiados desde el punto de vista neuropsicológico con los siguientes test:

(1) General: Mini-Mental (MMSE)

(2) Prueba de Vocabulario Test (WAIS-III)

(3) Memoria verbal (TAVEC-versión en español de la prueba CVLT)

Memoria visual

(5) Habilidades de Lenguaje

(6) Habilidades de percepción visual

(7) Habilidades de construcción visual

(8) Habilidades de atención y función ejecutiva

(9) Habilidades de fluidez verbal semántica

(10) Habilidades de fluidez verbal fonética

(11) Habilidades de trazabilidad A and B;

(12) Prueba de números clave (WAIS-III)

(13) Prueba de Stroop

(14) Prueba del Zoo

(15) Prueba de comportamiento y función ejecutiva (BADS)

(16) Prueba de praxias (WAB).

d) Estudio de Biomarcadores en LCR

Todas las muestras de LCR fueron estudiadas en el Hospital de Sant Pau mediante técnica de Innotest® para la determinación de Aβ1-42 , tau y p-tau. Se utilizaron los puntos de corte propuestos por Alcolea et al. (19) para los valores de estos biomarcadores: A-beta positivo si < 580 pg./ml, Tau total positivo si > 350 pg./ml Fosfo-tau positivo si > 50 pg./ml.

4) RESULTADOS

a) Sujetos a estudio

La muestra está compuesta por 482 sujetos de los que 72 se retiraron voluntariamente, 6 presentaron un MiniMental test con un rendimiento menor de 26 y fueron excluidos y por último en 44 de ellos el estudio de resonancia no reunió calidad suficiente para el análisis siendo también retirados del estudio, resultando una muestra final válida para el análisis de 360 sujetos. De esta muestra de 360 sujetos con RM válida, y MMSE mayor de 26, 345 mostraron CDR de 0 y 15 CD de 0,5. Los sujetos incluidos se encontraban en edades comprendidas entre los 39 y 79 años, con una edad media de 56 años. El 57,22% eran mujeres y el 42,77% hombres. El 93% de la muestra (n=335) eran diestros, un 2,2% fueron zurdos , un 3,3% ambidiestros y finalmente un 1,38% zurdos corregidos.

Se obtuvieron muestras de LCR en un 59,44% de los sujetos incluidos (n=213), de ellos el 92,9% (n=199) mostraban MMSE mayor de 26 y CDR de 0 mientras que el 6,9% (n=15) presentaron MMSE mayor de 26 y CDR de 0,5

La distribución de la muestra según la caracterización de la expresión de Apoe fue: 66,9% Apoe 3/3 (n=241), 23,6% Apoe 3/4 (n=85), 1,6% Apoe 4/4 (n=6) y 7,7% Apoe 2/3 (n=28).

La nueva escala se desarrolla en este estudio sobre la muestra final de 360 sujetos.

b) La identificación de la nueva escala EMTA

La EMTA está inspirada en la MTA propuesta por Scheltens et al. (5) desarrollada también como esta en plano coronal (7, 8) y fundamentada como la MTA en el estudio de la magnitud del ancho de la fisura coroidea , del ancho del asta temporal del ventrículo lateral y por la altura de hipocampo, pero incidiendo en los cambios mas incipientes de estas estructuras que periten identificar y sistematizar los mismos en el curso del envejecimiento, resultando así una nueva EMTA mas sensible para detectarlos.

La EMTA se fraguo basándose en el estudio de los espacios de LCR que rodean el comienzo del cuerpo del hipocampo (proceso unciforme del mismo), al nivel en el que la fimbria es identificable (ramificación distal del Fórnix), y la relación de esta con tela coroidea y plexo coroideo del asta temporal en todos los sujetos de la muestra a estudio, describimos

en cada uno de ellos el aspecto de estas estructuras y reflejando estos resultados en una tabla de Excel descriptiva. Se valoró al nivel referido (fimbria) el tamaño y forma de:

    i)   la cisura coroidea (medial a la fimbria).
    ii) la porción medial del asta temporal del ventrículo lateral (lateral a la fimbria) y localizada sobre el cuerpo del hipocampo.
    iii) la porción inferior y lateral del asta temporal del ventrículo lateral (lateral al cuerpo del hipocampo).
    iv) La cisura transversa peritroncular
    v)   el cuerpo del hipocampo.

Posteriormente agrupamos los sujetos incluidos en dicha tabla de Excel que mostraban coincidencia de patrones en todas estas estructuras. Así con esta información realizamos unas máscaras en el programa FSL-View (a modo de molde) que representarán cada uno de los patrones o estadios observados (resultaron seis en total que nombramos S1 a S6).

Posteriormente se clasificaron los hipocampos derecho e izquierdo de los 360 sujetos válidos de la muestra según la escala MTA de Scheltens y según los nuevos patrones o estadios que el estudio observacional anatómico había apuntado (S1 a S6). Por esta razón la nueva EMTA es capaz de reconocer y graduar la aparición de cambios incipientes, que son susceptibles de cuantificación mediante técnicas volumétricas.

A continuación estudiamos los sujetos clasificados mediante ambas escalas (MTA y la nueva EMTA) mediante técnicas volumétricas de morfometría basada en voxeles (first-vertex, SPM y Free-Surfer) lo que permitió conocer el volumen de sustancia gris del hipocampo, el volumen global de hipocampo y el volumen del conjunto de los espacios de LCR mencionados.

Estos resultados nos permitieron verificar que:

1- los sujetos graduados como MTA 0 o 1 eran distintos entre si (first-vertex).

2- que de entre los seis estadios o patrones observados en la nueva escala (S1 a S6) solo cuatro mostraban agrupaciones de voxeles que los demostraran distintos según las técnicas SPM y Free-Surfer

c) Reproducibilidad por dos radiólogos

La variabilidad intraobservador resultante para el NR mostró un índice Kappa de 0.72 para el lado izquierdo y 0,80 para el lado derecho. La variabilidad interobservador obtenida entre NR y rNR mostró un índice Kappa de 0.76 para el lado izquierdo y 0,82 para el lado derecho.

d) Cuantificar volumétricamente la EMTA: desarrollo de la nueva escala EMTA$_4$.

Primero clasificamos todos los sujetos mediante la MTA y la EMTA$_6$ y la EMTA$_4$, en segundo lugar verificamos mediante análisis a través de First-Vertex la presencia de diferencias estadísticamente significativas entre sujetos clasificados como MTA 0 y MTA1 (con correcciones para edad y sexo), en tercer lugar validamos mediante SPM8 y Free-surfer la presencia de diferencias estadísticamente significativas entre los estadios EMTA$_4$ (sin correcciones para edad y sexo)

i) Clasificación de los sujetos mediante las escalas clasificación de la MTA y las nuevas escalas EMTA$_6$ and EMTA (Tablas 33, 35, 37, 38).

Encontramos la siguiente distribución de sujetos según la MTA n=352 temporal derecho (TD) and n= 349 temporal izquierdo (TI):

	MTA 0	MTA1	MTA2	MTA3	MTA4
Left N=349	196	130	18	1	1
Right N=352	149	192	10	0	0

Por otro lado encontramos esta distribución según la EMTA$_6$ n=357:

EMTA$_6$	S1	S2	S3	S4	S5	S6
Left N=357	130	79	43	4	75	24
Right N=357	103	46	121	31	46	11

Después de la validación mediante la técnica de MBV los seis estadios de la nueva escala original EMTA$_6$ se fusionaron en cuatro EMTA$_4$ n=357:

EMTA$_4$	S1	S2	S3	S4
Left N=357	209	44	79	24
Right N=357	148	121	77	11

ii) Validación de la clasificación MTA 0 y MTA 1 mediante FIRST-VERTEX análisis.

Este análisis corregido por edad y sexo nos permitió demostrar que entre los dos estadios las formas de los hipocampos eran diferentes, y esta diferencia era significativa:

-MTA 0 (n= 149 TD y n=196 TI)

-MTA 1 (n=203 TD y n=153 TI)

Las agrupaciones de voxeles que marcaban las diferencias estadísticamente significativas mas acusadas eran:

-TD (p<0,001 , 85% cortex enthorinal, 67% subiculum y 16% cornu de ammnonis)

-TI (p<0,012 , 88% amígdala laterobasal, 48% subiculum y 29% cornu de ammnonis).

Tablas 30, 31

Una vez que tuvimos la evidencia de que la gran mayoría de los sujetos a estudio correspondían a cambios incipientes de atrofia continuamos nuestro estudio validando los estadios de la EMTA$_4$.

iii) Validación de los estadios EMTA mediante SPM and Free-Surfer: de la EMTA$_6$ a la EMTA$_4$.

En un primer paso validamos los seis patrones morfológicos que definen la EMTA$_6$. Primero estudiamos el efecto global (EG) de la escala EMTA$_6$ aplicada a nuestra población a estudio mediante técnicas de MBV para la escala en el lóbulo TD **(Figura 36)** (área de la fisura coroidea, fimbria, asta temporal medial e inferolateral, p<0,000). En segundo lugar, estudiamos las diferencias en el volumen de la sustancia gris (VSG) en el lóbulo TD entre los sujetos clasificados como estadios S1, S2, S3, S4, S5 y S6 de la EMTA$_6$ **(Figura 37)**. El VSG de los estadios S1, S2 y S2, S3 no mostró diferencias

estadísticamente significativas (DES). Por otro lado, el VSG del estadio S3 fue mayor que el del S4 (asta temporal medial, p<0,001), el VSG de S4 fue mayor que el de S5 (asta temporal inferolateral, p<0,001) y por ultimo el VSG de S5 fue mayor que el de S6 (asta temporal lateral, p<0,001). Ahora procedimos a validar mediante análisis Free Surfer los resultados obtenidos con SPM8-tool box para los estadios de la $EMTA_6$ **(Figura 38)**. Se demostraron DES entre estadios S1, S2, S3, S4, S5 y S6 (p<0,001); S2 y S3, S4, S5 and S6, (p<0,001); entre S3 y S4 y S6 (p<0,001) y entre S3 y S5 (p<0,09); en cuanto al volumen del asta temporal ínfero-lateral. Se demostraron DES entre estadios S6 *vs.* S1, S2, S3, S4 y S5 en cuanto al volumen del hipocampo (p<0,001) **(Figure 38).**

. Después de este análisis decidimos colapsar los estadios iniciales S1-S2 de la escala $EMTA_6$ dando lugar a la nueva escala $EMTA_5$, dado que no mostraban entre ellos DES.

En un segundo paso validamos mediante un análisis MBV-SPM8-tool-box los cinco estadios remanentes de la $EMTA_5$ para el lóbulo TD. En primer lugar estudiamos, el EG de la escala $EMTA_5$ en el lóbulo TD que mostró DES en las áreas de: la fisura coroidea, fimbria, asta temporal medial e inferolateral, p<0,000 **(Figura 40)**. En Segundo lugar, estudiamos las diferencias en el VSG correspondientes al lóbulo TD entre los estadios $EMTA_5$ S1-S2 vs. S3, S3 vs. S4, S4 vs. S5 and S5 vs. S6 **(Figura 41 y 42)**. El VSG de los estadios $EMTA_5$ S1 y S2 colapsados fue mayor con DES frente al de S3 (fimbria, p<0,001). El VSG de S3 fue también mayor con DES que el de S4 (fimbria-fisura coroidea, p<0,001). El VSG de S4 fue también mayor con DES que el de S5 (asta temporal inferolateral, p<0,001). El VSG de S5 fue también mayor con DES que el de S6 (asta temporal medial, p<0,001).

Luego validamos mediante Free Surfer los resultados obtenidos mediante los análisis SPM8-tool-box de los estadios de la $EMTA_5$ **(Figura 43)**. Se demostraron DES entre estadios S1 y S2 (colapsados) y S3, S4, S5, S6 (p<0,001), entre S3 y S4, S5, S6 (p<0,001) y entre S3 y S4 (p<0,09) en cuanto al volumen del asta temporal ínfero-lateral. Se demostraron DES entre estadios S6 *vs.* S1-S2, S3, S4 y S5 en cuanto al volumen del hipocampo (p<0,001). Analizando los estadios S4 y S5 de la $EMTA_6$, encontramos que había AV (agrupaciones de voxeles) con DES que indicaban que el VSG del estadio S4 era mayor que el del S5 (asta temporal inferolateral, p<0,001) y otras agrupaciones de voxeles que mostraban lo contrario (fimbria, p<0,01) **(Figura 44)**. Además el volumen del asta temporal lateral inferior correspondiente a S6 era mayor que el de S5 y el de S4 mayor que el de S3. Después de este análisis de la $EMTA_5$ decidimos fusionar los

estadios S4-S5 dando lugar a la nueva escala EMTA$_4$, dado que representan en conjunto un mismo estadio con similitudes en el VSG y de los espacio de LCR que rodean el cuerpo del hipocampo..

En ultimo lugar tratamos de validar mediante análisis VBM-SPM8-tool-box los estadios de la escala EMTA$_6$ para el lóbulo TI. No fue posible el análisis para el estadio S4 (debido a su n=3) **(Tabla 38)**. Por otro lado el resto de los resultados de la MBV del TI fueron comparables con los obtenidos para el lóbulo TD.

e) Comparación de resultados de la EMTA biomarcadores de LCR y cognitivos:

i) Correlación de los estadios EMTA$_4$ con los biomarcadores de LCR.

Una vez que validamos mediante MBV la escala EMTA$_4$ comenzamos un análisis exploratorio comparativo (AEC) de los biomarcadores de LCR en los estadios de la escala EMTA$_4$ en el lóbulo TD, n= 357. Así pudimos observar como había una DES en cuanto a la edad media de los estadios S4 (68,1) vs. S1(56,5) S2 (57,2), S3 (57,8). Además, había una DES entre los valores de los biomarcadores de LCR Aβ1-42/tau entre los estadios S1 y S4 (p<0,005), y también entre los estadios S2 y S3 frente a S4 (p<0,05). Cuando estudiamos el biomarcador de LCR Aβ1-42/p-tau también había una DES entre los estadios S1 y S4 (p<0,05) **(Tabla 40-41)**.

Al analizar el porcentaje de biomarcadores en LCR Aβ1-42 positivos para cada estadio de la clasificación EMTA$_4$ en el lóbulo TD encontramos que había una DES entre los estadios S4 y S1, S2 y S3 (p<0,000). De todas formas seguimos un AEC del porcentaje de biomarcadores en LCR Aβ1-42 positivos para cada estadio de la clasificación EMTA$_4$ en el lóbulo TI, n= 357. Pudimos observar como había una DES en relación a la edad media entre los estadios S4 y S1, S2 y S3 (61,8 años en S4 y una p<0,001). Además no encontramos DES en cuanto a los biomarcadores en LCR Aβ1-42/tau o LCRAβ1-42/p-tau entre los estadios EMTA$_4$ en el lóbulo TI. Por ultimo estudiamos el porcentaje de biomarcador positivo Aβ1-42 para cada uno de los estadios EMTA$_4$ del lóbulo TI. Encontramos DES a SSD relativa al porcentaje de biomarcador en LCR Aβ1-42 positivo entre los estadios S4 y S1, S2 y S3 aun cuando menos pronunciados que en el lóbulo TD (p<0,063) **(Tabla 42-43)**.

ii) Correlación de los estadios de la EMTA$_4$ con los biomarcadores neuropsicológicos.

Realizamos también un AEC de todos los biomarcadores neurocognitivos incluidos en el subtítulo 2.5 del apartado de métodos en n=357 voluntarios para el lóbulo TD y n= 356 para el lóbulo TI (un sujeto juzgado como ALTM 3 fue excluido de este análisis) en los estadios de la escala EMTA$_4$ mostrándose, solo aquellos resultados que presentaron DES. Así pues con respecto al lóbulo TD: solo encontramos DES entre los estadios S1,S4 en el test de alteración de la memoria-media- $p < 0,0054$. Con respecto al lóbulo TI encontramos DES entre los estadios S1 y S4 para: el test de alteración de la memoria-media-y el test compuesto global de memoria $p < 0,0074$ (en ambos casos), en el TAVEC recuerdo libre precoz $p < 0,48$, TAVEC recuerdo libre tardío $p < 0,464$ y TAVEC recuerdo reclamado precoz $p < 0,47$. Entre los estadios S1 y S3 en el TAVEC de ensayo inmediato $p < 0,0121$ y entre los estadios S1, S2, S3 y S4 en el test compuesto de memoria precoz ($p < 0,044$) **(Tabla 44)**.

Por otro lado no encontramos DES en cuanto a los test de: a) Lenguaje: test de nominación de Boston , Test de repetición y comprensión (Boston), b) test de percepción visual y práctica: Figura compleja de Rey, Juicio de orientación lineal, Poppelreuter (the 15-objects test(20), and c) Funciones de atención y función ejecutiva: Test de fluencia verbal, Digit Span (WAIS-III), Stroop Test, Test de realización de trazado, Zoo Mapa Test and (BADS) Test de codificación de símbolos digitales (WAIS-III).

5) DISCUSION

En el presente estudio desarrollamos y validamos a través del análisis con MBV la nueva escala EMTA$_4$ que tiene la capacidad de medir los cambios de atrofia de bajo grado que ocurren antes de que comiencen a ser detectables con la escala MTA.

El estadio S1 de la EMTA$_4$ (anterior S1 y S2 fusionados de la escala EMTA$_6$) así como el estadio S2 de la EMTA$_4$ (anterior S3 de la EMTA$_6$) corresponden a estadios 0 de la escala MTA. El estadio S3 de la escala EMTA$_4$ es equivalente al estadio 1 de la MTA. Este estadio S3 de la EMTA$_4$ tiene dos posibles patrones morfológicos que corresponden a los anteriores S4 & S5 de la escala EMTA$_6$. El estadio S4 de la EMTA$_4$por su parte coincide con el correspondiente a un incipiente estadio 2 de la MTA.

Aunque los estadios 0 y 1 de la MTA han sido considerados no relevantes clínicamente en la propuesta original de Scheltens et al. dado que se recomienda un punto de corte ajustado por edad de la MTA ≥2 en cualquiera de los dos hemisferios para ser considerado anormal por debajo de la edad de 75 años (5) y también otros autores (11, 14) propusieron un punto de corte para la MTA ≥1.5 basado en la graduación media de ambos hemisferios entre 45-65 años (el espectro de edad de la fase pre-clínica de la Enfermedad de Alzheimer), nosotros hemos encontrado un progresivo adelgazamiento de la corteza cerebral (CC) del hipocampo desde el estadio S1 al S3 de la EMTA$_4$ (estadios 0 y 1 de la MTA) acompañado también por un progresivo descenso de los niveles de Aβ1-42 en LCR (% de voluntarios con niveles <580pg/ml, es de: 9,8% S1, 16,4% S2, 17,1% S3 y 75% S4 en lóbulo TD así como de 13,3% S1, 10,3% S2, 19,5% S3 y 37,5% S4 en lóbulo TI).

Mientras que Sheltens et al. (5) propusieron un punto de corte de la escala MTA ≥2 en cualquiera de los hemisferios cerebrales como patológico para sujetos edades menores de 75 años, en nuestro trabajo hemos demostrado la existencia de una incipiente atrofia hipocampal (AH) en el estadio S4 de la EMTA$_4$ (estadio MTA 2 precoz) con una edad media de 68,1 años para el lóbulo TD y 61,8 años para el lóbulo TI ($p<0,001$ TI y $p<0,005$ TD) acompañados de un rendimiento bajo en los test de memoria verbal (TMV) para TD y sobre todo para el lóbulo TI y DES en LCR en los biomarcadores Aβ1-42/tau o CSF Aβ1-42/p-tau entre los estadios S1 vs S4 (MTA 0 vs. MTA 2 precoz) para lóbulo TD.

La sólida validación de la EMTA$_4$, tiene el mismo valor que el obtenido previamente por Sheltens et al. (5) en el estudio original de la MTA, o mas recientemente en los estudios de Wahlund et al. (aplicando la MTA al estudio de la Enfermedad de Alzheimer en fase de demencia, sujetos cognitivamente normales (CN) and y sujetos diagnosticados de otros tipos de demencia) (21), Westman et al. (utilizando la MTA para el estudio de la Enfermedad de Alzheimer en fase de demencia, sujetos cognitivamente normales (CN) y Enfermedad de Alzheimer en fase en fase de deterioro cognitivo ligero (DCL) (22) o Cavallin et al. (usando la MTA al estudio de una cohorte sujetos ancianos sanos ≥ 60 años de edad)(13).

Comparamos nuestros resultados (basado en voluntarios de la cohorte PGA (proyecto Guipúzcoa Alzheimer) con tres estudios relevantes: Wang et al.(23), Fortea et al. (24) y finalmente Jack et al. (25) que corresponden a estudios longitudinales de

envejecimiento y alteraciones de memoria (KADRC-Washington-USCM study(23), ADNI(24) y MACSA-Mayo study (25)). Hay diferencias entre estos cuatro trabajos relativas a los métodos utilizados: 1-en cuanto a la edad media: (71 años (23), 73,4 años (24), 72 años (25) and 56,6años PGA), 2- en relación al criterio usado apara etiquetar a un voluntario como CN; en el estudio de Wang et al. Definido como tener un CDR de 0, y en el de Fortea et al. (24) tener un MMSE de 29,1, mientras que en nuestro estudio incluimos n=199 sujetos con puntuación CDR ≤ 0.5 y también n=15 con MMSE < 26 pero puntuación CDR > 0.5 y 3-el número de voluntarios enrolado que oscila entre n=100 (23) y n=1246(25) pasando a través de n=145(24) and n= 214 en nuestra serie.

Por un lado las principales diferencias reflejadas entre nuestro estudio y los de Wang et al.(23), Fortea et al. (24) y finalmente Jack et al. (25) se concentran en: 1- este grupo(23) encuentra una elevación de tau en LCR asociado a disminución de grosor cortical en las áreas propias de la firma cortical de la EA pero no con AH, mientras que en nuestro trabajo encontramos los dos fenómenos asociados, 2- este trabajo (23) encuentra que la disminución en LCR de $A\beta1$-42 se relacionaba con un menor rendimiento en las pruebas de memoria episódica mientras que en nuestro estudio lo esta con un peor desempeño en los test de memoria verbal, 3- Jack et al. (25) encuentran empeoramiento progresivo de la memoria en el lapso de tiempo transcurrido entre los 30 años y 90 años mientras que en nuestro trabajo solamente hemos encontrado empeoramiento en el rendimiento de los test de memoria verbal para los sujetos clasificados como S4 de la $EMTA_4$ con edades medias de 68,1 años para el lóbulo TD & 61,8 años para el lóbulo TI. Ellos encontraron AH progresiva desde los 30 años hasta mediados los 60 años, cuando acelera su evolución mientras que en nuestro estudio solo demostramos AH incipiente para los sujetos clasificados como S4 de la $EMTA_4$.

Por otra parte las principales coincidencias con nuestro estudio de las series de Wang et al. (23), Fortea et al. (24) y por ultimo Jack et al. (25) se concentran en: 1- la observación del adelgazamiento de la corteza cerebral (23, 24) en las áreas propias de la firma cortical de la EA, 2- hallazgos que sugieren interacción entre los biomarcadores de LCR de la EA resultando un fenómeno bifásico de adelgazamiento cortical asociado con bajos niveles de $A\beta$ en LCR, seguido por AH una vez que en LCR la p-tau aparece(24) y 3- en estos trabajos como en nuestra serie la AH es el ultimo fenómeno en aparecer en el proceso del envejecimiento(24, 25).

Una limitación del presente estudio es que hemos incluido n=199 sujetos con puntuación de CDR ≤ 0.5 y también n=15 con MMSE < 26 pero puntuación de CDR score > 0.5; así pues nuestros resultados pueden estar influidos por esta circunstancia en comparación con los estudios de Wang et al. (23) que incluyen en su trabajo solo sujetos con CDR 0 o la serie de Fortea et al. (24) que incluyen voluntarios con MMSE 29,1. Otra limitación de nuestro estudio es relativa al tamaño de la muestra así de n=357 sujetos incluidos en nuestra serie para el análisis de MBV y del de los biomarcadores neuropsicológicos, la muestra se limitó a n=213 cuando correlacionamos los biomarcadores de MBV con los de LCR. Finalmente otra limitación de la aproximación del presente estudio es que hemos investigado la relación entre cambios morfológicos incipientes, biomarcadores de LCR y neuropsicológicos de modo transversal, y así no somos capaces de poder investigar si esos cambios se relacionan con un cuadro clínico final típico.

Un punto fuerte de nuestro trabajo, es el uso combinado de biomarcadores de LCR y neuropsicológicos para un limitado pero notable grupo de 213 voluntarios, mayor que la muestra de Wang et al (23) n=100 y Fortea et al (24) n=145. Actualmente se esta llevando a cabo un seguimiento longitudinal de los datos de la cohorte PGA. Estos datos nos permitirán investigar si la EMTA$_4$ puede ser usada como un biomarcador para el diagnostico precoz de la EA (mediante la medición del CDR registrado la evolución de los estadios de esta escala).

La variabilidad intraobservador registrada en la aplicación de la EMTA (0,72 valores kappa ponderados en el lado izquierdo y 0,80 en el lado derecho) fue inferior a la observada por Ferreira et al. (0,93 en el lado izquierdo y 0,94 en el lado derecho) (14) o Cavallin et al. (0,88 en el lado izquierdo y 0,89 en el lado derecho) (13) en la aplicación de la MTA. La variabilidad interobservador observada aplicando la EMTA (0,76 valores kappa ponderados en el lado izquierdo y 0,82 en el lado derecho) también fue un poco más baja que la observada para la escala atrofia PA (0,85 en los lados izquierdo y derecho)(26). La explicación de estas peores variabilidades intra e interobservador obtenidas con la EMTA en comparación con las publicadas para las escalas MTA (13, 14) y PA (26)podría estar relacionada con la propia naturaleza del EMTA, diseñada y validada para detectar cambios de atrofia de bajo grado del lóbulo temporal medial.

6) CONCLUSIONES

a) Hemos confeccionado una nueva escala de medir la atrofia temporal medial (EMTA), mediante RM craneal, más sensible que la utilizada habitualmente (MTA).

b) La EMTA fue primero diseñada sobre un análisis visual de las RM craneales basada en estrictos criterios anatómicos

c) La EMTA ha sido validada mediante estudios de morfometría basada en voxeles resultando 4 estadios según el grado de atrofia: S1 a S4

d) Los estadios S1 y S2 de la EMTA corresponden al estadio 0 de la MTA. El estadio S3 corresponde al estadio 1 de la MTA. El estadio S4 al MTA2 en su fase inicial.

e) La EMTA es fácil de aplicar y tiene una buena correlación inter e intraobservador.

f) Los individuos en estadio S4 tienen una edad más avanzada que la de los estadios S1 a S3.

g) Los individuos en estadio S4 en el lado derecho muestran alteraciones de biomarcadores en LCR (Aβ1-42/tau o CSF Aβ1-42/p-tau) comparados con los que están en el estadio S1

h) Los sujetos en S4 en lóbulo temporal izquierdo muestran rendimientos alterados en los test cognitivos de memoria verbal.

i) Creemos que la EMTA puede considerarse un marcador precoz de la neurodegeneración en la fase preclínica de la Enfermedad de Alzheimer.

1) INTRODUCTION

The preclinical Alzheimer's disease (PcAD) concept and definition has been possible due to the appearance and development of specific biomarkers for Alzheimer's disease (AD) (3, 4). However in the biomarkers models developed by IWG and NIAA-AA, the structural magnetic resonance imaging (MRI) (3, 6, 15, 27) has been entitled either as a late appearance biomarker in the pathophysiology of preclinical AD (15, 27) or it has been eventually excluded (4, 6). The current accepted preclinical & clinical biomarkers are: cerebral spinal fluid (CSF), biomarkers (Aβ $_{1-42,}$ T-tau or P-tau) or amyloid positron emission tomography (PET) (3). However these by themselves are not sensitive enough in clinical practice to detect the early phases of the neurodegenerative process.

The present thesis is focused on the study of the low-grade atrophy prior to the diagnosis of AD. We aim to develop an anatomically based radiological scale of atrophy of the medial temporal lobe (MTL). Furthermore, we will compare the anatomical scaling with corresponding volumetric measures as well with other AD biomarkers in order to test its sensitivity as biomarker for preclinical AD.

a) Definition, pathology and diagnosis of the Alzheimer's Disease

Alzheimer's disease is a chronic neurodegenerative disease that usually starts slow and get worse over the time. The most common early symptom is difficulty in remembering recent events (short-term memory loss). As the disease advances symptoms can include: language problems, disorientation, mood swings, loss of motivation, not managing self-care and behavioural issues (28).

Pathologically AD is characterising by an abnormal protein deposits: Aβ plaques and neurofibrillary tangles (NFTs) formed by hyper phosphorylated tau. Neurodegeneration is as important as these hallmark pathological lesions of AD, and manifests as atrophy, neuron loss, and gliosis, which are routinely noted in research post-mortem examinations. Although the loss of synapses also is highly significant for the clinical manifestations of AD, this is difficult to assess without the use of labour-intensive morphometric methods, so it is not routinely measured in most AD research

centres. Neurodegeneration and NFT deposition are both neuronal processes and occur in roughly the same topographic distribution. Aβ plaques are extracellular and occur in a different, but to some degree overlapping, topographic distribution from NFT and neurodegenerative pathological changes (27).

The distribution pattern and packing density of amyloid deposits turned out to be of limited significance for differentiation of neuropathological stages. Neurofibrillary changes occurred in the form of neuritic plaques, neurofibrillary tangles and neuropil threads. The distribution of neuritic plaques varied widely not only within architectonic units but also from one individual to another. Neurofibrillary tangles and neuropil threads, in contrast, exhibited a characteristic distribution pattern permitting the differentiation of six stages. The first two stages were characterized by an either mild or severe alteration of the transentorhinal layer pre-alpha (transentorhinal stages I-II). The two forms of limbic stages (stages III-IV) were marked by a conspicuous affection of layer pre-alpha in both transentorhinal region and proper entorhinal cortex. In addition, there was mild involvement of the first Ammon's horn sector. The hallmark of the two-isocortical stages (stages V-VI) was the destruction of virtually all isocortical association areas. The investigation showed that recognition of the six stages required qualitative evaluation of only a few key preparations. AD is an age-related, not an age-dependent disease. The degree of brain destruction at stages III-IV frequently leads to the appearance of initial clinical symptoms. The stages V-VI representing fully developed AD are increasingly prevalent with increasing age. The arithmetic means of the stages of both the amyloid depositing and the neurofibrillary pathology increase with age. Age is a risk factor for AD (29, 30) **(Figure 1).**

Development of neurofibrillary changes
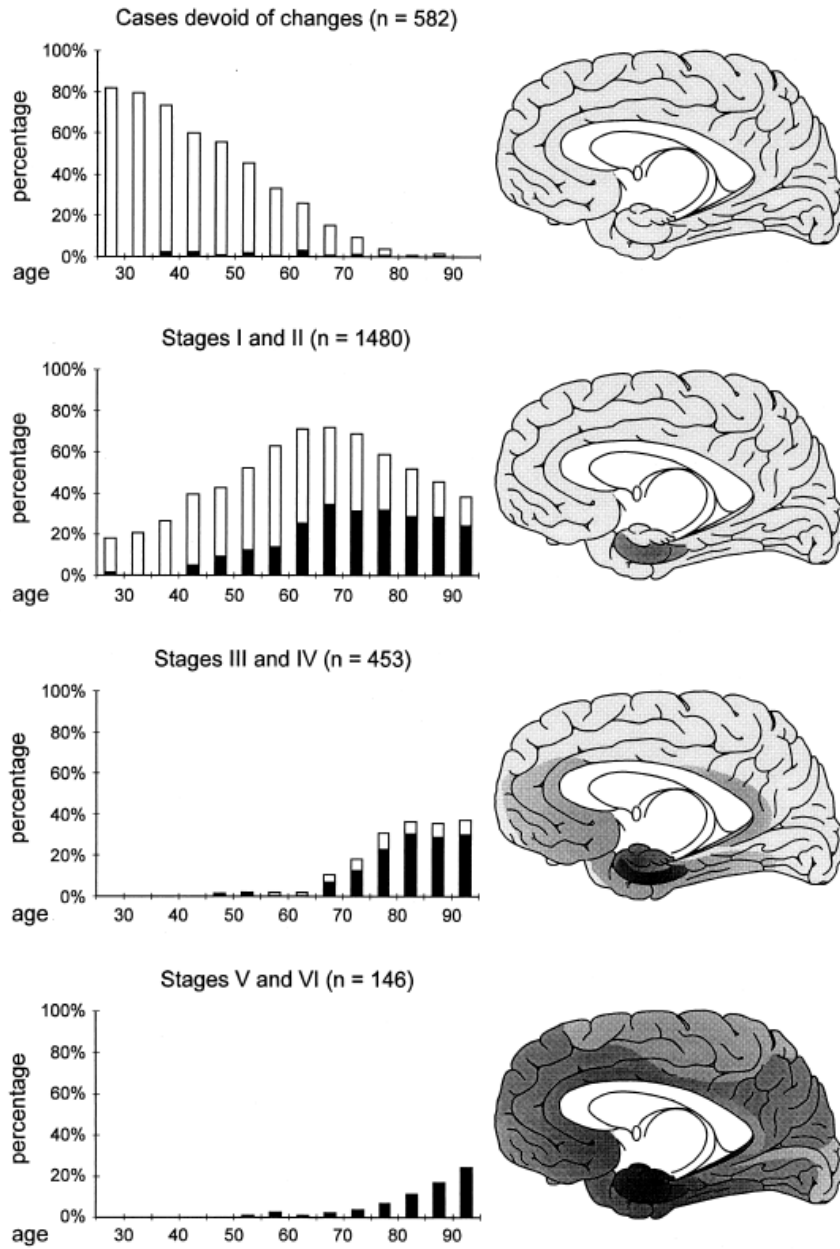
Figure 1- Frequency of stages of Alzheimer-related lesions in different age categories.

[Modified Braak H and Braak E (24)].

Traditionally AD has been define as a type of dementia [accounts for 60% to 70% of cases (28)], a notion brought into existence with the publication of criteria from the National Institute of Neurological and Communicate Disorders and Stroke-Alzheimer's Disease and Related Disorders Association (NINCDS-ADRDA) in 1984 (3, 31). Two major principles of these criteria were: 1) the clinical diagnosis of AD could only be designated as "probable" as the patient was alive and could not be made definitively until Alzheimer's pathology had been confirmed post mortem; and 2) the clinical diagnosis of AD could be assigned only when the disease had advanced to the point of causing functional disability and met the threshold criteria of dementia (31). The absence at that time of clinical criteria for the other dementias and the lack of biomarkers resulted in a low specificity in differentiation AD from other dementias (3).

In the past eight years, both the International Working Group (IWG) and the US National Institute on Aging-Alzheimer's Association Working Group (NIA-AA-WG) have contributed criteria for the diagnosis of Alzheimer's disease (AD) that better define clinical phenotypes and integrated biomarkers into the diagnostic process, covering the full staging of the disease (3, 4, 6, 32-34).

Table 1- Diagnosis criteria Alzheimer´s disease depending the sponsor society

NINCDS-ADRDA	1984	Probable-in vivo Clinically advanced
IWG	2007	in vivo Prodromal Episodic memory Biomarker-MRI-PET-CSF
	2010	New Lexicom Preclinical AD "Asymptomatic at risk" "Presymtomatic" Clinical AD "Atypical AD" "Mixed AD" Biomarker-MRI-PET-CSF Less complex in semiology Consistency Applicable Clinical Trials
NIAA-AA	2011	Preclinical AD Pre dementia AD (MCI) Dementia AD Each of them with its on diagnostic criteria Asymptomatic AD-biomarkers evidence of Aβ accumulation Pre dementia AD (MCI) Dementia AD – probabilistic likelihood Applicable without support of Biomarkers Less specificity

b) Pathophysiology of Alzheimer's disease

Spearling *et al.* propose a theoretical model of the physiological cascade of AD to facilitate the discussion of the concept of a preclinical stage of AD (4). They proposed model of AD views Aβ peptide accumulation as a key early event in the pathophysiological process of AD. However the acknowledge of the aetiology of AD remains uncertain and several mechanism have been proposed (synaptic, mitochondrial, metabolic, inflammatory, neuronal, cytoskeletal and other age-related alterations) as well to play an even earlier role, more central than Aβ peptide accumulation (4). There are also a significant debate about whether abnormal processing versus clearance of $A\beta_{42}$ the aetiology event in sporadic AD (late onset).

Some investigators have suggested that the sequestration of Aβ fibrillar forms may even serve as a protective mechanism against oligomeric species, which may be the more synaptotoxic forms of Aβ (4). However of all the known autosomal dominant, early onset forms of AD are thought to be, at least in part, due to alterations in amyloid precursor protein (APP) production or cleavage. Similarly, trisomy 21 invariably results in AD pathological individuals (4). Autopsy and biomarkers studies suggest that Aβ$_{42}$ accumulation increases with advanced aging (the greatest risk factor). It is also clear that synaptic depletion, intracellular hyper phosphorylated forms of tau, and neuronal loss invariably occur in AD and in autopsy seem to correlate better than plaque counts or total Aβ load with clinical impairment (4) Usually the presence of markers "upstream" Aβ accumulation is associated with markers of "downstream" pathological changes (such abnormal tau, neural dysfunction, glial activation and neuronal loss and atrophy). However remains to be proven that Aβ accumulation is sufficient to incite the downstream pathological cascade of AD. It is also unknown whether this neurodegenerative process could be related to direct synaptic toxicity due to oligomeric forms of Aβ, or a "second hit" that results in synaptic dysfunction, neurodegeneration, neurofibrillar tangle formation, and eventually neuronal loss (4) **(Figure 2).**

Hypothetical model of AD pathophysiological cascade
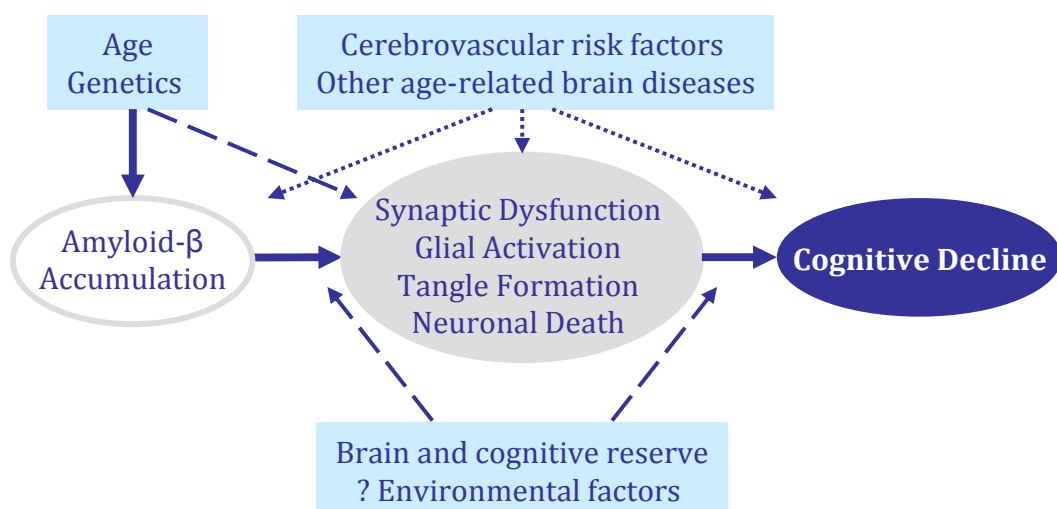
Figure 2- Hypothetical model of the Alzheimer's disease (AD) pathophysiological sequence leading to cognitive impairment. This model postulates that amyloid beta (Aβ) accumulation is an "upstream" event in the cascade that is associated with "downstream" synaptic dysfunction, neurodegeneration, and eventual neuronal loss. Note that although recent work from animal models suggests that specific forms of Aβ may cause both functional and morphological synaptic changes, it remains unknown whether Aβ is sufficient to incite the neurodegenerative process in sporadic late-onset AD. Age and genetics, as well as other specific host factors, such as brain and cognitive reserve, or other brain diseases may influence the response to Aβ and/or the pace of progression toward the clinical manifestations of AD. [Modified Sperling *et al.* (4)].

Norton *et al.* (35) present a model that estimates the modifiable component of the risk of AD in relation to seven key risk factors based on a previous work of Barnes *et al.* (36). They estimate that one in three AD cases worldwide is attributed to diabetes, midlife hypertension, midlife obesity, physical inactivity, smoking, depression or low educational attainment, taking into account the frequent co-occurrence of these factors. Based on this estimate, they show, in their most optimistic scenarios, that relative reductions in the prevalence of each of the seven risk factors of 20% per decade might reduce the number of cases of AD in 2050 by 15.3%, which would translate into a reduction in the number of individuals with AD from 106 million expected without intervention to 90 million worldwide by 2050 (35). According to the models, most AD cases worldwide are attributed to low educational attainment (35). In the USA, Europe and UK, the largest proportion of cases is attributed to physical inactivity (35) **(Figure 3).**

_____
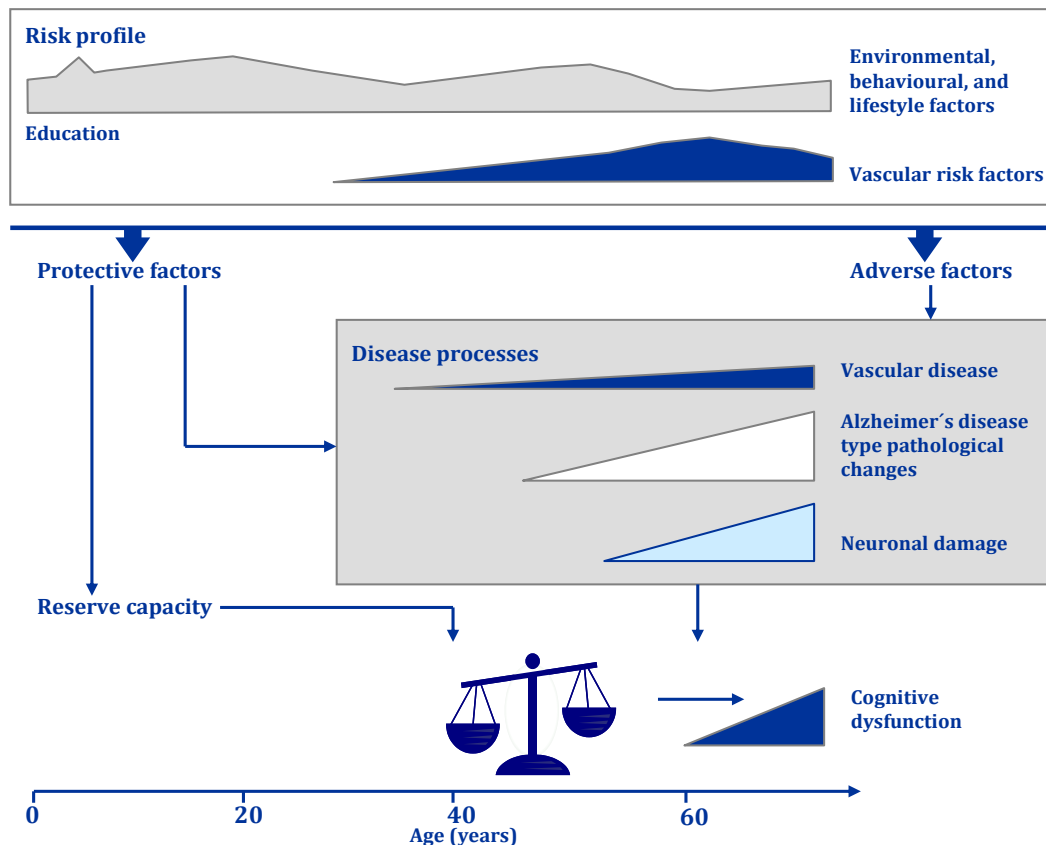
Figure 3- Modifiable risk factors for Alzheimer's disease across life

An individual's profile of modifiable risk factors includes adverse and protective factors. These factors include education and environmental, behavioural, and lifestyle factors. Examples are physical activity, diet, smoking, and depression—factors that can fluctuate over the course of life. Vascular risk factors—e.g., diabetes, hypertension, and obesity—generally occur from midlife onwards, under the influence of environmental, behavioural and lifestyle factors, on a background of genetic predisposition. Adverse factors induce disease processes in the brain that generally start to develop later in life. Protective factors might attenuate disease processes and can also contribute to cerebral reserve capacity. Disease processes include cerebrovascular disease and Alzheimer's disease type pathological changes, the combined burden of which leads to progressive neuronal damage in the brain. Once the balance between the burden of neuronal damage and cerebral reserve capacity is disturbed, cognitive dysfunction ensues. [Modified Norton *et al.* (35)].

Following Norton *et al.* (29) maintaining mental health up to the late life requires a life spam perspective on prevention. AD is at least partially preventable and that several known risk factors for poor health also substantially contribute to dementia risk. In fact, the potential for prevention might be even larger if other modifiable risk factors for dementia (e.g., diet and leisure activities) are consider (37).

51

Pathogenesis is not restricted to the neuronal compartment, but includes strong interactions with immunological mechanisms in the brain (38). Misfolded and aggregated proteins bind to pattern recognition receptors on microglia and astroglia, and trigger an innate immune response characterised by release of inflammatory mediators, which contribute to disease progression and severity (38). Genome-wide analysis suggests that several genes that increase the risk for sporadic AD encode factors that regulate glial clearance of misfolded proteins and the inflammatory reaction (38). External factors, including systemic inflammation and obesity, are likely to interfere with immunological processes of the brain and further promote disease progression. Modulation of risk factors and targeting of these immune mechanisms could lead to future therapeutic or preventive strategies for AD (38) **(Figure 4).**
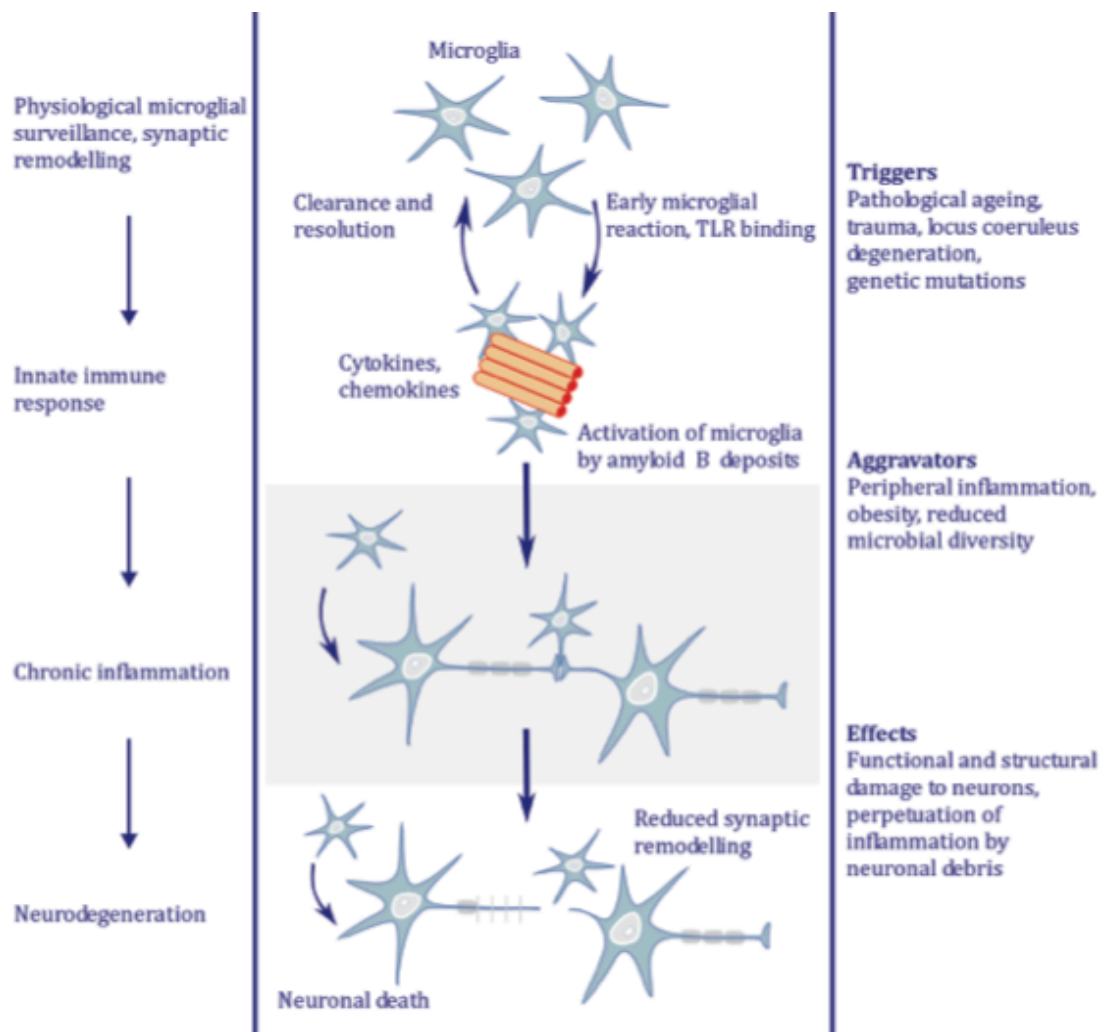
Figure 4- Pathomechanistic sequelae of microglia activation

Physiological functions of microglia, including tissue surveillance and synaptic remodelling, are compromised when microglia sense pathological amyloid β accumulations. Initially, the acute inflammatory response is thought to aid clearance and restore tissue homoeostasis. Triggers and aggravators promote sustained exposure and immune activation, which ultimately leads to chronic neuroinflammation. Perpetuation of microglia activation, persistent exposure to proinflammatory cytokines, and microglial process retraction cause functional and structural changes that result in neuronal degeneration. TLR=Toll-like receptor. [Modified Heneka *et al.* (32)].

c) Biomarkers of Alzheimer's disease

Over the past two decades, it has become increasingly possible to identify *in vivo* evidence of the specific neuropathology of AD by use of validated and disease specific biomarkers(6). Laboratory and neuroimaging biomarkers are very highly correlated with neuropathological lesions of AD (6). From the point of view of IWG represented by Dubois *et al.* (1), these biomarkers can be divided into pathophysiological and topographical markers **(Table 2).**

Table 2- Biomarkers division following IWG criteria

	Pathophysiological markers	Topographical markers
Cerebrospinal fluid		
Amyloid β42	Yes	No
Total tau, phospho-tau	Yes	No
PET		
Amyloid tracer uptake	Yes	No
Fluorodeoxyglucose	No	Yes
Structural MRI		
Medial temporal atrophy	No	Yes

[Modified Dubois et al. (1)].

Pathophysiological markers correspond to the two aetiological degenerative processes that characterise Alzheimer's pathology: The amyloidosis path to neuritic plaques and the taupathy path to neurofibrillar tangles. They include CSF measurements of reduced concentrations of amyloid β, increase total tau, and increasing phospho-tau, and amyloid PET scanning with Pittsburg compound B (PiB) or other radioligands (florbetaben, ^{18}F-AV-45, etc).

_____

CSF biomarkers (low amyloid β and, even more specifically, abnormal ratio of tau to amyloid β) are associated with very high rates of progression from amnesic mild cognitive impairment (MCI) to AD dementia, and have shown a consistently high sensitivity and specificity in predictive models (6). High mean cortical binding values for PiB-PET are predictive of cognitive decline and development of AD clinical signs in cognitively normal elderly individuals (6). In vivo pathophysiological markers correlate very well with their respective neuropathological lesions, including CSF amyloid β and PiB-PET with senile plaques, and total tau and phospho-tau with neurofibrillar tangles (6).

Topographical markers are used to assess the less specific and downstream brain changes that correlate with regional distribution of Alzheimer's pathology and include medial temporal lobe atrophy and reduced glucose metabolism in temporo-parietal regions on fluorodeoxyglucose PET. These markers are valuable indicators because structural brain changes accurately map to the Braak stages of neurofibrillar tangle deposition (6). These MRI and PET topographical markers have been shown consistently to predict the development of AD dementia in MCI cohorts and to correlate with disease severity (6). In 2007 there was no empirical basis for assessing weightings to pathophysiological versus topographical changes associated with neurodegeneration. Since then, understanding of the timing of pathological events has increased, with pathophysiological changes preceding the topographical changes associated with neurodegeneration (more related the latter with the emergence of cognitive symptoms (6).

Nevertheless CSF and amyloid PET have both shown the highest specificity when correlated with the underlying Alzheimer's pathology in post-mortem studies. Conceptually, they are the most specific biomarkers to determine that an individual is within the AD continuum even several years before the clinical onset of disease (3). A marked reduction in CSF $A\beta_{1-42}$ and in the $A\beta_{1-42}/A\beta_{1-40}$ ratio has consistently been noted in patients at different stages of AD. However, an isolated low $A\beta_{1-42}$ is not sufficiently specific to diagnose AD, in view of similar findings in some patients with non-AD dementias (Lewy body disease or vascular dementia), given its presence long before onset of clinical AD, or given AD copathologicaly in patients with Lewy body disease. Additionally $A\beta_{1-42}$ concentrations are particularly sensitive to preanalytical and analytical biases and make it difficult to achieve the requisite low coefficiency of variation and quality control (3).

The added value of the combination of CSF markers has been tested in predictive studies of progression to AD dementia. Individuals with a high ratio of T-tau to Aβ $_{1-42}$ or of P-tau$_{181}$ to Aβ $_{1-42}$ progress to symptomatic cognitive impairment (ie, CDR>0) more quickly than do the remainder of the cohort. This result was not observed for Aβ $_{1-42}$ concentrations alone for the duration of the longitudinal studies (3-5 years) completed to date. The combination of T-tau, Aβ $_{1-42}$ and P-tau is highly predictive of dementia, which has been confirmed in three large multicentre studies namely the Alzheimer's Disease Neuroimaging initiative (ADNI) study, the Development of Screening Guidelines and Criteria for Predementia Alzheimer's Disease (DESCRIPA) study, and the Swedish Brain Power (SBP) project. A meta-analysis recently confirmed that the combination of CSF Aβ $_{1-42}$ with either T-tau or P-tau has the highest predictive accuracy, whereas individual markers were also predictive but with lower accuracy (odds ratio [OR] 7.5-8.1). Studies of autosomal dominant mutation carrier, including the Dominantly Inherited Alzheimer's Disease (DIAN) project, also show that high CSF T-tau and P-tau combined with a decrease in CSF Aβ $_{1-42}$ and the ratio of Aβ $_{1-42}$ /Aβ $_{1-40}$ are present 10-15 years before the first symptoms of dementia (3).

Additionally the combined analysis of the CSF biomarkers provides the best accuracy in the differential diagnosis between AD and others degenerative dementias, with a good concordance with post-mortem diagnosis. In particular, the ratio of T-tau to Aβ $_{1-42}$ was the best biomarker to differentiate AD from frontotemporal lobar degeneration, and showed a specificity of 96.6% in a series of patients with diagnostic confirmation either by genetics or by post-mortem examination (3). PET imaging with amyloid tracers, including ^{11}C-PiB, florbetapir (AV-45), flutemetanol (^{18}F-PiB derivative), florbetaben (AV-41) and AZ4694, provide important information about the extent of Aβ neuritic plaque burden in the brain. Amyloid PET is therefore considered as a surrogate marker of brain fibrillary amyloid pathology (neuritic plaques and amyloid angiopathy) and by extension a good marker of Alzheimer's pathology (3).

From the point of view of NIAA-AA represented by Jack *et al.* a model of AD biomarkers intended to be a framework for *in vivo* staging of the disease. The model was initially presented at the International Conference on Alzheimer's disease in July 2009, and published in January 2010 (27). New evidences in this field have been accumulated since that time and

modifications to this model has been proposed by the same group and published in February 2013 (15). Following this proposal biomarkers of AD can be divided into two major categories: a) measures of brain amyloid β (Aβ) deposition and b) measures of neurodegeneration (defined as progressive loss of neurons or their processes [axons and dendrites] with a corresponding impairment in neuronal function) (15). Brain Aβ deposition is assessed by measurements of CSF Aβ $_{1\text{-}42}$ and PET amyloid imaging. Increased concentrations of CSF T-tau and P-tau, hypometabolism on PET-FDG and atrophy on structural MRI are measurements of neurodegeneration. PET-FDG and MRI follows a modality-specific topology that is characteristic of AD (6, 15).

This NIAA-AA biomarkers model is predicated on the assumption that biomarkers are related to specific pathophysiological processes. Low CSF Aβ $_{1\text{-}42}$ and uptake of amyloid PET tracers are associated with fibrillar Aβ deposits. Increase in T-tau and P-tau is associated with neurofibrillar tangle (NFT) burden at autopsy, and in AD, T-tau and P-tau behave very similarly to each other. Atrophy in MRI studies correlates with neuron loss and are measurements of tau-related degeneration. Ante-mortem PET FDG hypometabolism is also correlated with NFT burden and not with plaque burden at autopsy (15).

The basic principles of this model at its original description were: a) the major AD biomarkers become abnormal in a temporally ordered manner (CSF Aβ $_{1\text{-}42}$ and amyloid PET are dynamic earliest, followed by CSF tau and PET FDG, then structural MRI followed by clinical symptoms. The model assumes that the maximum rate of change moves sequentially from one biomarker class to the next, and as the disease progresses all biomarkers become progressively more abnormal simultaneously, b) Aβ deregulation, which leads to plaque formation, is necessary but not sufficient to produce the clinical AD syndrome. Cognitive decline is only loosely coupled with rate of magnitude of amyloid PET and CSF Aβ $_{1\text{-}42}$, but is closely coupled with the magnitude and rate of change on neurodegenerative biomarkers (CSF T-tau and P-tau, hypo-metabolism on PET-FDG and atrophy on structural MRI), c) rates of change in each biomarker follow a non-linear temporal course, which these authors postulate to be sigmoid-shaped with time, d) a subject-specific lag in time exists between biomarker evidence of *in situ* AD pathophysiology and the emergence of cognitive impairment, which is mediated by differences in brain resiliency or cognitive reserve and e) the added contributions of other pathologies (e.g., vascular disease, Lewy bodies, TDP-43 inclusions) that often co-occur with

aging also contribute substantially to interindividual variations in clinical disease expression (27) **(Figure 5).**
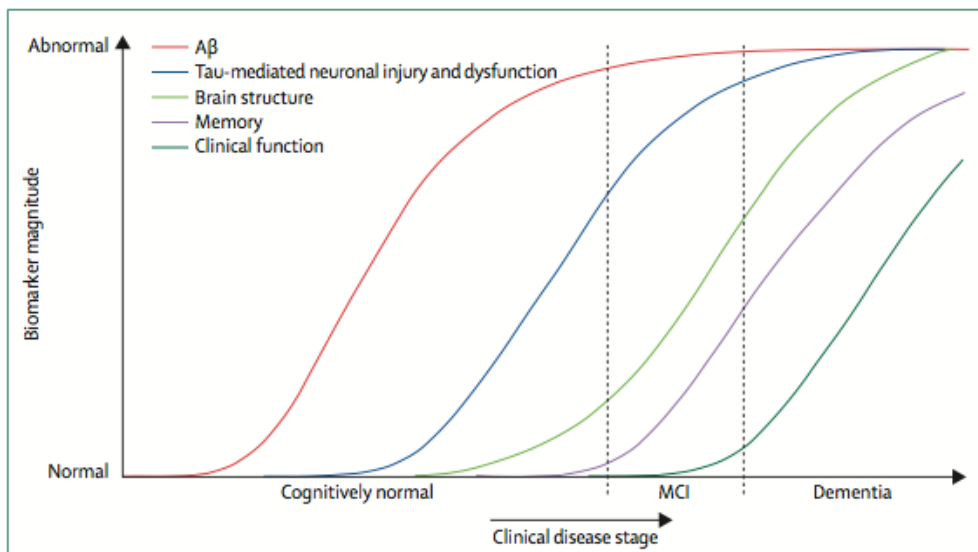
Figure 5- Biomarkers NIAA-AA 2010 model.

Evidence has been accumulated since the original description of this NIAA-AA biomarkers model that clearly supports the general temporal ordering framework describe above in which amyloid biomarkers become abnormal first, followed by biomarkers of neurodegeneration, and the clinical symptoms. However, less evidence has been obtained to define the relative temporal ordering of CSF tau, PET FDG, and structural MRI (15). In fact results as whose derived from this thesis tend to probe the early cortical hippocampal thickness changes that occurs before the AD clinical onset. Regarding the sigmoid-shape of the biomarkers curve evolution over time, it has to be said that several sources reinforce the idea that amyloid biomarkers do follow a sigmoid-shape trajectory over time although related PET FDG and MRI atrophy measurements some evidences suggest that their slopes curves may not be parallel to the amyloid biomarker curve and continue to change substantially through the dementia phase of the disease (15).

Due to AD pathophysiology usually coexists with other pathophysiology changes, particularly cerebrovascular disease and synucleinopathy (bearing in mind that hippocampal sclerosis, TDP-43 and potentially non-AD taupathies such as argyrophylic grain disease are also important contributors), this reality could be a confounder factor when studying a

determinate elderly cohort for which one possible solution is to analyse the subset of participants who tested positive for AD biomarkers to screen out people who are not following the AD pathophysiological pathway (15).

The original NIAA-AA biomarkers model was design to have quantifiable horizontal and vertical axis. Progressive clinical stages disease stages were place on the horizontal axis. Although it is certainly true that every person who develops AD exhibits progressive cognitive decline, indexing of individuals on the horizontal axis by clinical stage or continuous measurements of cognitive impairment has proved to be a flawed approach due mainly to the fact that important pathophysiological changes occur on the preclinical phase (that might constitute half or more of the total disease duration) in which measurements of cognitive decline are most imprecise (15). A new NIAA-AA biomarkers model version therefore has been proposed (15) **(Figure 6).**
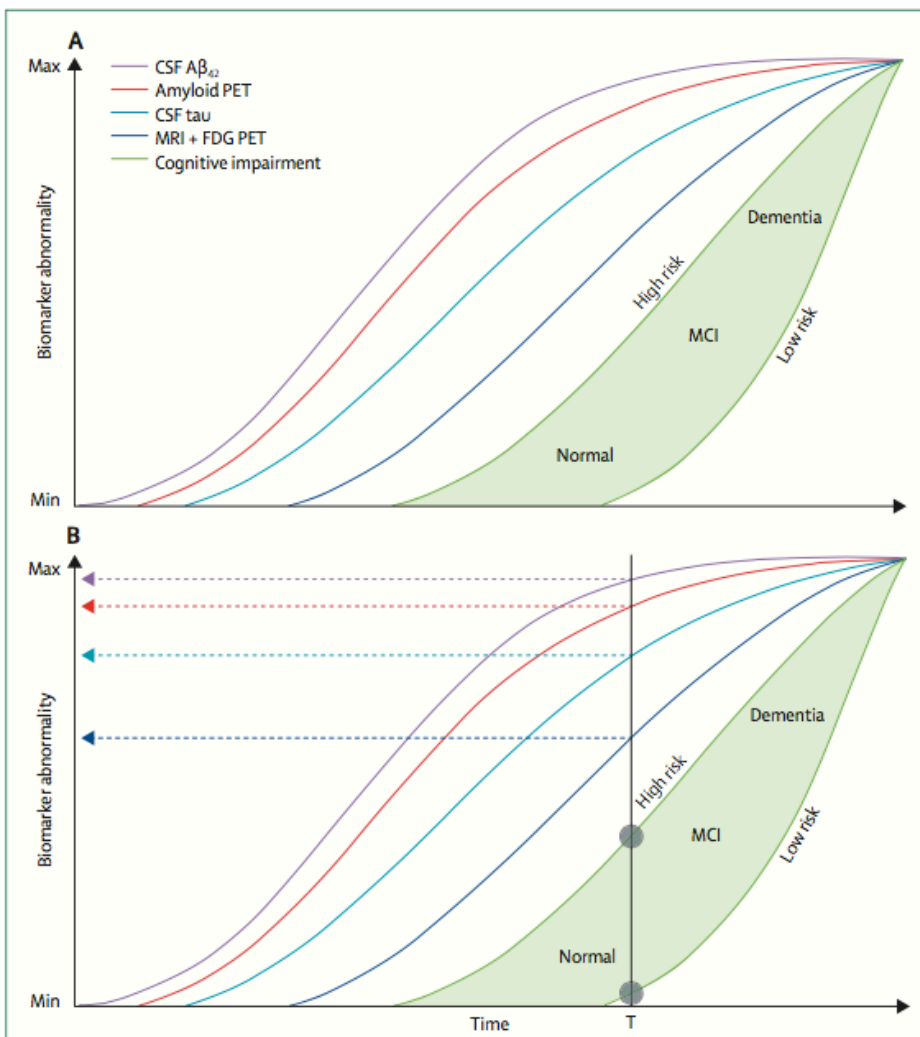
Figure 6- Biomarkers NIAA-AA 2013 model.

The main differences with respect to the 2010 version are: a) the horizontal axis is now expressed as time, not clinical stage, b) a range of possible cognitive outcomes is shown at given positions along the horizontal axis reflecting the fact that each individual responds to AD pathophysiological process uniquely (high risk of cognitive impairment profile people shows a curve that is shifted to the left in time), c) modifications of the specific ordering of some biomarkers (CSF Aβ $_{1-42}$ is now positioned slightly before amyloid PET, which is followed by CSF tau. PET FDG and MRI are drawn coincidentally as the last biomarkers to become abnormal), d) The biomarker curves (still sigmoid-shaped) have a progressively steeper slope in the right-hand tail for later-changing biomarkers and e) the biomarkers curves are drawn closer together in the revised model indicating less distinct temporal separation (15).

One of the most important criticisms of this model was that originally did not account for the fact that medial temporal limbic tau pathology is a nearly universal feature of ageing and that tau pathology typically appears in individuals at a younger age than do Aβ (therefore AT8-positive pretangles (i.e., positively stained perikarya) were reported in a high proportion of young individuals (as young as 6 years of age) in selected subcortical areas (15). Braak and Del Tredici (39)propose that tau pathology begins in the locus coeruleus (changes then spread to other brainstem nuclei and to the entorhinal cortex, perhaps by direct cell-to-cell transmission) and that the subcortical deposition of tau is the starting point of the AD pathophysiological cascade, beginning as early as the first decade of life (15).

Small and Duff (40)have suggested that tau hyper phosphorylation and Aβ accumulation might be independent pathophysiological processes that share a common upstream cause. Mesulam(41) specifically suggested that protracted exposure to up regulation of cellular activity related to neural plasticity could represent the common upstream cause of both tau hyper phosphorylation and Aβ accumulation. Duykaerts (42)has also suggested that tau and Aβ pathological changes could be independent processes but with pathogenic synergy (15).

Several independent sources of AD biomarker evidence suggest that the sequence of events depicted by these biomarkers is Aβ pathophysiology first, and then tau related neurodegeneration. However autopsy data suggest on the other hand that AD-like taupathy

precedes Aβ deposition. One way to integrate this information could be the idea that tauopathy and Aβ pathophysiology arising independently.

In this proposed integrating model (Figure 6), subcortical tauopathy is the first AD pathophysiological process to arise in many individuals and is detectable only by immunostaining methods. This tauopathy however does not by itself lead to AD. Aβ pathophysiology arises later and independently from pre-existing tauopathy. Through unknown mechanisms Aβ pathophysiological changes qualitatively transform and, as proposed by Price and Morris(43), accelerate the antecedent subcortical tauopathy leading to neocortical spread of NFTs. So acceleration of the initial slow developing subcortical tauoptahy occurs after Aβ biomarkers become abnormal (15). In elderly people this theory is consistent with the notion of an age-related failure to clear misfolded proteins, or failure of normal protective mechanisms to sequester toxic soluble forms of these proteins or both. An independent Aβ pathophysiology can accelerate an antecedent tauopathy as probed by: a) the fact that genetically determine Aβ overproduction leads to AD, whereas genetically determine tauopathis doses not, which support a casual instigating role for Aβ and not tau in early-onset AD, b) a recent discovered coding mutation in the amyloid precursor protein gene that protects against late-onset AD (so there are casualty points to Aβ as the disease initiator in early-onset AD, and as either initiator or an accelerator in sporadic AD. In a subject specific manner, probably at least two pathways to sporadic AD might exists (15) **(Figure 7).**
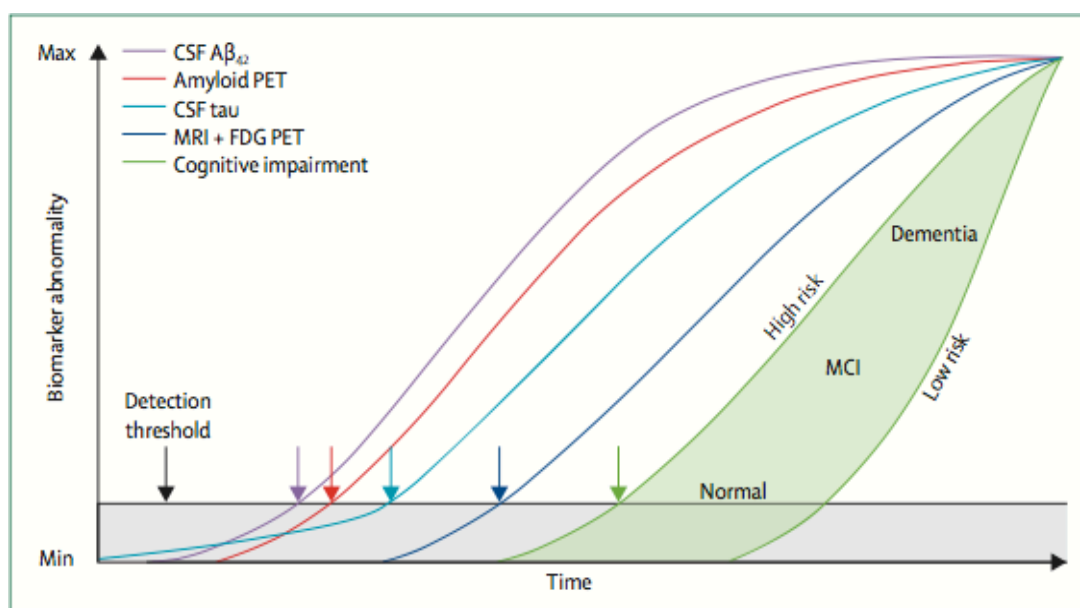
Figure 7- Model integrating Alzheimer's disease immunohistology and biomarkers

The black horizontal line denotes the threshold for biomarker detection of pathophysiological changes. The grey area denotes the zone in which abnormal pathophysiological changes lie below the biomarker detection threshold. In this figure, tau pathology precedes Aβ deposition in time, but only early on at a sub threshold biomarker detection level. Aβ deposition then occurs independently and rises above the biomarker detection threshold (purple and red arrows). This induces acceleration of tauopathy and CSF tau then rises above the detection threshold (light blue arrow). Later still, FDG PET and MRI (dark blue arrow) rise above the detection threshold. Finally, cognitive impairment becomes evident (green arrow), with a range of cognitive responses that depend on the individual's risk profile (light green-filled area). Aβ=amyloid β. FDG=fluorodeoxyglucose. MCI=mild cognitive impairment.

Table 3-Biomarkers sum up following IWG vs. NIAA-AA criteria

IWG	NIAA-AA
a) Pathophysiological CSF Aβ $_{1-42}$ **T-tau and P-tau** PET **Pib-PET** b) Topographical PET **FDG-PET** Structual MRI **Medial temporal lobe atrophy**	**a) Sigmoid Shaped** have a progressively steeper slope in the right-hand tail for later-changing biomarkers **b) Specific ordering** 1ª CSF Aβ $_{1-42}$, 2ª PET-PiB, 3ª CSF tau, 4ª PET FDG and MRI are drawn **c) Horizontal axis is now expressed as time** **d) Range of possible cognitive outcomes** (high risk shows a curve that is shifted to the left in time) **e) Aβ pathophysiology first, then tau related neurodegeneration** acceleration of the initial slow developing subcortical tauoptahy occurs after Aβ biomarkers become abnormal

d) Preclinical Alzheimer disease.

A new version of the diagnostic criteria for preclinical AD that was proposed in 2014 by Dubois *et al* (20) is summarizing in Table 4.

IWG-2 criteria for asymptomatic at risk for AD (A plus B)

A Absence of specific clinical phenotype (both are required)
  • Absence of amnestic syndrome of the hippocampal type
  • Absence of any clinical phenotype of atypical AD

B In-vivo evidence of Alzheimer's pathology (one of the following)
  • Decreased Aβ1–42 together with increased T-tau or P-tau in CSF
  • Increased retention on fibrillar amyloid PET

IWG-2 criteria for presymptomatic AD (A plus B)

A Absence of specific clinical phenotype (both are required)
  • Absence of amnestic syndrome of the hippocampal type
  • Absence of any clinical phenotype of atypical AD

B Proven AD autosomal dominant mutation in *PSEN1*, *PSEN2*, or *APP*, or other proven genes (including Down's syndrome trisomy 21)

AD=Alzheimer's disease.

A new version of the diagnostic criteria for preclinical AD that was proposed in 2011 by Sperling *et al* (2) is summarizing in Table 5.

Table 5- Staging categories for preclinical AD research

Stage	Description	αβ (PET or CSF)	Markers of neuronal injury (tau, FDG, sMRI)	Evidence of subtle cognitive change
Stage 1	Asymptomatic cerebral amyloidosis	Positive	Negative	Negative
Stage 2	Asymptomatic amyloidosis + "downstream" neurodegeneration	Positive	Positive	Negative
Stage 3	Amyloidosis + neuronal injury + subtle cognitive/behavioral decline	Positive	Positive	Positive

Abbreviations: AD, Alzheimer's disease; Ab, amyloid beta; PET, positron emission tomography; CSF, cerebrospinal fluid; FDG, fluorodeoxyglucose (18F); sMRI, structural magnetic resonance imaging.

There are five cohorts nowadays studying the preclinical AD that are:

a) MAYO-MCSA(1)

   296 subjects enrolled, mean age 78 years, biomarkers obtained PET-PiB, PET-FDG. And MR-VBM.

b) KADRC- WUSM(2)

   311 subjects enrolled, mean age 65 years, biomarkers obtained Aβ $_{1-42}$, T-tau or P-tau in CSF.

c) Cita (unpublished yet).

   213 subjects enrolled, mean age 56 years, biomarkers obtained Aβ $_{1-42}$, T-tau or P-tau in CSF.

d) BIOCARD-JHSM (44)

   245 subjects enrolled, mean age 57 years, biomarkers obtained MRI-VBM.

e) WRAD-WUSM (45)

   211 subjects enrolled, mean age 60 years, biomarkers obtained Aβ $_{1-42}$,T-tau or P-tau in CSF.

The characteristic of these five cohorts are summarizing in tables 6 and 7.

Table 6- Preclinical AD cohorts description.-I-

Series	Number Subjects	Age	Cohort	Biomarkers	Cutoff points
Knopmann 2012 ADMADRC	296	**78y**	MAYO MCSA	PET-PIB. PET-FDG RM-VBM.	GCR 1,5 HPR 1,35 Hva -0,70
Vos 2013 Youden Index	311	**65y**	KADRC WUSM	$A\beta_{42}$ TauTotal Tau Fosforilada	<459pgr/ml >339pgr/ml >67pgr/ml
Cita	214	**56y**	CITA PGA	$A\beta_{42}$ TauTotal Tau Fosforilada	<550pgr/ml >350pgr/ml >59pgr/ml

Table 7- Preclinical AD cohorts description.-II-

Series	Number Subjects	Age	Cohort	Biomarkers	Cutoff points
Soldan 2012 Own data	245	**57y**	BIOCARD JHSM	RM-VBM No CSF	Hazard Model APOE status CR (cognitive reserve)
Almeida 2015 Own data	211	**60y**	WRAD WUSM	$A\beta_{42}$ Tau Total Tau Fosforilada	=734ngr/ml =295ngr/ml =42,14ngr/ml

The distribution of subjects from cohorts: MAYO-MCSA (1), KADRC- WUSM (2) and Cita classified by NIAA-AA preclinical stages of AD are displayed in Table 8 and Table 9. As you can appreciate the lower mean age of Cita-cohort condition in the one hand the relative high percentage of volunteers corresponding to Stage 0 (63%) comparing with the results obtained with the other two cohorts compared (43%-MAYO/MCSA, 41%-KADRC-WUSM) and in the other hand the relatively low figures of volunteers included in Stage 2 (5%) comparing with the results obtained with the other two cohorts compared (13%-MAYO/MCSA, 12%-KADRC-WUSM).

Table 8- **The distribution of subjects from cohorts: MAYO-MCSA (1), KADRC- WUSM (2) and Cita classified by NIAA-AA preclinical stages of AD.**

Series	Stage 0	Stage 1	Stage 2	Stage 3	Stage 4
MAYO MCSA 2012 78y	43%	15%	13%	2%	23%
KADRC WUSM 2013 65y	41%	15%	12%	4%	23%
PGA Cita **56y**	**63%**	10%	**5%**	1%	21%

Table 9- **The percentage of conversion to at least CDR 0.5 of MAYO-MCSA and KADRC-WUSM**

Series	Stage 0	Stage 1	Stage 2	Stage 3	Stage 4
MAYO MCSA 2012 15 months	**5%**	11%	21%	**43%**	10%
KADRC WUSM 2013 5 years	**2%**	11%	26%	**56%**	5%

e) Therapies for Alzheimer disease

i) Amyloid chelation therapy

(1) Targeting AB production and removal: Inhibiting β secretase activity.

One type of disease-modifying approach traetment involves β-secretase inhibitors, designed to block the production of amyloid β, which are now being tested in phase 2 and phase 3 clinical trials. These studies are bolstered by target engagements of more than

80% lowering of amyloid β production. Together, these clinical trials suggest that the magnitude of target engagement and stage of disease are crucial, and provide tantalising evidence that these disease-modifying approaches could be nearing confirmation (17).

(2) Immunotherapy

(a) Active-vaccination-ADEM

Immunotherapy in AD aimed at β-amyloid covers 2 types of vaccination: active vaccination against Aβ42 in which patients receive injections of the antigen itself, or passive vaccination in which patients receive injections of monoclonal antibodies (mAb) against Aβ42. Three of the peptide vaccines for active immunizations, CAD106, ACC001, and Affitope, are in phase 2 clinical trials. Three of the mAbs solanezumab, gantenerumab, and crenezumab, are or were in phase 2 and 3 clinical studies. While the phase 3 trials failed, one of these may have shown a benefit at least in mild forms of AD without ADEM phenomena. There is a need for a greater initiative in the development of immunotherapeutics. Several avenues have been explored and still to come (46).

(b) Passive Aβ$_{1-5}$ immunotherapies

Although a highly effective drug has not yet been approved for the treatment of AD, pivotal advances were made in 2014, leading to substantial knowledge about therapeutic targets and early stages of disease (17). Two phase 3 trials of anti-amyloid-β monoclonal antibodies did not show significant benefits in cognitive or functional primary outcomes; however, they revealed insights into the disease course and suggested improvements in trial methodology. Bapineuzumab had no effect on cognition, while showing minimal effects on biomarkers, including a slight decrease in accumulation of fibrillar amyloid only in individuals who carried the *APOE4* allele and a slight lowering of CSF phospho-tau. Solanezumab bound significant amounts of soluble amyloid-β, its biomarker of target engagement, but did not show significant benefits in the primary cognitive outcome. However, there were benefits in secondary outcome measures of cognition only in patients with mild dementia, but not in those with moderate dementia, suggesting that earlier stages of disease are more amenable to therapeutic benefits. Similarly, in a phase 2 study of crenezumab, an antibody which also targets soluble amyloid β in addition to aggregated forms, cognitive benefit was detected only in patients with mild AD and at the highest doses of crenezumab used in the study (17).

Several monoclonal antibodies, including solanezumab, gantenerumab, and crenezumab, are in late-stage clinical development in trials of populations at early disease stages.

As a summary of the neurotransmitter, amyloid chelation therapy and immunotherapy despite the early promise of these therapies, none has proved effective at stopping or reversing the neurodegenerative process, nor clear cognitive benefits have been observed. However, some evidence suggests that the early application of some of the treatments (mild AD dementia) might have a cognitive benefit.

ii) Prevention trials

Several prevention trials have launched to test prevention in dominantly inherited AD and in people thought to be at high risk of AD due to the presence of fibrillar amyloid deposits in the brain. The Alzheimer's Prevention Initiative (API) Colombian trial and the Anti-Amyloid Treatment in Asymptomatic Alzheimer's Disease trial (A4 trial) launched in the past year, and the Dominantly Inherited Alzheimer Network Trials Unit (DIAN-TU) prevention trial continued from the year before. In 2014, three new prevention efforts were announced. The API announced a future prevention trial in *APOE4* homozygous participants. The DIAN-TU trial platform announced the next stage to prevent cognitive decline in a platform prevention trial of the DIAN-TU Adaptive Prevention Trial (DIAN-TU APT) and the European Innovative Medicines Initiative (IMI) announced the European Prevention of Alzheimer's Disease study, a cohort study to initiate adaptive prevention trials (17).

In support of these novel approaches to treat or prevent Alzheimer's disease, there has been rapid development of trial methodology, biomarkers, and cognitive measurements. The specialty continues to move into the investigation of early disease stages, aiming to treat before symptoms manifest. On the basis of trial results showing that one in four trial participants did not have cerebral amyloidosis, biomarkers are playing an ever more important part in the selection of participants, through screening for the presence of cerebral amyloid by PET scan and CSF measures (17).

Approaches to accelerate drug development are underway, bolstered by international efforts initiated at the G8 dementia summit, and establishment of the World Dementia Council. Rapid

development of tau PET imaging measures has shown strong correlations of tau deposits with gold standard clinical and cognitive measures. Tau PET imaging is being added to trials, in addition to amyloid imaging, CSF biomarkers, and MRI, to provide insight into the *in vivo* actions of the drug candidates, and to develop surrogate biomarkers to accelerate future trials. Cognitive tests continue to evolve with the development of sensitive measures of cognitive decline associated with amyloid pathology, several novel cognitive composites, and frequent longitudinal assessments promising better metrics to judge drug effects (17).

Increased governmental support is essential to address the burden of AD; however, the future of research funding is uncertain. There is a wealth of basic science knowledge, hypotheses, and targets whose translation into clinical therapies is constrained by limited fiscal resources. In support of the efforts to develop effective treatments and prevention strategies, public–private partnerships such as the NIH Advanced Medicines Program have accelerated implementation of tau PET imaging and RNA analysis in trials. In addition to the multi-national Alzheimer's Disease Neuroimaging Initiative (ADNI) and the global DIAN, several observational cohorts are also being established, with networks to better understand frontotemporal dementia and dementia in Down's syndrome. The European IMI has initiated several AD programmes to understand and accelerate therapeutics development. The global coordination of these efforts will be instrumental to address the global burden of AD (17).

f) Hippocampal formation anatomy

i) Gross anatomical features of hippocampal formation

(1) Rostrocaudal extent of the hippocampal fields

The **Figure 8** provides a histological estimate of the locations, along the temporal lobe rostrocaudal axis, of the different components of the hippocampal formation. The length of each component has been calculated relative to the distance to the frontotemporal junction, also known as the limen insulte (47). The rostrocaudal extent of the major portion of the hippocampal formation occupies the cavity of the temporal extension of the lateral ventricle for approximately 4 cm **(Figures 8 and 9)**(47).

0	Temporal pole
1 cm	
22	Frontotemporal junction
24	Anterior limit of the entorhinal cortex
29	Anterior limit of the amygdala
33	Anterior limit of the lateral ventricle
35 *	Anterior limit of the subiculum
41	Anterior limit of the dentate gyrus
48	Posterior limit of the uncus
50	Posterior limit of the entorhinal cortex
51	Anterior limit of the lateral geniculate nucleus
58	Posterior limit of the lateral geniculate nucleus
65	Anterior limit of the calcarine sulcus
68	Posterior limit of the dentate gyrus
75 mm *	Posterior limit of the hippocampal formation

Figure 8- Entire human hippocampal formation has a rostrocaudal extent of approximately 5 cm. A representation of the approximate linear extents of each of the subdivisions of the hippocampal formation and related structures as reconstructed from a series of coronal sections through the temporal lobe of one brain. Numbers on the left show the distances in millimetres from the rostral pole of the

temporal lobe to each of the anatomical points indicated on the right side of the bold vertical line. The distance between the asterisks indicates the length of all hippocampal formation fields excluding the entorhinal cortex
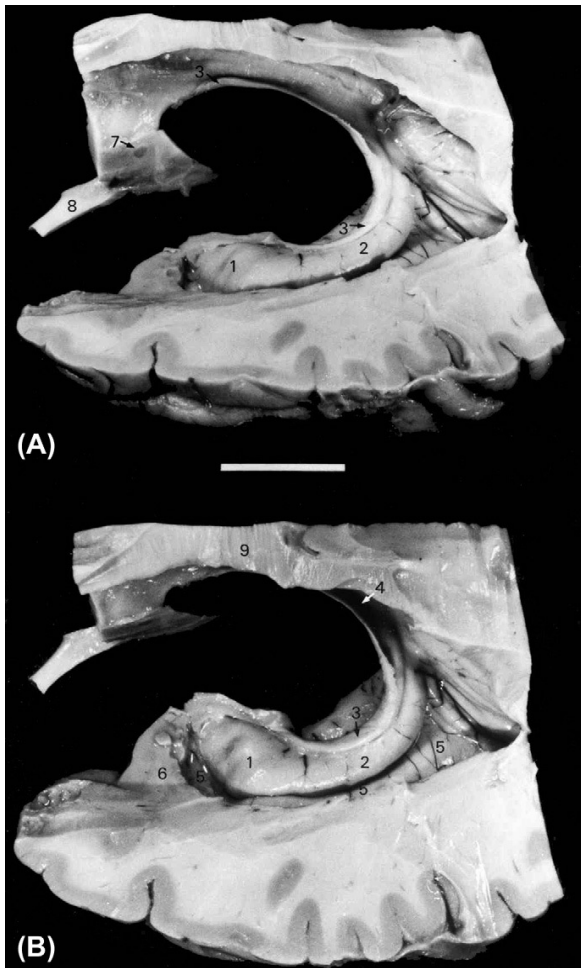
Figure 9- Dorsolateral view of the human hippocampus after removal of the overlying structures. The preparation is seen from slightly different angles in (A) and (B). The lateral ventricle (5) has been opened, thus exposing the shape of the hippocampus. It is possible to follow the hippocampus caudally as it ascends toward the retrosplenial region. Ultimately, the fornix (3) extends rostrally and then ventrally to bifurcate around the anterior commissure (7) and innervate the septal nuclei and diencephalon. The lateral surface of the temporal lobe can be seen at the bottom of the two views. Scale bar equals 2 cm. 1, pés hippocampus; 2, hippocampus (body); 3, fimbria-fornix; 4, hippocampal commissure; 5, temporal horn of the lateral ventricle; 6, amygdala, 7, anterior commissure; 8, optic nerve; 9, corpus callosum.

The entorhinal cortex is the most rostrally situated of the hippocampal formation regions, and it can be identified just behind the limen insulae. The entorhinal cortex begins rostrally at approximately 2.5 cm from the temporal pole. The rostral most 5 mm of the entorhinal cortex

is located rostral to the amygdaloid complex. The next 5 mm lies in a position ventromedial to the amygdaloid complex. Thus, approximately a full centimetre of the entorhinal cortex is located rostral to any other component of the hippocampal formation. The dentate gyrus, hippocampus, subiculum, presubiculum, and parasubiculum bend medially and then take a caudal direction at the rostral limit of the lateral ventricle, forming the uncus. The subiculum makes this bend most rostrally and thus forms the most rostral portion of the hippocampal formation (excluding the entorhinal cortex). The subiculum is the first visible hippocampal structure inside the lateral ventricle, i.e. in a rostrocaudal series of MRI coronal sections through the brain. The dentate gyrus makes the medial bend most caudally; it becomes visible around 6 mm from the anterior pole of the hippocampus in coronal sections. The medial or "uncal" region of the hippocampal formation makes up a large portion of what is usually referred to as the uncus **(Figures 10, 11 and 12)**(47).
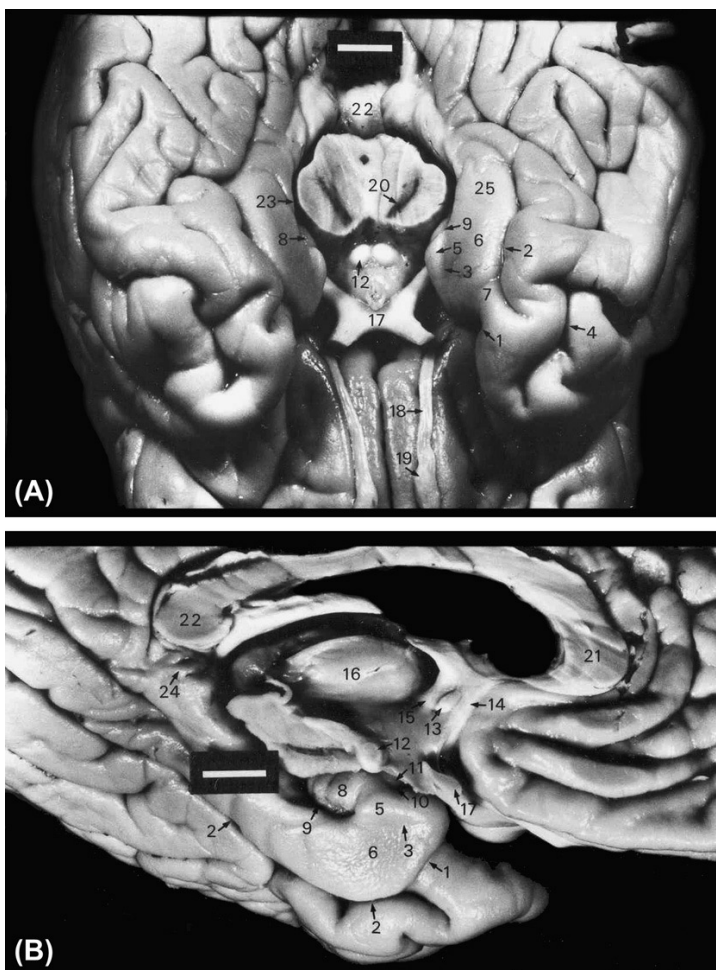
Figure 10- Ventral and ventromedial surface of the human brain (A) Ventral surface of the human brain after removal of the brainstem and the cerebellum. The gyri and sulci of the ventral surface of the

temporal lobe are clearly exposed, and the relationships of the medial temporal lobe to other diencephalic and mesencephalic structures can be seen. (B) The ventromedial aspect of the left temporal lobe of the same brain after being bisected along the midline. The hippocampal structures situated at the medial and dorsal aspect of the temporal lobe that could not be demonstrated in the ventral view are now visible. The scale bar in both panels equals 1 cm. 1, rhinal sulcu; 2, collateral sulcus; 3, intrarhinal sulcus; 4, occipitotemporal sulcus; 5, gyrus ambiens; 6, entorhinal cortex; 7, perirhinal cortex (anterior portion); 8, uncus; 9, hippocampal fissure; 10, sulcus semiannularis; 11, gyrus semilunaris; 12, mammillary bodies; 13, anterior commissure; 14, precommissural fornix; 15, postcommissural fornix; 16, thalamus; 17, optic chiasm; 18, olfactory tract; 19, olfactory bulb; 20, substantia nigra; 21, corpus callosum (rostrum); 22, corpus callosum (splenium); 23, choroidal fissure; 24, gyri Andreae Retzii; 25, parahippocampal gyrus.

This uncal portion extends for a rostrocaudal distance of approximately 1 cm and, as we will discuss later, comprises several different hippocampal fields(47). The various hippocampal fields also have different caudal termination points. The entorhinal cortex ends first, approximately 1.7 cm caudal to the anterior limit of the lateral ventricle and approximately 1.5 cm caudal to the start of the subiculum. The caudal border of the entorhinal cortex generally takes place approximately at the end of the gyrus intralimbicus (the most caudal portion of the uncus) and roughly coincident with the rostral limit of the lateral geniculate nucleus (Figures 12 and 13)(47) if the plane of the section is orthogonal to a horizontal line through the anterior and posterior commissures. The parasubiculum ends at approximately the same level as the entorhinal cortex. However, the caudal border of the presubiculum is more difficult to determine precisely. This is because near the caudal border of the hippocampus there is a subtle change in the cytoarchitectonic characteristics of the presubiculum, which, in the monkey (48), marks the transition to a ventrotemporal extension of the retrosplenial cortex (49).

_____
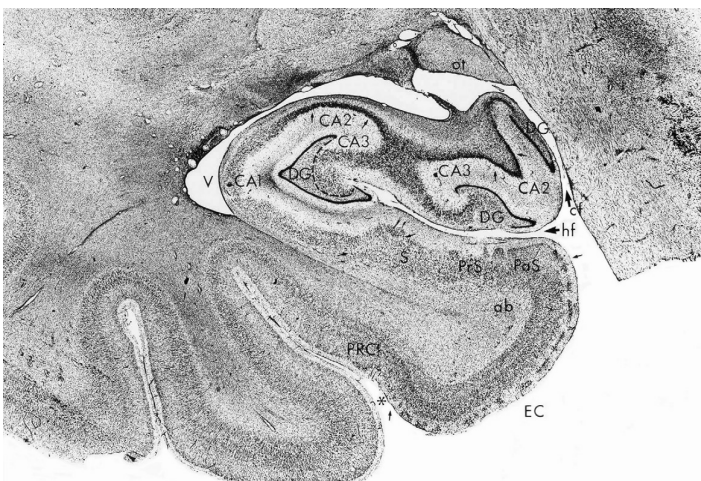
Figure 11- Dentate gyrus border from the CA3 field of the hippocampus. .Dashed line in the dentate gyrus separates the polymorphic layer (hilus) of the dentate gyrus from the CA3 field of the hippocampus. Note that both the hippocampal fissure (hf) and the choroidal fissure (cf) are apparent at this level of the medial or uncal hippocampal formation. Note also that the border between CA1 and the subiculum (marked by arrows) is obliquely oriented relative to the pyramidal cell layer.
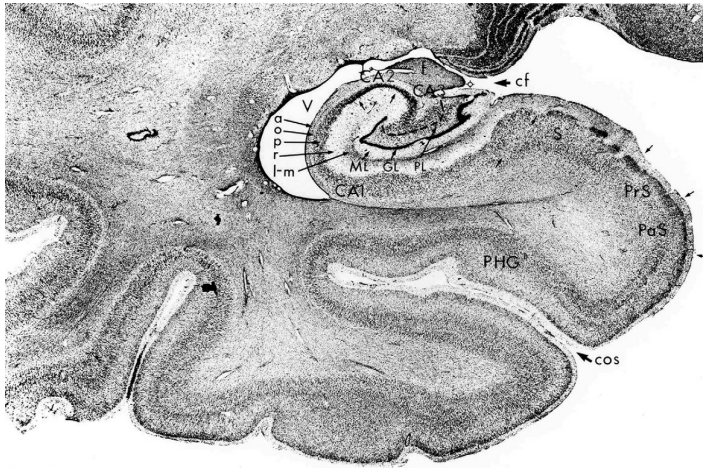
Figure 12- Dashed line in the dentate gyrus indicates the border between the polymorphic layer of the dentate gyrus (PL) and the CA3 field of the hippocampus. Note that at this level the entorhinal cortex is no longer present and the parasubiculum (PaS) of the hippocampal formation abuts the parahippocampal cortex (PHG), which has replaced the perirhinal cortex in, a caudal continuation of the parahippocampal region. Note also that a small groove (target sign) called the fimbriodentate sulcus separates the molecular layer of the dentate gyrus from the fimbria.
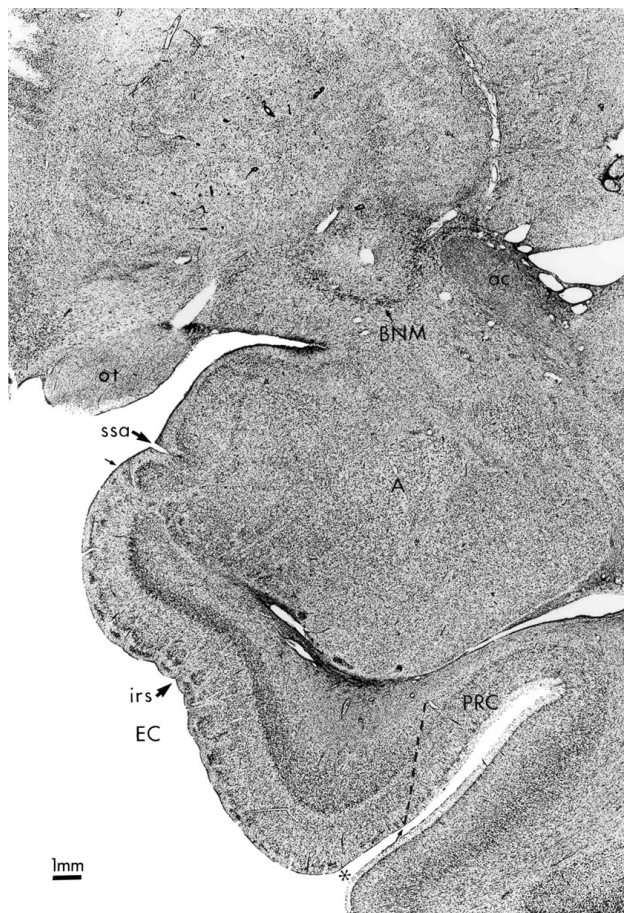
Figure 13- A representative series of coronal, thionin-stained sections (arranged from rostrally (Figure 13) to caudally (Figure 14)) through the human hippocampal formation. A, amygdaloid complex; a, alveus; ab, angular bundle; ac, anterior commissure; AHA, amygdalohippocampal area; BNM, nucleus basalis of Meynert; CA1, CA1 field of the hippocampus; CA2, CA2 field of the hippocampus; CA3, CA3 field of the hippocampus; cas, calcarine sulcus; cf, choroidal fissure; cos, collateral sulcus; DG, dentate gyrus; EC, entorhinal cortex; f, fimbria; gl, GL, granule cell layer of the dentate gyrus; hc, hippocampal commissure; hf, hippocampal fissure; irs, intrarhinal sulcus; LGN, lateral geniculate nucleus; l-m, stratum lacunosum-moleculare of the hippocampus; ml, ML, molecular layer of the dentate gyrus; o, stratum oriens of the hippocampus; ot, optic tract; p, pyramidal cell layer of the dentate gyrus; PaS, parasubiculum; PHG, parahippocampal gyrus (areas TF and TH); pl, PL, polymorphic layer of the dentate gyrus; PRC, perirhinal cortex (areas 35 and 36); Prs, presubiculum; r, stratum radiatum of the hippocampus; RSP, retrosplenial cortex; S, subiculum; ssa, sulcus semiannularis; V, temporal horn of the lateral ventricle. A dashed line indicates the oblique border between the entorhinal cortex and the laterally adjacent perirhinal cortex. Here, and in Figures 17 and 19 small arrows mark the dorsomedial and ventrolateral extents of layer II of the entorhinal cortex and an asterisk marks the collateral sulcus (9).

As the remaining fields of the hippocampal formation curve dorsally to meet the retrosplenial region **(Figure 9),** their cytoarchitecture becomes increasingly difficult to interpret. As a rule, the hippocampal fields that make up the rostral extreme of the hippocampus (i.e., the

subiculum and CA1 of the hippocampus) also makes up the caudal extreme. Therefore, the other hippocampal fields are enclosed at the rostral and caudal extremes by CA1 and the subiculum (the dentate gyrus, CA3, and CA2). For this reason, the dentate gyrus and CA2 and CA3 fields of the hippocampus appear to end at a more rostral level than the CA1 field and subiculum **(Figures 9 and 10).** The dentate gyrus ends approximately 7 mm in front of the caudal pole of the hippocampal formation at a level that is just caudal to the emergence of the calcarine sulcus of the occipital lobe **(Figure9)(47).**
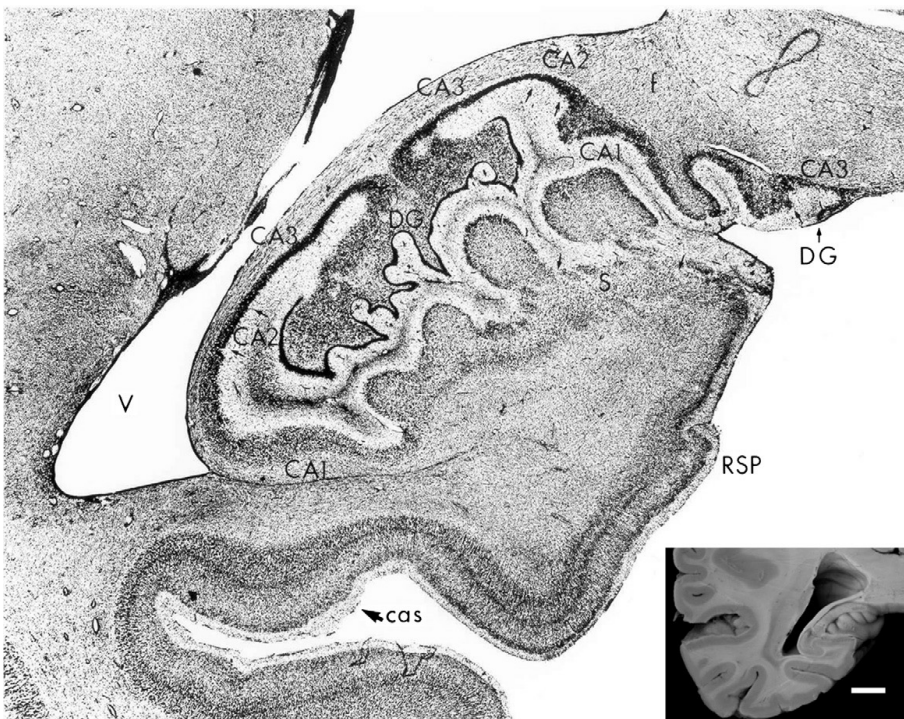
Figure 14- A coronal section near the caudal pole of the hippocampal formation. The hippocampal formation is bending dorsally and medially toward the corpus callosum. It is at about this level that the dentate gyrus and the CA2 and CA3 fields end, though CA1 and the subiculum continue caudally for some distance. The presubiculum and parasubiculum are replaced by the retrosplenial cortex (RSP) and the collateral sulcus is replaced by the calcarine sulcus (cas). Fibers of the hippocampal commissure (hc) are apposed to the ventral surface of the corpus callosum (9).

(2) Ventromedial Surface Anatomy

In the following paragraphs, we will describe the surface appearance of the temporal lobe regions that contain the hippocampal formation and associated structures. We will refer to illustrations showing the ventral and medial surfaces of the human brain **(Figures 9 and 10)** and to illustrations showing dorsolateral views of the hippocampal formation as seen through

dissection of the temporal lobe **(Figure 9)(47)**. We will then relate the gross anatomical features visible in these views to the familiar cytoarchitectonic terms of the hippocampal fields. The ventral and medial surfaces of the temporal lobe are organized into longitudinal strips by two prominent, rostrocaudally-oriented sulci. As illustrated in **Figure 16**, the more lateral of the two is the occipito-temporal sulcus, which is often broken, forming small, transverse gyri. The more medial of the sulci, and the one that is more highly associated with the hippocampal formation, is the collateral sulcus (47) .

The collateral and the occipitotemporal sulcus are often continuous with each other. The collateral sulcus is continuous rostrally with the rhinal sulcus in about 40% of human brains (50), although there is a remarkable amount of individual variability in the configuration of these sulci (51-54). These rhinal and collateral sulci form the lateral border of the parahippocampal gyrus (55). The parahippocampal gyrus has been broken up into an anterior part that is made up mainly of the entorhinal cortex and associated perirhinal cortex and a posterior part that includes the TF and TH fields (56, 57) in non-human primates, the parahippocampal gyrus consists only of the TF and TH fields (48). As we will describe in more detail in the cytoarchitectonic description, the collateral sulcus does not provide a discrete lateral boundary for the entorhinal cortex, which ends somewhere along the medial bank of the sulcus. The two fields of the perirhinal cortex (58) actually form the remainder of the medial bank, fundus, and a portion of the lateral bank of the collateral sulcus **(Figure 9).**

_____
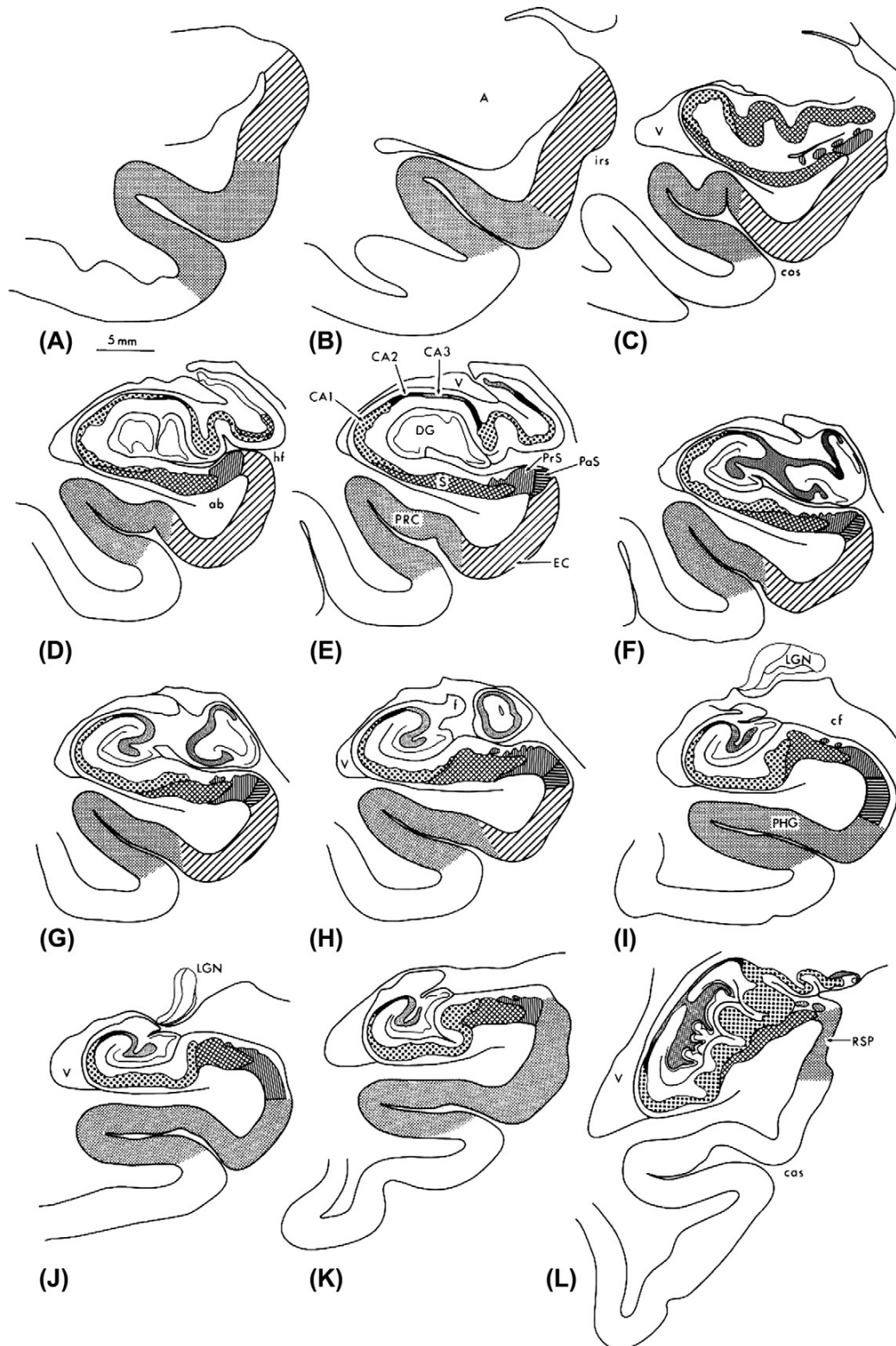
Figure 15- A series of coronal sections of the human temporal lobe arranged from rostral (A) to caudal (I). The various cytoarchitectonic fields of the hippocampal formation have been shaded with different hatching patterns (panel E is marked as a template) to show the varying extents of each of the fields at different rostrocaudal levels (9).

The perirhinal cortex may or may not extend onto the most medial surface of the fusiform gyrus (the cortex located lateral to the collateral and/or occipitotemporal sulci) in different brains (51). This appears to depend on the depth of the collateral sulcus. The perirhinal cortex not only covers all the surface of the lateral bank of the collateral sulcus but also extends a variable distance lateral to the collateral sulcus along the ventral surface of the temporal lobe (53); this is important to remember when segmenting the medial temporal lobe in MRI coronal sections **(Figure 16).**
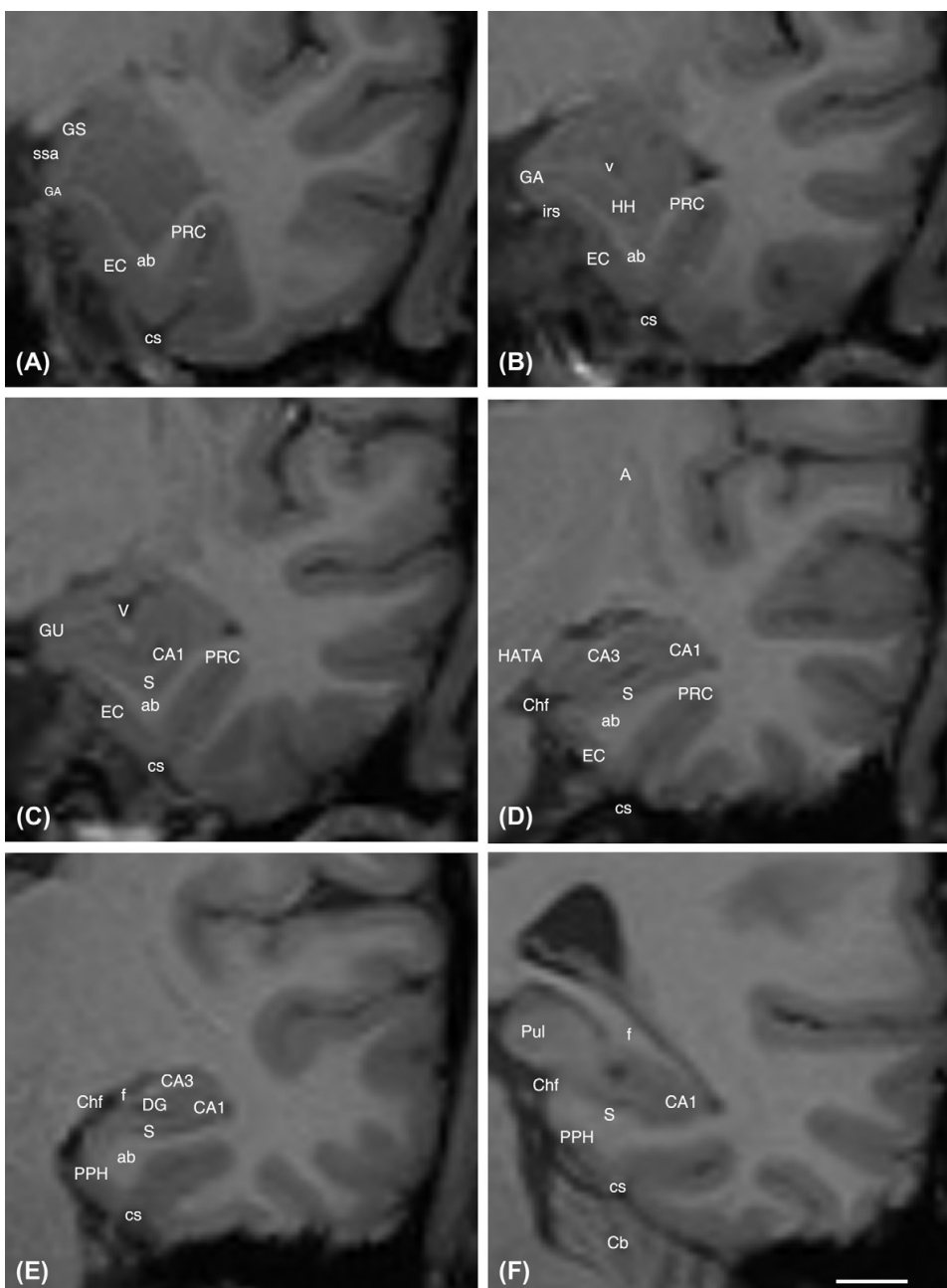
Figure 16- MRI representative levels through the hippocampal formation through a rostral (A) to caudal (F) sequence of levels approximately at comparable levels as shown in Figures 13. Abbreviations are as in Figure 13; Cb, cerebellum; cs, collateral sulcus; Chf, choroidal fissure; GA, gyrus ambiens; GS, gyrus semilunaris; GU, gyrus uncinatus corresponding to HATA, hippocampoamygdaloid transitional area; PPH, posterior parahippocampal cortex (areas TF and TH); PUL, pulvinar complex of the thalamus (9).

The entorhinal cortex **(Figures 10 and 17)** forms much of the anterior portion of the classically defined parahippocampal gyrus. The entorhinal cortex may be localized visually by identifying the conspicuous bumps (verrucae (or warts) (59); that mark its surface, and that are best developed in humans (60), although they can be observed in apes as well (55). These bumps are located above the islands of cells that form layer II of the entorhinal cortex (61). Interestingly, in unfixed specimens of the entorhinal cortex, grayish patches are evident on the surface of the entorhinal cortex that gives it a lattice-like appearance **(Figure 23).** Tangential sections through the superficial layers of the entorhinal cortex yield a similar appearance (50, 62). The dorsomedial aspect of the human entorhinal cortex forms a conspicuous mound or prominence referred to as the gyrus ambiens **(5 in Figure 16).** The ventral limit of the gyrus ambiens is separated from the rest of the entorhinal cortex by a shallow sulcus that Retzius (63) referred to as the inferior rhinal sulcus.

Because of the verticality and shortness in longitudinal extent of this sulcus, its lack of relationship with the more vertically oriented rhinal sulcus and the fact that it is inside the limits of the entorhinal cortex, we have referred to it as the intrarhinal sulcus. This sulcus can be seen in **Figures 9 and 10**. The intrarhinal sulcus is thought to be formed as an indentation of the tentorium cerebelli (50, 64); _in vivo_ MRI images indicate that the inferior rhinal sulcus may not always be coincident with the tentorium cerebelli. The dorsomedial limit of the entorhinal cortex becomes marked by the shallow sulcus semiannularis **(10 in Figure 10).** The gyrus semilunaris that is situated just dorsal to the sulcus semiannularis is made up of the periamygdaloid cortex **(11 in Figure 10).**
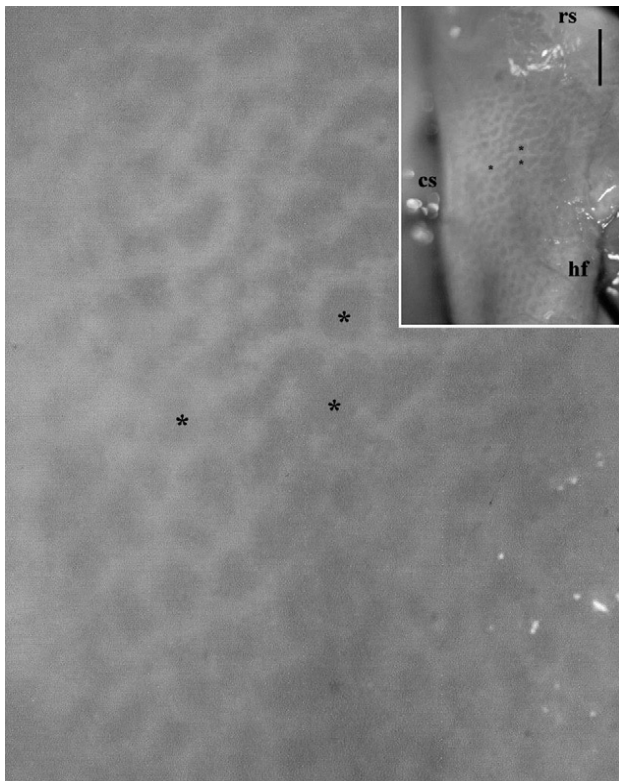
Figure 17- Detail of the unfixed surface of the human entorhinal cortex in a 72-year-old control case. Differences in density allow the clear appreciation of a latticework design that corresponds to cell islands in layer II. Note also the white matter surrounding the darker patches of layer II cell islands, the so-called substantia reticularis alba of Arnold. Scale bar equals 5mm (9).

There is a series of prominent bulges located caudal to the gyrus ambiens that is generally called the uncus **(or hook**, **8 in Figure 16).** The uncus, which comprises portions of several fields of the hippocampal formation, is one of various useful landmarks used in neurosurgical resections of the medial temporal lobe. The gyrus uncinatus forms the most rostral of the uncal bulges. In histological sections, the gyrus uncinatus corresponds to the hippocampo-amygdaloid transitional area. The middle bulge is called the band or limbus of Giacomini and is formed mainly by the most medial bend of the dentate gyrus **(Figure 11).** The most caudal of the uncal bulges is the gyrus intralimbicus and is composed mainly of field CA3 of the hippocampus. As seen in **Figure 16,** and in the coronal sections in **Figures 19 and 24**, the ventral boundary of the uncus is formed by the rostral extension of the hippocampal fissure, also known as the uncal sulcus or uncal notch **(9 in Figure 10).**

Caudal to the level of the uncus, the hippocampal fissure becomes attenuated **(Figure 14),** and the choroidal fissure **(23 in Figure 10)** faces the medial surface of the dentate gyrus and

_____

fimbria **(Figure 10).** A small indentation between the fimbria and the molecular layer of the dentate gyrus has been called the fimbriodentate sulcus by Gastaut (65) in this region **(Figure 12, target sign).** At rostral levels of the hippocampal formation, the hippocampal fissure extends laterally to separate the dentate gyrus or hippocampus from the underlying subiculum. Rostral to the medial closure of the hippocampal fissure, there is a narrow region between the hippocampus and the subiculum that corresponds to a rostral extension of the lateral ventricle cavity **(Figure 19).** Klingler (47) has labelled this ventricular pocket the diverticulum unci.

 As the parahippocampal gyrus meets the retrosplenial region caudally, the medial surface presents a group of small bumps known as the gyri Andreae Retzii **(24 in Figure 10; see also inset in Figure 14).** This irregular region of cortex marks the caudal limit of the hippocampal formation; it is composed mainly of the CA1 field of the hippocampus and the subiculum. Although they are difficult to see in **Figure 16**, two obliquely oriented small gyri are located deep to the gyri Andreae Retzii. The medial one is called the fasciola cinerea and corresponds to the caudalmost part of the dentate gyrus. The lateral gyrus is the gyrus fasciolaris, and corresponds to the caudal end of the CA3 field. There is still some dispute about which of the fields of the hippocampal formation surround the splenium to form the induseum griseum, or supracommissural hippocampus (66). Our analysis indicates that the subiculum and field CA1 mainly form this small band of supracallosal tissue.

Figure 18- Numbers at the top right of this illustration indicate the layers of the entorhinal cortex. Note the shallow intrarhinal sulcus (irs) that is located in the entorhinal cortex (9).

(3) Dorsomedial Surface Anatomy

The classical gross anatomical image of the human hippocampal formation is of a prominent, bulging eminence in the floor of the temporal horn of the lateral ventricle **(Figure 9).** As seen in the coronal histological sections **(Figures 11–13),** a number of distinct cytoarchitectonic fields, including the dentate gyrus, hippocampus, and subicular cortices, are included in this region. The anatomist Arantius (67) first used the term "hippocampus" (or sea horse); he considered the three-dimensional form of the grossly dissected human hippocampus to be reminiscent of this sea creature. It is actually unclear from the account of Arantius (67) which particular aspect or surface of the hippocampal formation reminded him of the sea horse since he also likened the hippocampus to a silkworm. An historical and amusing account of the etymology of the term "hippocampus" is provided by Lewis (68). As he noted, others such as Winslow (69) likened the hippocampus to a ram's horn and de Garengeot (70) named the hippocampus Ammon's horn after the mythological Egyptian god. The term Cornu Ammonis was appropriated by Lorente de No' (71) for his terminology of the hippocampus proper (CA1–CA4), and Ammon's horn has been used synonymously with the hippocampus. Recent use favors the term "hippocampus", however.

The ventricular portion of the hippocampus is presented in two slightly different views in **Figure 9**. This portion of the hippocampal formation is widest at its anterior extent where the structure bends toward the medial surface of the brain. The subtle gyri (or digitations hippocampi) formed in this region (which can range from two to five in number), (72) give it a foot like appearance and the name pes (foot) hippocampus (1) has classically been applied to this area **(Figure 9).** The pes hippocampus contains several hippocampal fields, and the constituents change at different rostrocaudal levels. Its convoluted appearance adds complexity in coronal sections in the identification of individual hippocampal fields. Continuing caudally from the pes hippocampus, the unreflected "body" of the hippocampus **(Figure 9,** (2)**)** becomes progressively thinner as it bends upward toward the splenium of the corpus callosum.
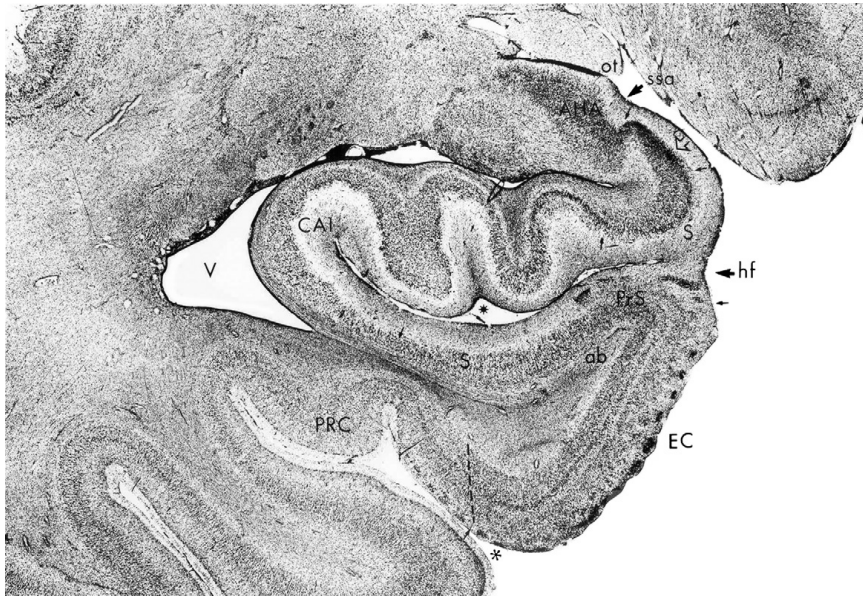
Figure 19- In Figures 11–13, small arrows marks the borders of each of the cytoarchitectonic fields of the hippocampal formation. A dashed line indicates the oblique border between the entorhinal cortex and the adjacent perirhinal cortex. The open arrow at top right indicates a transition region between the amygdala and hippocampal formation, which appears to be cytoarchitectonically distinct from other hippocampal fields. The asterisk in the center of the field marks the enclosed region of ventricular cavity called the diverticulum unci (9).

The medial surface of the hippocampus presents a fringe of fibers named the **fimbria**. Fibers originating from the pyramidal cells of the hippocampus and subiculum travel in the white matter which sheaths the hippocampus (the alveus) and coalesce in the medially situated fimbria **(Figure 9** (3)**)**. At rostral levels, the fimbria is thin and flat, but it becomes progressively thicker caudally as more fibers are continually added to it. As the **fimbria** leaves the caudal extent of the hippocampus, it fuses with the ventral surface of the corpus callosum and travels rostrally in the lateral ventricle forming the fornix, which has different portions. The region between the caudal limit or the hippocampal formation and the fusion with the corpus callosum forms the crus of the fornix, whereas the major portion of the rostrally directed fiber bundle is called the body of the fornix. At the end of its rostral trajectory, the body of the fornix takes a ventral course and descends, forming the columns of the fornix. The fornix then divides around the anterior commissure to form the anterior column of the fornix or precommissural fornix, which innervates the septal region, and the posterior column of the fornix or post commissural fornix, which terminates in the diencephalon (**Figure 9A).**

About at the point where the **fimbria** fuses with the posterior portion of the corpus callosum, fibers extend across the midline to form the hippocampal commissure. A variety of gross anatomical terms have been applied to this commissural projection but the term "psalterium" or David's lyre (alluding to an ancient instrument "psaltery" made of strings stretched over a board and cited in the Bible) is most common. The psalterium makes up the dorsal hippocampal commissure. As we will discuss below, the primate hippocampal commissural connections are much more limited than in the rodent, (73, 74). Stereotaxic depth encephalography indicates that, as in the monkey, there is little commissural interaction of the human hippocampal formation (75). Gloor *et al.* (76)4) have confirmed that the ventral hippocampal commissure is virtually absent in the human brain whereas the dorsal hippocampal commissure is similar to that observed in the non-human primate brain.

ii) Cytoarchitectonic Organization of the Hippocampal Formation

(1) Topographycal considerations

We presented a description of the topographical organization of the human hippocampal formation in the preceding section that should facilitate the interpretation of the cross-sectional photomicrographs shown in **Figures 8 to 13**. Much of the hippocampal formation lies in the floor of the temporal horn of the lateral ventricle **(Figure 9, A and B).** The individual fields of the hippocampal formation can be envisioned as adjacent bands of brain tissue, running rostrocaudally in the temporal lobe, mostly made up of a dominant single cell layer. The distinctive C-shape of the hippocampal formation is obtained when the fields fold over each other in the mediolateral direction. This highly recognizable interlocking fashion is best shown in its midportion or "body" **(Figures 12 and 20)** where every field sequentially follows one another, beginning with the dentate gyrus and finishing at the border with the cortex at the parahippocampal region, in an orderly fashion that can be appreciated in coronal sections through his region. Perhaps the most distinctive feature of the hippocampal formation in humans as well as in experimental animals is the rigid step-by-step progress of the information flow, starting and finishing at the entorhinal cortex, always unidirectional, albeit not excluding other inputs and outputs from other sources.

As the hippocampal formation approaches the rostral limit of the ventricle, it bends sharply in a medial direction and then in a caudal direction and loses the simple display of the

hippocampal formation fields. The photo-micrographs **(Figures 11 and 18)** of coronal sections through "uncal" levels show complex arrangements of the hippocampal formation fields. It is difficult to determine solely with Nissl-stained coronal sections which fields of the hippocampal formation are seen at these levels. Only with the aid of other histochemical and inmunohistochemical series is one able to differentiate the fields that are designated in **Figures 13 and 14 and schematically shown in Figure 9.**

At caudal levels, the human hippocampal formation again loses its simple C-shaped organization. It bends dorsally as it ascends toward, and ultimately bends around, the splenium of the corpus callosum. Coronal sections through these caudal levels **(Figure 14)** again provide complex images with discontinuous representations of several of its fields.

(2) Dentate Gyrus, Hippocampus, Subiculum

As in other species, the human dentate gyrus is a trilaminate cortical region. Its organization is most easily appreciated at mid rostrocaudal levels of the hippocampal formation (**Figures 12 and 20).** Here it forms a C-shaped structure separated ventrally from the CA1 field of the hippocampus and the subiculum by the fused hippocampal fissure **(Figures 13 and 19).** The principal cell layer of the dentate gyrus is the granule cell layer. Primarily one class of neuron, the granule cell, which sends a unipolar dendritic tree into the overlying molecular layer, populates it.

Dendritic staining of human granule cells show that they are invested with spines except for the most proximal 20–30 mm (77). Earlier estimates of granule cell number (78) concluded that there are about 9x 10^6 granule cells in the human dentate gyrus. However, more recent estimates using unbiased stereological techniques have come up with figures that are substantially higher (i.e., 15 x10^6) (79). Interestingly, Sa´ *et al.*(80) report a right–left asymmetry in the number of dentate granule cells, which are 20% more numerous on the right side. Human dentate granule cells often give rise to basal dendritic trees that extend into the subjacent polymorphic layer. Lim *et al*. (77) noted the presence of basal dendrites in 30% of the neurons they investigated. Such basal dendrites are seldom observed in non-primates.

The third layer of the dentate gyrus is generally called either the polymorphic layer or the hilus of the dentate gyrus. This is a complex region (81), and there has been substantial

confusion as to whether it should be included as a part of the dentate gyrus or is another, independent field of the hippocampus proper (the so-called field CA4). The situation is further complicated by the fact that the appearance of the region enclosed by the granule cell layer varies from species to species. With the use of powerful anatomical techniques in this region, there is increasingly convincing evidence in the rat and non-human primate that the polymorphic layer is a part of the dentate gyrus. Perhaps the most salient data come from connectional studies of the hilus, which indicate that its cells give rise to projections only to the dentate gyrus and not to any other field of the hippocampal formation (82). Connectional studies in the in vitro human hippocampal slice preparation also support the distinction of the polymorphic layer from the hippocampus. Lim *et al.* (77) demonstrated a dense plexus of fibers arising from the polymorphic layer that separates it from the remainder of CAE3.

_____
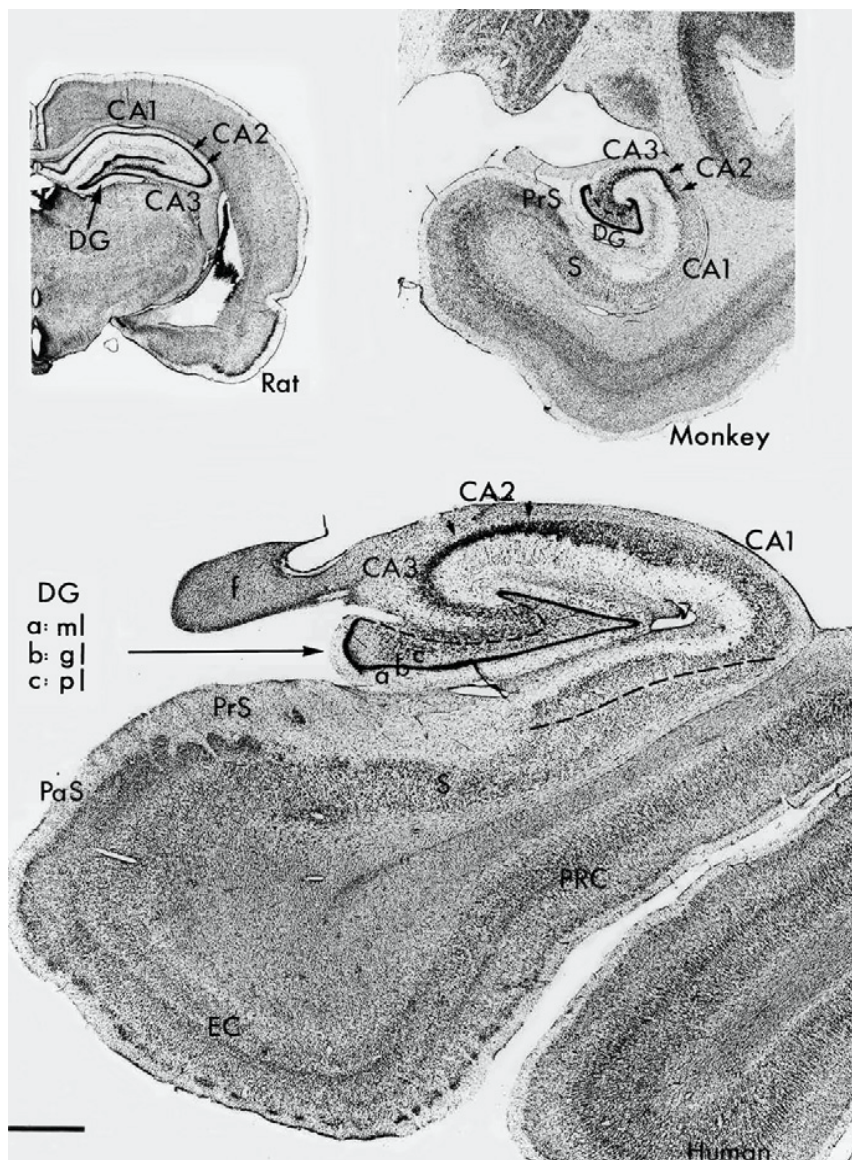
Figure 20- Coronal sections through the hippocampal formation of the rat, monkey, and human brains presented at the same magnification. Preparations are stained with thionin for the demonstration of neuronal cell bodies. The dashed line in the monkey and human dentate gyri separates the polymorphic layer of the dentate gyrus from the CA3 field of the hippocampus. In the human section, a dashed line also indicates the oblique border between field CA1 and the subiculum (9).

In the human dentate gyrus, it is not easy to differentiate the cells of the polymorphic layer from those of the hippocampus in standard Nissl preparations. Yet both Timm's stained preparations **(Figure 21A),** which yield a patchy distribution of dark precipitate in the polymorphic layer, and acetylcholinesterase preparations **(Figure 21 B)**, which demonstrate numerous precipitate-laden cells in the polymorphic layer, make the establishment of the border much easier. In **Figures 11, 20, 21 A and B, and 22A,** a dashed line indicates the border of the polymorphic layer with the hippocampus.

_____
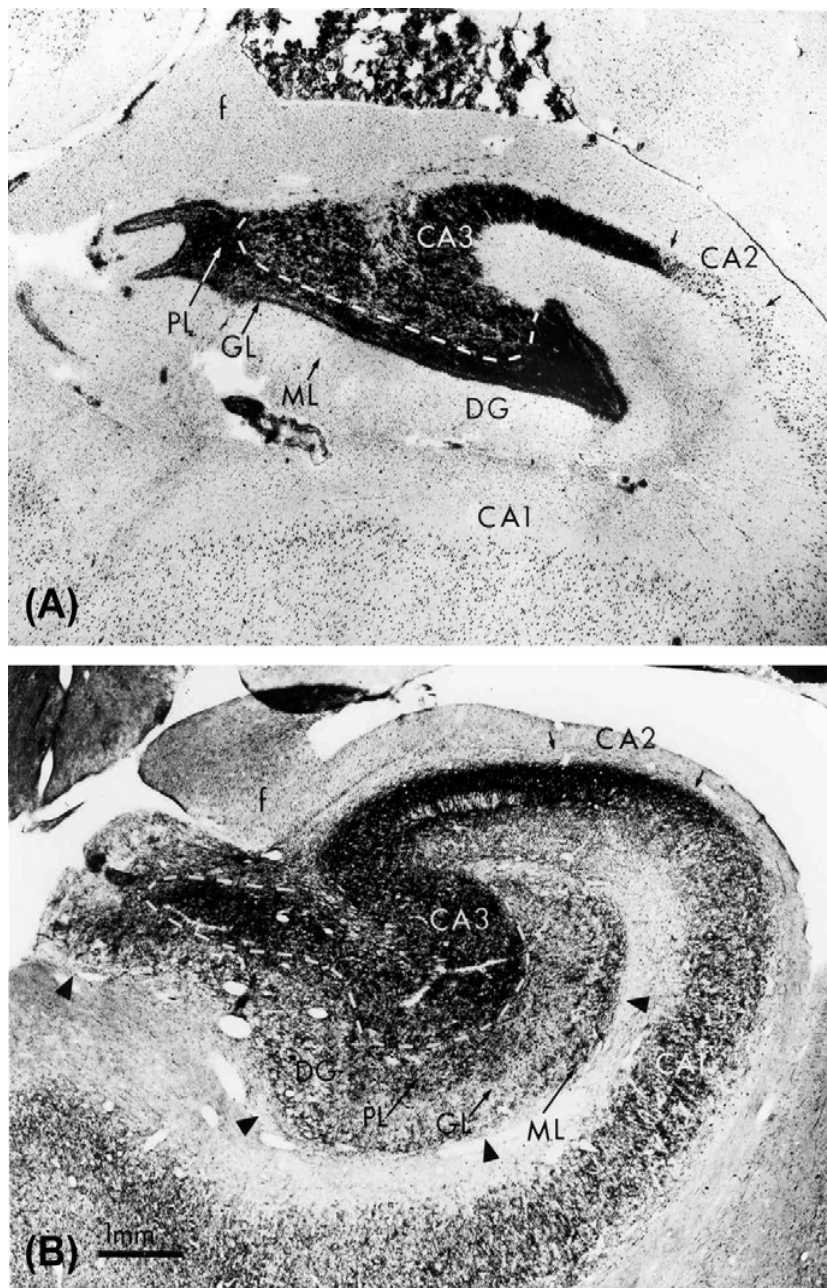
Figure 21- (**A) A coronal section through the human hippocampal formation stained by the Timm's sulfide silver method for the demonstration of heavy metals**. The section has also been counterstained with cresyl violet for the demonstration of neuronal cell bodies. Dark precipitate is confined to the polymorphic layer of the dentate gyrus and to the region within and immediately surrounding the CA3 pyramidal cell layer. The region of dark precipitate corresponds to the distribution of the mossy fiber axons arising from the granule cells of the dentate gyrus. Staining is attributable to the high level of zinc contained in the en passant presynaptic mossy fiber boutons. The termination of staining in the hippocampus marks the border between the CA3 and CA2 fields. This section was prepared and kindly made available to us by Carolyn Houser, University of California, Los Angeles. (**B) A coronal hipppocampal section stained for the demonstration of AchE. In** the dentate gyrus, staining is dense in the outer portion of the

molecular layer (the superficial limit of which is marked with arrowheads) and in the polymorphic layer. There are numerous AchE-positive neurons in the polymorphic layer that distinguish it from the adjacent CA3 field. AchE staining is heavy in the CA3 field, especially in stratum oriens, and it gets somewhat darker in area CA2. There is a marked decrease in staining in CA1 and a further decrease in the subiculum (9).

The other question that commonly arises concerning this region is what to label the portion of the hippocampal pyramidal cell layer that is enclosed by the granule cell layer. As illustrated in **Figures 11 and 12**, these cells are rather numerous in the human hippocampal formation and are organized in a complex pattern. In fact, the pyramidal cell layer typically makes a sharp bend as it extends towards the hilus and folds back on itself (the so-called end blade). Lorente de No' (71) included some portion of the enclosed pyramidal cell as his field CA4. However, in some illustrations, he also appears to have applied the term "CA4" to the cells of the polymorphic layer of the dentate gyrus. Because there is no cytoarchitectonic or connectional reason to distinguish the CA3 pyramidal cells enclosed within the granule cell layer from those that are outside it, we have dropped the use of the confusing term "CA4" and simply referred to the entire hippocampal pyramidal layer in this region as CA3.

(a) Hippocampus

The human hippocampus can be divided into three distinct fields, CA3, CA2, and CA1 according to the nomenclature of Lorente de No' (71). In most respects, the overall organization of these fields is similar to that observed in the macaque monkey (83).

Field CA3 borders the hilus of the dentate gyrus, where it terminates in a complex fashion (as described earlier). At its other end, it borders field CA2. Cassell (84) and Seress (78) have estimated that there are about 2.1×10^6 neurons in the CA3 region and Cassell (84) has estimated that there are about 0.22×10^6 pyramidal cells in CA2. More recent accounts of the number of neurons for CA3–CA2 combined using stereological techniques offer a figure of approximately 2.8×10^6 neurons (79). Sa´ *et al* (80) reported hemispheric asymmetry so that CA3–CA2 contains 14% more neurons on the right side compared to on the left hippocampus. The CA3 pyramidal cells are the largest of the hippocampus and stain darkly in Nissl stains. While the layer is approximately ten cells of thickness, it nonetheless has a relatively homogeneous appearance. There is no indication of sub lamination or marked variation of neuronal size or shape in different mediolateral sectors of CA3. The hallmark of CA3 is that its neurons receive input on their proximal dendrites from the axons of the dentate

granule cells (the mossy fibers). The mossy fiber projection is located either within or immediately above the pyramidal cell layer in what is generally called stratum lucidum. The pattern of mossy fiber termination is best illustrated in Timm's silver sulfide preparations **(Figure 21A)**, in which the terminal varicosities of the mossy fibers are densely labeled with precipitate, presumably owing to their high content of zinc (85). Lim *et al* (77) analysed the mossy fiber projection in slices of hippocampal tissue from human temporal lobe. Immunohistochemical stains have also been used to map the projections of the mossy fibers (86). Most of the dentate gyrus granule cells are immunoreactive for calbindin, as are interneurons in the external part of the molecular layer of the dentate gyrus (87). The mossy fibers occupy the pyramidal cell layer. Fascicles of mossy fibers cross the pyramidal cell layer of CA3 to accumulate in the stratum lucidum, where they form the so-called end-bulb, and form presynaptic terminals on dendrites (mossy fiber giant boutons). Also, at this point intrahippocampal mossy fibers travel for some distance along the longitudinal axis of the hippocampus.

_____
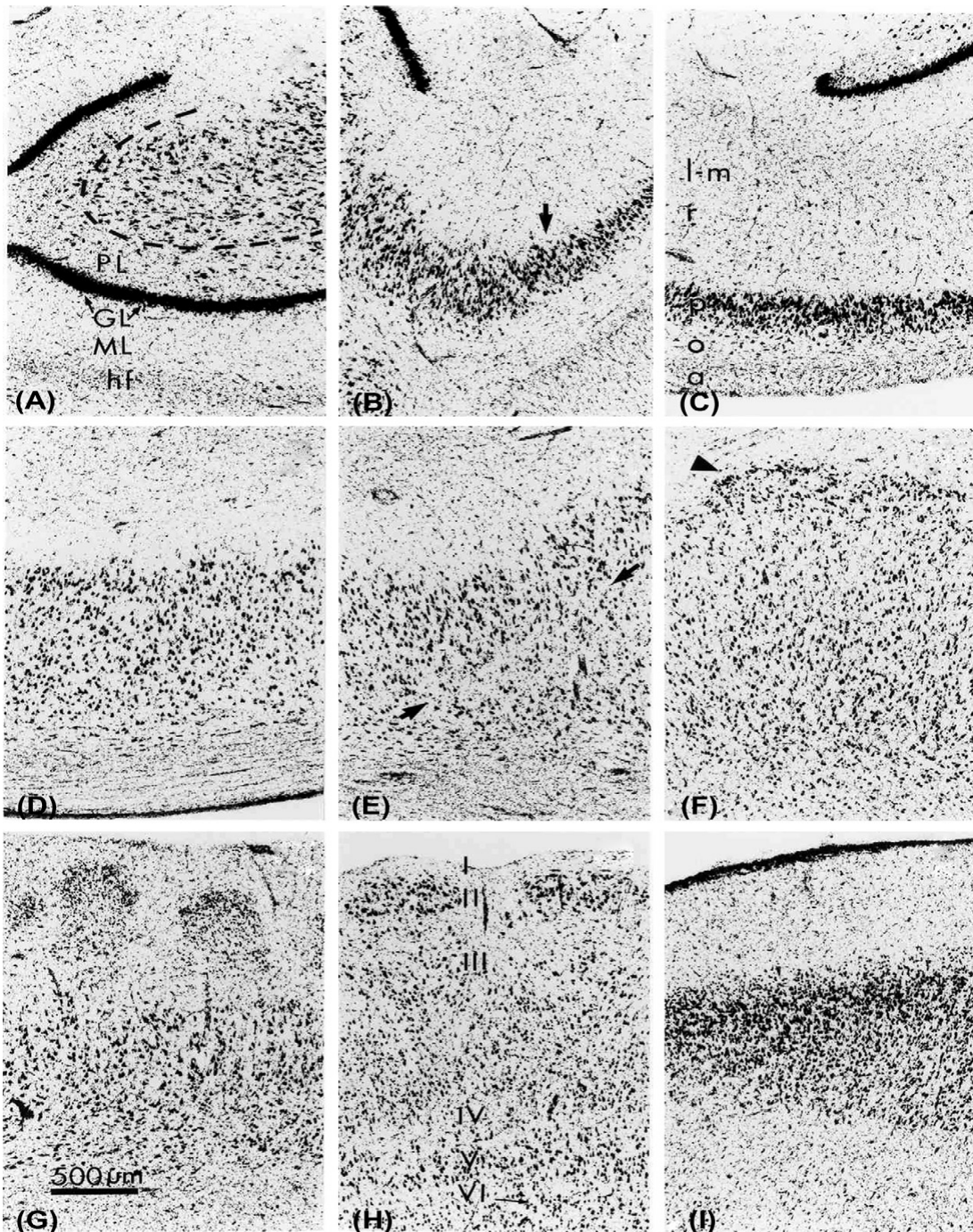
Figure 22- Higher-magnification photomicrographs to demonstrate the major cytoarchitectonic features of each of the fields of the human hippocampal formation. (A) The molecular (ML), granular (GL), and polymorphic (PL) layers of the dentate gyrus are indicated. The dashed line marks the border between CA3 of the hippocampus and the polymorphic layer (hf, hippocampal fissure). (B) Region of transition between the CA3 (on the left of the arrow) and CA2 (on the right) fields of the hippocampus. Note that the pyramidal cell layer in CA3 is both wider and more diffusely organized than in CA2. (C) Field CA2 of the hippocampus has the narrowest and most densely packed pyramidal cell layer of the hippocampal fields. The principal laminae of the hippocampus are also indicated: a, alveus; o, stratum oriens; p, pyramidal cell layer; r, stratum radiatum; l-m, stratum lacunosum-moleculare. (D) Field CA1 of the hippocampus has a wider pyramidal

cell layer than fields CA3 or CA2 and the cells tend to be smaller and more widely separated. The most superficial pyramidal cells are more tightly packed, are somewhat larger, and stain somewhat darker than the deeper cells. (E) Transition region between CA1 (on the left side) and the subiculum (on the right). A narrow cell free zone (marked by arrows) often corresponds to the oblique border between the two fields. The region of overlap of the two pyramidal cell layers varies from brain to brain but in some cases can extend for several millimeters. (F) The pyramidal cell layer of the subiculum is often wider than of CA1. There are roughly two major layers of pyramidal cells, with the superficial ones being somewhat smaller than the deeper ones. Islands of small also characterize the subicular pyramidal cell layer darkly stained cells (arrowhead) that lie at its superficial edge. (G) The presubiculum is characterized by a densely packed layer II that, at rostral levels (as illustrated in this photomicrograph), breaks up into spherical islands. The outer cap of layer II cells is more densely packed and somewhat darker staining than the cells in the remainder of the layer. (H) The entorhinal cortex is a multilaminate region that is generally considered to make up at least six distinct layers. The most distinctive feature of the entorhinal cortex is the islands of darkly stained modified pyramidal and stellate cells that make up layer II. In some regions, the surface of the entorhinal cortex forms bumps (verrucae or warts in the gross anatomical terminology) above the islands of layer II cells; these bumps are present in this section (compare with Figure 24.3 for a surface view). Another distinguishing characteristic of the entorhinal cortex is the lack of an internal granular layer (layer IV). In its place through much of the entorhinal cortex is a cell-free space, the socalled lamina dissecans. (I) Transition region between the amygdala and hippocampus. This field is located in the rostral aspect of the uncal hippocampal formation (open arrow in Figure 24.5). Its small, darkly stained, and tightly packed neurons do not resemble those in any other hippocampal field (9).

Before proceeding, it might be appropriate to review the laminar nomenclature of the hippocampus. While the hippocampus has essentially one cellular layer, the pyramidal cell layer, the plexiform layers above and below all have been given distinctive names. Axons of the pyramidal cells form the limiting surface with the ventricular cavity, and this fiber band is called the alveus. Between it and the pyramidal cell layer is the stratum oriens, which is occupied mainly by the basal dendrites of the pyramidal cells, though it also harbors a variety of neurons, many of which are interneurons. The region opposite to the pyramidal cell axons (and closer to the hippocampal fissure) contains the apical dendrites of the pyramidal cells as well as a number of interneurons. This plexiform region has historically been divided into a number of laminae. These include:

1. Stratum lucidum (meaning clear for its transparent aspect in the unfixed hippocampus), in which the mossy fibers travel and form *en passant* synapses on the proximal dendrites of the pyramidal cells, is located immediately above the pyramidal cell layer in CA3.

As noticeable decrease in glial staining, it is not as prominent in Nissl-stained sections of the human hippocampus because many of the mossy fibers also travel within the pyramidal cell layer and the difference in background glial staining is ɴᴏᴛ as distinctive. Stratum lucidum is missing in fields CA2 and CA1 because pyramidal cells in these fields do not receive mossy fiber input.

2. Stratum radiatum is distal to stratum lucidum and contains the axons of the associational connections (in CA3) or the Schaffer collaterals (in CA1) – see below.

3. Stratum lacunosum-moleculare is located closest to the hippocampal fissure.

In stratum radiatum (as well as in stratum oriens), the CA3 and CA2 cells receive associational projections from other rostrocaudal levels. Kondo *et al*. (82) have recently reported in the non-human primate an associational fiber system that extends for as much as three-fourths of the longitudinal extent of the hippocampus, and is considerably less defined relative to the rodent hippocampus. Other subcortical inputs arise from regions such as the septal nuclei and the supramammillary region. In CA1, the projections from CA3 and CA2 (the so-called Schaffer collaterals) terminate in stratum radiatum and stratum oriens. The perforant pathway projection from the entorhinal cortex to the dentate gyrus and CA3 travels, in part, in stratum lacunosum-moleculare of the hippocampus and makes en passant synapses on the distal apical dendrites of the hippocampal pyramidal cells (88).

The border between CA3 and CA2 is not readily apparent in Nissl-stained sections. This is because CA3 cells appear to extend under the border of CA2 for a short distance. The CA2 region has the most compact and narrow pyramidal cell layer of the hippocampus **(Figure 28C)**. Its cells are about as large and darkly stained as those in CA3, but there is far less space between the cell bodies. These characteristics, coupled with the lack of mossy fiber input, are the distinguishing features of the CA2 field. Even though the borders of CA2 are among the most difficult to establish with confidence, it clearly deserves to be thought of as a distinct cytoarchitectonic field, since CA2 has distinct connectional characteristics. In the macaque monkey, for example, it receives a particularly heavy input from the supramammillary region of the hypothalamus (89), as well as a distinctive substance P projection from the hypothalamus (90). It appears to be particularly insensitive to pathology (it is the so-called resistant sector of classical neuropathology (81, 82).

Field CA1 is unquestionably the most complex subdivision of the human hippocampus. According to Stephan (91) and Stephan and Manolescu (92), it is also one of the most phylogenetically progressive of the hippocampal fields. Not only does it appear to be populated by a far more heterogeneous group of neurons than the other hippocampal fields, but its appearance also varies substantially along both its mediolateral and its rostrocaudal axes. The border of CA1 with CA2 is not sharp because some CA2 pyramidal cells extend over the emerging CA1 pyramidal cell layer. The boundary between CA1 and CA2 can be placed, however, shortly after the pyramidal cell layer starts to broaden. The border with the subiculum is equally difficult to place because it forms a rather oblique border zone. As shown most clearly in **Figures 11, 20 and 22E**, the pyramidal cell layer of CA1 overlaps that of the subiculum for a considerable distance. There is often a cell-free zone between the two layers that helps to define the border **(Figure 22E)**. Once the overlapping nature of this border is recognized, using cytoarchitectonic criteria in Nissl-stained material can then readily place the boundary.

Before describing the features of field CA1, we should discuss the origin and usefulness of the term "prosubiculum". Lorente de No' (71) used it to describe a field situated between CA1 and the subiculum. Analysis of his **Figures 22 and 33** indicates that the area he illustrated as the prosubiculum is actually much of what contemporary authors consider subiculum proper. Some authors continue to use the term "prosubiculum" to label the region of overlap of CA1 and the subiculum (93). However, we would agree with Braak (94) **(see Figure 23)**, Braak (95) **(see Figure 17)** and Cassell (84) that overlap of elements from two adjacent fields does not constitute sufficient grounds for defining the existence of a new field. If the cells in this region are ultimately shown to have input and output characteristics distinctly different from other parts of CA1 or the subiculum, then use of the term "prosubiculum" might be warranted. Until then, we have separated this border region into CA1 and subicular components.

Earlier studies (84), indicated that the CA1 field of the human hippocampus contains approximately 4.6×10^6 neurons. Of these, Olbrich and Braak (96) have estimated that 9.4%, or approximately 430000, are interneurons while the remainder are pyramidal cells. More recent studies using unbiased counting methods, yield counts that are three to four times higher, as reported by Sa' et al. ((80); 11×10^6), West and Gundersen (79), West *et al* (14.4×10^6 (97)7)), and Simic *et al.* (20×10^6(98)) without detectable differences between left and

right sides of the hippocampus. As Braak (95) pointed out, the human CA1 pyramidal cell layer generally can be subdivided into two main laminae that are each many cells thick. At many levels of the hippocampus, however, each of the sublayers also appears multilaminate. The pyramidal cell layer varies in thickness from about ten cells to more than 30 cells. In general, the outer layer of pyramidal cells is more compact, and the cells tend to stain somewhat more darkly than the more deeply placed cells **(Figure 23).**

The CA1 pyramidal cell layer has a variable appearance at different rostrocaudal levels of the hippocampus. At any particular level, there is a gradient of changing organizational features along the mediolateral axis. Close to the CA2 border, the CA1 pyramidal cell layer is at its thinnest, and the cells of both sublayers appear most tightly packed **(Figures 17 and 18).** Toward the subicular border, the pyramidal cell layer gets appreciably thicker and more loosely organized. It is often difficult to identify two discrete sublayers of CA1 in this region because the cells are patchier. Stratum radiatum is much broader in the region of CA1 closest to CA2 and becomes much thinner toward the subiculum **(Figures 11, 12 and 20).**

(b) Subiculum

An early estimate of the number of pyramidal cells in the subiculum was approximately 2.55 x 10^6 (84). However, more recent studies yield counts that are nearly twice as high (98), that is, around 5 x 10^6 neurons. The subiculum (among others) is the origin of major subcortical projections to the septal complex, nucleus accumbens, anterior thalamus, and mammillary nuclei, as well as projections to the entorhinal cortex, and to some cortical regions in the non-human primate (93). However, these projections are poorly understood, even in experimental animals. Moreover, the cellular and laminar organization of this region has not yet been clearly delineated.

As noted earlier, the subiculum and field CA1 of the hippocampus overlap at their border **(Figures 11, 20 and 22E)**. The laminar organization of both regions is complex in this zone. Medially (closer to the presubiculum), the subiculum can easily be divided into three layers. Superficially, there is a wide molecular layer into which the apical dendrites of the subicular pyramidal cells extend. The molecular layer of the human subiculum tends to be relatively wider than in the monkey and rat and, as in those species; it is distinct from the stratum radiatum of CA1. At some levels, islands of what appear to be layer II presubicular cells invade

the distal portions of the subicular molecular layer (99). The pyramidal cell layer of the subiculum is 30 or more cells thick, and can be divided into at least two sublaminae. Relative to CA1, the subicular pyramidal cells tend to be somewhat larger and more widely spaced. Braak (99) has labeled the two sublaminae of the pyramidal cell layer the external (nearest the molecular layer) and internal layers. The cells of the external pyramidal cell layer are larger than those in the internal pyramidal layer, and many contain a dense accumulation of lipofuscin in the proximal portion of their apical dendrites. Neither of the subicular pyramidal cell layers is homogeneous. In particular, the superficial limit of the external pyramidal cell layer contains islands of small, darkly stained cells **(Figures 27 and 28F)**. This characteristic also distinguishes the subiculum from CA1, which contains large, darkly stained cells at its superficial limit **(compare Figure 28 F)**. The deepest portion of the subicular pyramidal cell layer contains a variety of smaller neurons, which appear to be analogous to the polymorphic layer identified in the monkey (83). As indicated in **Figure 21**, the subiculum makes up much of the rostral uncal flexure of the hippocampus. We should note also that cells **(Figure 29 I)** that a unique field lays between the rostromedial subiculum and the amygdalohippocampal area of the amygdaloid complex **(Figure 25, open arrow)**. This transition region contains a high density of small, darkly stained cells that are unlike neurons in any of the other hippocampal fields. This region has been termed hippocampoamygdaloid transitional area (HATA) by Rosene (93).

(3) Presubiculum and Parasubiculum

The laminar organization of the presubiculum and parasubiculum is complex and only poorly understood. It is perhaps most useful to consider that the presubiculum consists of a single, superficially located cellular layer made up of an external principal (layer II) and an internal principal cellular layer (62), which is formed by densely packed, small, modified pyramidal cells **(Figure 23 G).** Layer II of the presubiculum tends to be narrow and continuous at posterior levels of the hippocampal formation but breaks up into larger-diameter islands at more rostral levels. As in the monkey (83), layer II in the human can be further divided into a narrow, superficial rim that contains more densely packed and darkly stained neurons and a broader band of more widely separated cells.

The parasubiculum also contains a single cellular layer that is difficult to clearly differentiate from the presubiculum. The layer II cells of the parasubiculum tend to be somewhat larger than those in the presubiculum and more widely spaced.
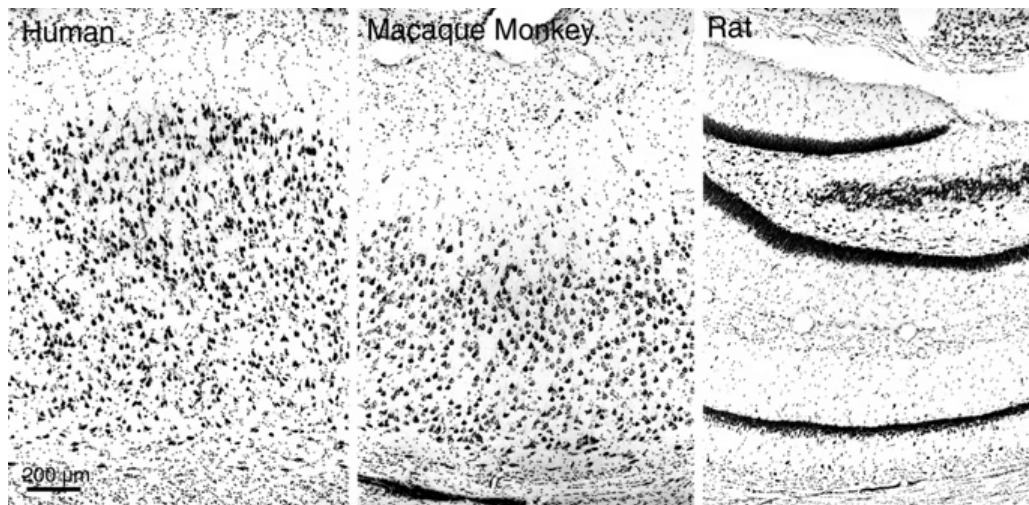
Figure 23- Higher-magnification photomicrographs of approximately the same region of the CA1 field of the hippocampus in the rat, monkey, and human. This is a standard Nissl-stained preparation, and all of the images are at the same magnification. The calibration bar at the lower left applies to all three panels. Note that CA1 in the rat, which is the dark line at the bottom of the image, consists of three to five layers of tightly packed pyramidal cells (individual cells are difficult to resolve at this magnification). The monkey pyramidal cell layer, in contrast, is approximately 30 cell layers thick and there is a hint of sub lamination within the top half of the layer having a slightly higher density of neurons. The pyramidal cell layer in the human CA1 field is even thicker and has a much more heterogeneous or laminated appearance (9).

(4) Entorhinal Cortex

The term "entorhinal cortex" was coined by Brodmann (58) as a synonym for his area 28. More than any other hippocampal field, the entorhinal cortex has undergone substantial regional and laminar differentiation in the primate brain relative to the rodent (91). In the rat, the entorhinal cortex comprises two regions (medial and lateral) that were originally proposed by Brodman, his areas 28a and 28b. In the macaque monkey, the entorhinal cortex demonstrates a marked gradient of cytoarchitectonic changes from rostral to caudal extents, and can be partitioned into at least seven different cytoarchitectonic fields ((100); **Figure 24 upper part)**. Classically, the human entorhinal cortex has been studied by several authors (101), who have partitioned it into as many as 23 fields (101). Our own studies suggest that the laminar organization of the human entorhinal cortex is not nearly as distinct as in the macaque monkey. Nonetheless, we have observed the same rostrocaudal gradient of cytoarchitectonic differentiation in the human entorhinal cortex. Using similar criteria, up to

eight fields, largely comparable with those defined for the monkey, can be distinguished in the human entorhinal cortex ((53); **Figure 24 lower part**). Other cytoarchitectonic parcellations for the human entorhinal cortex have also been proposed, based either on the peculiarities of the pigment staining of layer II neurons ((50); 12 subfields) or more classical cyto- and myeloarchitectonic approaches ((102); 9 subfields). In the monkey, the entorhinal cortex is spatially associated with the amygdaloid complex rostrally and the other fields of the hippocampal formation caudally. It extends rostrally to about the mid rostrocaudal level of the amygdala and caudally to the level of the anterior limit of the lateral geniculate nucleus or about midway back through the hippocampus **(Figure 8)**. In the human, the entorhinal cortex appears to extend relatively more rostrally than in the monkey.

Structures that form the medial and lateral borders of the entorhinal cortex are different at various rostrocaudal levels. At rostral levels, the entorhinal cortex borders the periamygdaloid cortex medially, and the boundary is marked approximately by the sulcus semiannularis **(Figure 13).** As the other fields of the hippocampal formation emerge at more caudal levels of the entorhinal cortex, the medial boundary is formed either by the pre-subiculum or the parasubiculum. Unlike in the rat and monkey, where the lateral border of most of the entorhinal cortex is coincident with the rhinal sulcus, there is no easily identifiable lateral limit of the human entorhinal cortex. In fact, the rhinal sulcus in the human is, for the most part, situated rostral to the entorhinal cortex (38, 42). Although the collateral sulcus lies laterally to the entorhinal cortex for its full rostrocaudal extent, at no level does it form its lateral border. As in the monkey, the human entorhinal cortex is laterally adjacent to the perirhinal cortex (areas 35 and 36 of Brodmann) for much of its rostrocaudal extent. In the monkey, we have found that area 35 forms the lateral border of rostral levels of the entorhinal cortex, whereas area 36 (which is differentiated from area 35 principally by the presence of a distinct layer IV) borders caudal levels (100). In the human brain, the lateral border of the entorhinal cortex is formed throughout its rostrocaudal extent by a cortical field that lacks a distinct layer IV and has many of the other cytoarchitectonic characteristics of area 35, although with some peculiarities (54). However, the border between area 35 and the entorhinal cortex is not easily placed. As indicated in **Figures 19 and 25**, these two fields appear to have an obliquely oriented boundary. The deep layers of the entorhinal cortex appear to extend somewhat more laterally than the superficial layers. This distinctly oblique border between area 35 and the entorhinal cortex has been emphasized by Braak (62), who

has labelled the region of overlap the "transentorhinal zone", and by Ding *et al*. (54) as area 35 u (for "unique"). The caudal limit of the human entorhinal cortex also presents a complex cytoarchitectonic appearance. In the monkey (100), the entorhinal cortex is continuous caudally with a lateral extension of what appears to be the parasubiculum, and then with fields TH and TF of the parahippocampal gyrus. For some distance, however, neural elements from all these fields appear to be intermixed. A similar situation also holds true for the human entorhinal cortex.
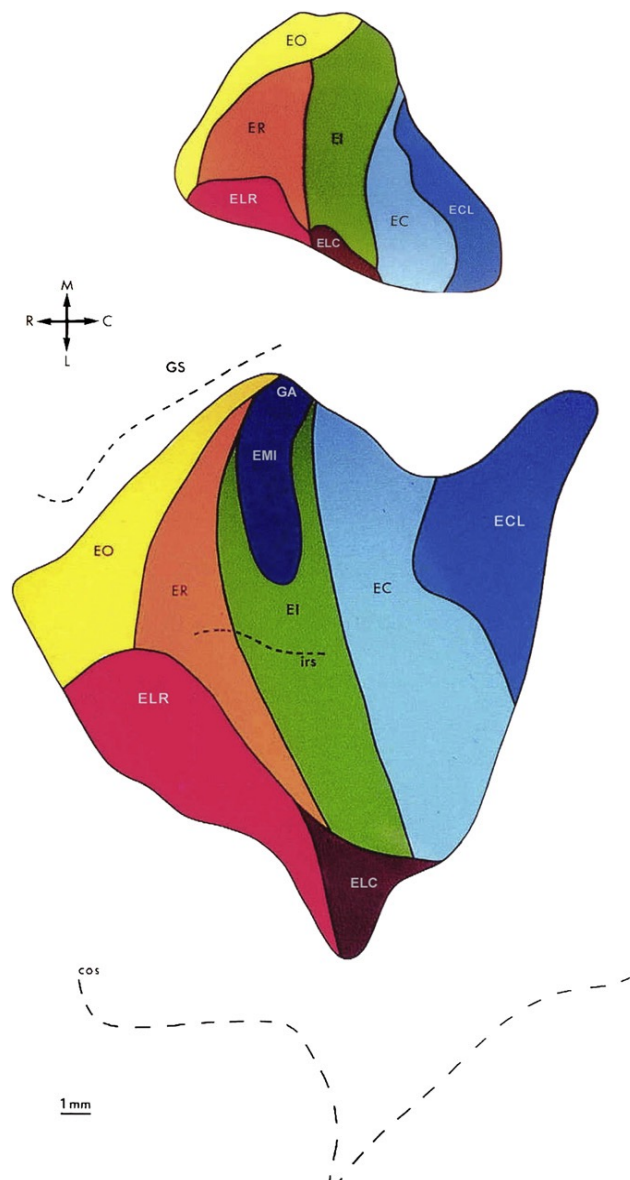
Figure 24- Two-dimensional unfolded maps of the entorhinal cortex in the nonhuman primate (Macaca fascicularis monkey, upper panel) and in the human brain (lower panel). In both cases, the same scale and orientation (arrows) applies to both species. While in the non-human

primate, no special mention to adjacent sulci (the rhinal sulcus in particular) is made, in the case of the human entorhinal cortex, the location of the the gyrus semilunaris (GS) above the upper dashed line (sulcus semiannularis), the location of the intrarhinal sulcus (irs) in the middle of the mediolateral extent of the entorhinal cortex, and the fundus of the collateral sulcus (cs) separated some distance from the lateral border of the entorhinal cortex by the laterally adjacent perirhinal cortex are indicated. Subfields of the entorhinal cortex, which presumably share homology between both species, are color-coded in a similar way. Despite the fact that only one more subfield could be reliably identified, note the expanse of the caudal and lateral entorhinal portions of the human brain compared to nonhuman primates (9).

While the entorhinal cortex is a multilaminate structure, its cellular constituents and laminar organization are quite distinct from those of other neocortical regions. Several numbering schemes have been adopted for its various layers. According to Ramón y Cajal (103), Hammarberg (104) provided the first account of entorhinal lamination and recognized five distinct layers. Ramón y Cajal (103) described seven cellular and plexiform layers in the entorhinal cortex, while Lorente de No' (71) assigned six. Other authors (38, 40, 93, 95), have not numbered the layers of the entorhinal cortex but simply divided it into two laminae, the laminae principalis externa and principalis interna, with a cell-free space, the lamina dissecans, interposed. By doing this, they stressed the perceived impropriety of associating layers of the entorhinal cortex with those of the neocortex. We (Amaral *et al.*,(100)) have adopted with minor modifications **(Figure 24)** the scheme of layering proposed by Ramón y Cajal (103). Because there has been substantial confusion concerning the laminar organization of the human entorhinal cortex, it is worthwhile to review briefly the major characteristics of each of its laminae.

The entorhinal cortex can be conveniently divided into six layers **(Figure 22H).** Layer I, closest to the pial surface, is an acellular or plexiform layer that tends to be somewhat thicker at more posterior levels. Layer II is a cellular layer made up of islands of relatively large and darkly stained, modified pyramidal and stellate cells **(Figure 22H).** Layer II is one of the most outstanding and distinguishing characteristics of the entorhinal cortex **(see Figure 17 for unfixed appearance).** The islands are distributed all over the entorhinal cortex, although they tend to be thinner, more elongated, and less noticeable rostrally, at dorsal and medial portions (38, 41, 50). In the fixed brain, the cell islands of layer II form small mounds **(Figure 23H)** on the surface of the brain that can be observed with the naked eye **(Figures 8, 9 and 13)**. These raised bumps on the surface of the entorhinal cortex (the verrucae hippocampi illustrated by Klingler (59)) provide a useful macroscopic indication of the rostral entorhinal

location. Layer II cell islands are surrounded by white strands of fibers that have been referred to as substantia reticularis alba of Arnold. The presence of modularity in the human entorhinal cortex has been demonstrated with cytochrome oxidase activity in the upper layers of the human entorhinal cortex (105). Interestingly, the cytochrome oxidase pattern loses the patchy appearance at the caudal limit of the entorhinal cortex. Further evidence of modularity in the human entorhinal cortex is demonstrated by immunoreactivity for non-phosphorylated neurofilaments and the calcium-binding proteins, calbindin and parvalbumin (106). The reader interested in this aspect of entorhinal morphology is referred to the detailed study by Solodkin and Van Hoesen (107). Although there are no reported studies of the ultrastructure of layer II neurons in the human entorhinal cortex, the study by Goldenberg *et al.* (108) in the rhesus monkey shows differences along the rostrocaudal extent of the entorhinal cortex. Rostrally, neurons are grouped in clusters with frequent appositions of their somata. These appositions were absent at intemediate and caudal levels. In contrast, axosomatic synapses and the presence of myelinated fibers increase at progressively more caudal levels in the entorhinal cortex. Usually, there is an acellular gap between layer II and the broad layer of medium-sized pyramidal cells that populate layer III. This gap increases at more posterior levels of the entorhinal cortex so that, in myelin-stained preparations, the layer II cell islands are conspicuous negative images outlined by the dense fiber labelling in layer I and in the space between layers II and III. Layer III contains a relatively homogeneous population of pyramidal cells. Layer III cells have a columnar appearance at caudal levels of the entorhinal cortex but tend to be arranged in large patches rostrally. In myelin preparations, layer III contains delicate bundles of radially oriented fibers that extend to the pial surface. These bundles of fibers are more noticeable at rostral levels of the entorhinal cortex, and they become particularly dense close to the boundary with the perirhinal cortex. Golgi studies of the monkey entorhinal cortex (100) show that dendrites of layer III pyramidal neurons bend and pass through the interstices of layer II cell islands, a morphological feature that has also been observed in the human entorhinal cortex after intracellular filling of neurons in fixed slices (109).

One of the most characteristic features of the entorhinal cortex in all species is the absence of an internal granule cell layer. In its place there is an acellular region of dense fiber labelling, the lamina dissecans (101), which is most noticeable at mid rostro-caudal levels of the entorhinal cortex. In the entorhinal regions where the lamina dissecans is not prominent,

layers III and V are apposed. Fiber preparations through these regions, however, still demonstrate a heavy plexus of fibers at the interface of the two layers. To emphasize the lack of a typical internal granule cell layer in the entorhinal cortex, the lamina dissecans has been labeled as layer IV. In some reports of the human entorhinal cortex, the term "layer IV" has been applied to the layer of large pyramidal cells that lies deep to the lamina dissecans (110). To avoid the confusion that might arise from labelling a layer of large pyramidal cells with the same number typically applied to a layer of small granule cells in the neocortex, we have followed Ramón y Cajal's lead and labelled the large cells deep to lamina dissecans as layer V. Layer V is about five or six cells deep and comprises primarily large and darkly stained pyramidal cells. At rostral levels of the entorhinal cortex, layer V merges with layer III while at midlevels the lamina dissecans clearly separates the two layers. Layer V becomes most highly developed at mid to caudal levels of the entorhinal cortex, and here three sublaminae can be differentiated. The most superficial layer (sublayer Va) contains the largest pyramidal cells in the entorhinal cortex, while the middle sublayer (Vb) contains somewhat smaller and more loosely arranged cells. The deep sublamina (layer Vc) contains fewer neurons and a fairly dense plexus of fibers **(Figures 18 and 19**, (53)**)**. At the same time that the lamina dissecans becomes less noticeable in the caudal half of the entorhinal cortex, layer Vc becomes much more pronounced, and it is easy to mistake Vc for a caudal extension of the lamina dissecans. At rostral levels of the entorhinal cortex, layer VI is not easily distinguished from layer V. Close to the border with the perirhinal cortex, layer VI is rather broad and diffuse. The border of layer VI with the white matter is not sharp rostrally, and there is a gradient of decreasing cell density from this layer into the white matter. Caudally, however, layer VI presents a sharp border at the transition with the white matter **(Figures 11 and 19).** The subcortical white matter situated deep to the subicular complex is called the angular bundle **(Figures 11 and 19)** because of its trajectory in non-primates. It is within this region that the perforant path fibers travel to caudal levels of the hippocampal formation. At the border of the entorhinal cortex with the perirhinal cortex, layer VI tends to fade out in a gradual fashion and finally ends somewhat more laterally than the termination of layer V. This contributes to the oblique orientation of the border between the entorhinal and perirhinal cortices discussed earlier.

Several estimates of the number of neurons in the human entorhinal cortex have been made (19, 40, 106-108). The counts generally are carried out relative to layers but do not take into consideration the various subfields of the entorhinal cortex. The number of neurons in the human entorhinal cortex is on the order of $7-8 \times 10^6$. Of these, about 10% are in layer II,

approximately 45% are located in layer III, about 15% of the total number populate layer V, and 31% are in layer VI. Comparing these numbers to estimates of neuron number in other hippocampal fields, emphasizes how divergent the axonal projection of layer II neurons must be both to the dentate gyrus, which contains 15×10^6 granule cells and CA3, which contains 2.8×10^6 pyramidal cells (111). It is important to note that 3.6×10^6 neurons in layer III of the entorhinal cortex project to 16 x 106 neurons in the human CA1 field of the hippocampus. This means that almost half of the total number of neurons in the human entorhinal cortex project to CA1 (112). Therefore, CA1 is under very heavy direct influence from the entorhinal cortex.

iii) Clinical hippocampus anatomy- normal aging vs Alzheimer disease.

A recurrent question in aging research is to what extent humans lose neurons, as they grow older. Until a few years ago, the common assumption was that the hippocampus begins to lose neurons in midlife and the loss continues into old age. However, this view had to be corrected after studies that used unbiased sampling strategies. Recent numerical counts by West *et al.* (113), and Simic *et al.* (98) show that the hippocampal formation does not generally suffer any age-related loss of neurons. Only the subiculum (52% or 7.3% per decade) and the hilus of the dentate gyrus (31% or 4.2% per decade) demonstrate substantial cell loss in normal aging (113); however, in these studies it is important to include young subjects for comparison, and consider gender differences. In contrast, neuronal loss in the hippocampal formation of AD patients is much higher, even in very mild cases (97). Studies on the entorhinal cortex (114) reveal a similar trend (0.7% of neuron loss per year, and, specifically 1.2% for layer II neurons). The analysis of the extent of atrophy in the human entorhinal cortex in normal aging (age range of the series, 12–110 years old) based on the areal measurement of two-dimensional reconstructions of the entorhinal cortex reveals a decrease up to 4% in size over the life range (115).

Among the many conditions that produce patholological changes in the hippocampal formation, AD is probably the most devastating (49, 105, 106, 111-115). Myriad studies have come to the clear conclusion that this disorder is distinctly different from an elaboration of normal aging. AD is associated with four neuropathological correlates in the hippocampal formation: neuronal cell loss, neurofibrillary tangles, neuritic plaques, and granulovacuolar

degeneration (for more information about each one of these lesions, see Tomlinson (116) and Braak and Braak (117)).

Corsellis (118) first drew attention to complete cell loss in the CA1 field of the brains of Alzheimer patients. Ball (111) subsequently conducted systematic analyses of cell loss in the hippocampal formation, and he estimates that there is a decrease of some 56% in the number of hippocampal pyramidal cells (versus 12% in age-matched controls). These early studies have been confirmed by more recent studies using unbiased sampling procedures (97). These studies demonstrate that CA1 suffers a profound neuron loss (an average of 68%), in contrast to normal aging where neuron loss is negligible. Hyman *et al.* (105, 113) have emphasized that the cell loss is pronounced not only in CA1, but that the subiculum and layers II and V of the entorhinal cortex are also depleted of neurons. More recent studies (114) show that there is already profound neuron loss (35% in the entorhinal cortex as a whole, of which 50% is in layer II, and 46% in CA1, in mild clinical cases of Alzheimer disease). Interestingly, despite the fact that neurons in layers II and V of the entorhinal cortex are nearly eliminated, layers III and VI have a relatively normal appearance.

Neurofibrillary tangles, while occasionally observed in the normal-aged brain, are more numerous in the Alzheimer brain and are located in the same regions that undergo the greatest amount of cell loss (119, 120). Ball (119) noted that a greater number of neurofibrillary tangles occur in the posterior part of the hippocampus. Neuritic plaques are spherical foci, 5–200 mm in diameter, which may have a central amyloid core surrounded by argyrophilic rods and granules. They are very numerous in the hippocampal formation of patients with AD and show a preference for the molecular layer or the dentate gyrus (105). The fourth pathological correlate of AD is granulovacuolar degeneration (120). Neurons demonstrating granulovacuolar degeneration contain one or more 3–5-mm vacuoles that hold 0.5–1.5-mm argyrophilic granules. These profiles are numerous in the subiculum and CA1 of the Alzheimer brain but are not frequently found in the entorhinal cortex.

It has been suggested that, as AD develops, the hippocampal formation, especially the entorhinal cortex, becomes, in essence, functionally disconnected from its major afferent and efferent interactions, as a result of the cell loss and other pathological sequelae of AD (see Hyman *et al.* (110), and Braak and Braak (117), for a comprehensive review of the human

entorhinal cortex in various pathologies). Given the important role the hippocampal formation is known to play in certain forms of memory, it is likely that a major portion of the problems with memory function observed in AD is attributable to damage of the anatomical connections of the hippocampal formation (121).

The importance of the hippocampal formation morphology has been stressed by the clinical use of structural MRI as a useful method for evaluation of the atrophy degree which correlates with the neurodegeneration (124-129, and for a recent review, see Frisoni *et al.* (122)). The volumetric measurement of the hippocampal formation is a useful aid in the diagnosis and prognosis of the disease, and the importance of the correct identification of the anatomical structures is crucial to make accurate measurements (reviewed in Konrad *et al.* (123)).

Elaboration on anatomical and MRI studies of the human entorhinal cortex (124), have favoured the application to clinical studies. Recent clinical reports (125, 126), advanced the diagnosis and conversion of mild AD to full clinical symptoms by measuring the thickness, among other areas, of the entorhinal cortex. These methods have been also applied to the whole cerebral cortex in a longitudinal study where only the areas around the central sulcus showed no differences in thickness between controls and AD patients. Still, the early diagnosis of AD based on structural MR is elusive, as it seems that biomarkers (β-amyloid, tau protein) of the disease become abnormal at an earlier stage relative to neurodegeneration markers such as brain atrophy (27).

g) Neuroimaging and neuroradiology of Alzheimer's disease and aging (temporal and parietal scales).

i) Structural neuroimaging MRI studies in Alzheimer's disease.

Voxel based morphometry (Voxel-based morphometry [VBM]) is a free method of bias that in a relatively short time allows the verification of atrophy changes in different brain regions. Publications based on this technique applied to the study of AD have shown how the disease spreads from the medial temporal lobe to the lateral temporal lobe and then to the parietal lobe and finally to the frontal lobe, reproducing pathological studies about AD proposed by Shiino *et al.* (127)

Based on this description Shiino *et al.* (139) studied 40 non-familiar AD, 20MCI, 88 controls above 60 years and 40 below this age. The authors of this paper describe progressive atrophy in controls at the perisylvian cortex, anterior cingulate cortex, caudate head, dorsomedial and parahippocampal cortex and thalamus in subjects with AD further involvement of the amygdala, hippocampus, subcallosa region of the posterior cingulate cortex and posterior association cortex parietooccipital.

Shiino *et al.* (139) propose four subtypes of AD for its selective atrophy patterns: amygdala-hippocampal involvement (Hipp), hippocampal-amygdala, posterior cingulate cortex and precuneus (Hipp / PCC-PRCC), hippocampus-amygdala and posterior parietal-occipital cortex (Hipp / TOP) and the posterior cingulate cortex, precuneus and posterior cortex (PCC-PRCC / TOP). The PCC-PRCC or PCC-PRCC / TOP EA pattern occurs in 90% under 65 years. 100% of the Hipp patterns AD carrying more than 36 months of clinical evolution. Karas *et al.* (128) shown in AD overall cortical atrophy with preservation of sensory-motor cortex, cerebellum and occipital pole in addition to those already mentioned in hippocampus, insula and temporal pole.

Several studies focus on the earliest changes in AD like Whitwell *et al.* (129) (the most early changes evident in the prodromal phase-DCL/ EA-amygdala-hippocampus focus on entorhinal cortex and anterior-fusiform gyrus), Desikan *et al.* (130) (changes are in the etnorhinal cortex and inferior parietal turn predict the transformation of MCI due to AD) and Weimer (131) (the size of the ventricular system increases with age but the pace increases, years before the development of MCI). Others do it in determining the subjects at risk of developing the disease as Stoub *et al.* (132) (studying the volume of the parahippocampal white matter (PWM) in two samples of 65 subjects followed for 8.5 years, concluding statistically significant differences in baseline volume PWM from the group that is stable and that evolves MCI). Moreover, Franko and Joly (133) found the highest rates of atrophy in the anterolateral right hippocampus in those subjects with MCI that progress to AD versus those that remain stable MCI. These areas of the anterolateral right hippocampus concentrate the largest deposits of tau. The parietal cortex is involved in the processes of attention and episodic memory formation (134) particularly the dual involvement of dorsal parietal cortex (superior parietal lobe-precuneus) and parietal cortex ventral (supramarginal angle and rotation) in search functions, attention and verification for memory formation.

The parietal lobe involvement in the EA focused studies like Ross *et al.* (135) (which stresses that derioration in the profile of these subjects predominates disorder morphology, dysgraphia and difficulty bimanual tasks), or Jacobs *et al.* (136) (described as the volume of the inferior parietal lobe versus other lobes is the one which best discriminates in a cohort follows the stable group, the one which progresses and those subjects that in an evolution of 6 years it is shown that they were on preclinical disease stage).

Several studies focus on the differentiation patterns of early (under age 65) or late onset of AD have been done: Karas *et al* (137) (EA early debut show a disproportionate involvement precuneus), Ishii *et al* (138) (parietotemporal and posterior cingulate atrophy in AD debut early but not late), Shibuya *et al.* (139) (AD early onset shows less involvement at entorhinal cortex that late onset AD subjects) or Moller *et al.* (140) (late AD subjects show debut with hippocampal atrophy, right temporal lobe and cerebellum compared to early onset of AD showing hippocampal atrophy, temporal lobe, precuneus, frontal and cingulate gyrus lower. The direct comparison between the two groups result in individuals early-onset AD show more atrophy in the precuneus and late-onset AD in medial temporal lobe).

The value of family history of AD to predict patterns of atrophy has also been studied by Okonkwo *et al.* (141) (in a follow-up period of four years middle-aged adults with a family history showed changes in the posterior hippocampus atrophy in the absence cognitive impairment without accredited effect factor APOE4) or pattern of familial AD by Schott *et al.* (142) (annual checks in familial AD show etorhinal hippocampus and cortex atrophy that occurs early in AD at the rate 5 % per year vs. controls).

(1) Clinical radiological diagnostic criteria-medial temporal lobe atrophy scale (Sheltens) and parietal atrophy scale (Koedam).

(a) Scheltens (MTLA-scale)

Voxel based morphometry is not an affordable method in clinical practice that is why visual rating scale temporal atrophy given by Sheltens *et al.* (5) still in use was developed. This scale developed in coronal plane (7, 8) consisting of five grades (0-4) **(Table10, Figure 25)** which value the width of the choroidal

fissure and the medial temporal horn and as the height of the hippocampus has been validated against studies volumetric, neuropsychological and disease for the past 20 years (9) as a diagnostic tool for grading patterns temporal atrophy in moderate to severe AD and control subjects with a sensitivity of 70- 100% and specificity of 67-96%.

Table 10- MTA visual rating scale

MTA visual rating scale

Score	Width of choroid fissure	Width of temporal horn	Height of hippocampal formation
0	N	N	N
1	↑	N	N
2	↑↑	↑↑	↓
3	↑↑↑	↑↑↑	↓↓
4	↑↑↑	↑↑↑	↓↓↓

F Barkhof, M Hazewinkel, M Binnewijzend and R Smithuis. 2012
http://www.radiologyassistant.nl/en/p43dbf6d16f98d/dementia-role-of-mri.html
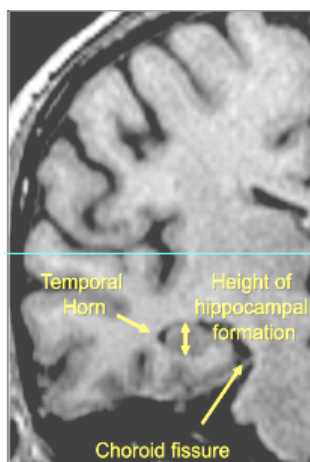
Below 75 years
  ✓MTA-score of 2 is abnormal
  ✓MTA-score of 1 de may be normal

Above 75 years
  ✓MTA-score of 3 or 4 is abnormal
  ✓MTA-score of 2 may be normal

F Barkhof, M Hazewinkel, M Binnewijzend and R Smithuis. 2012
http://www.radiologyassistant.nl/en/p43dbf6d16f98d/dementia-role-of-mri.html
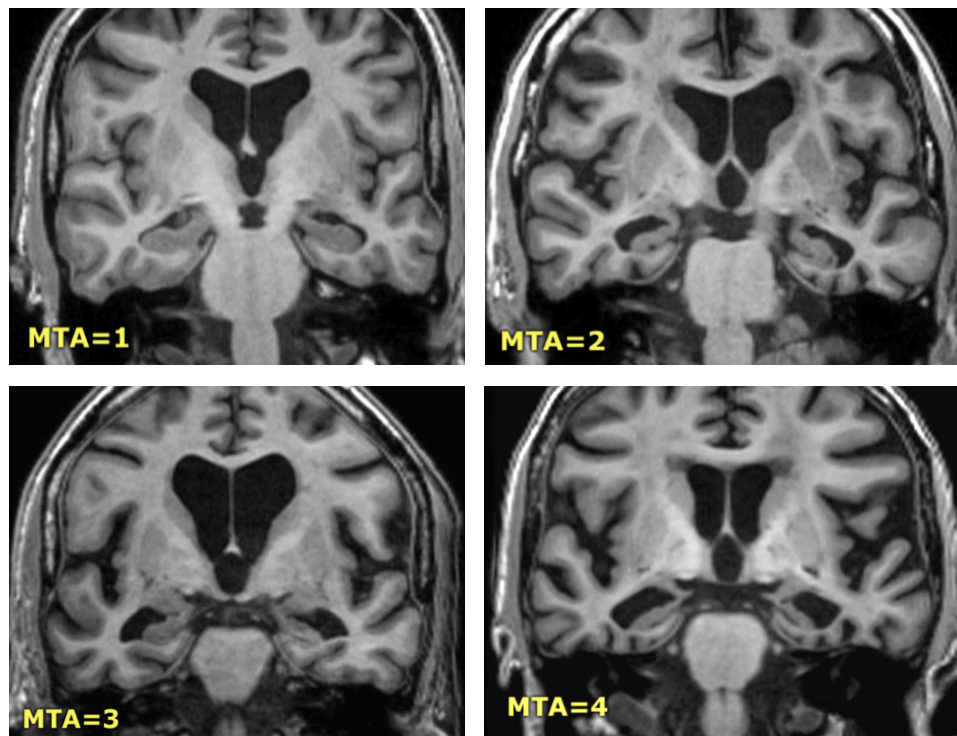
Figure 25- **Examples of MTA scales scores.**

It seems justified to take account of the degree of atrophy registered on the scale of temporal atrophy in combination with clinical information when AD individual patients are diagnosed in clinical practice.

The original proposal by Scheltens and colleagues consisted of an age-adjusted cut-off of MTA score ≥2 in either of the two hemispheres considered abnormal below the age of 75 years, with an MTA score ≥3 required to be abnormal above 75 years of age(5). This cut-off has shown low specificity (67%) (10). A cut-off of ≥1.5 based on the average score of both hemispheres has also been proposed (11). This cut-off has shown higher specificity (94%), but at the expense of lower sensitivity (46%). Further, a cut- off of ≥2 based on the average score of both hemispheres has been reported to have higher sensitivity in patients with AD older than 75 years (12), and a score of 3 might be considered normal in individuals above 80 years of age (13). Between 45-65 years a cut-off of ≥1.5 based on the average score of both hemispheres has also been proposed (11, 14). The age-decades-adjusted cut-off resulted in the best performance for MTA is AUC = 78.5 (14). So for the study of PcAD the MTA has a limited value as far as only a cut-off of ≥1.5 on the average score of both hemispheres have been proposed so there is a necessity to describe a new sensible and specific new

scale of medial temporal lobe atrophy for judging subjects between 40 and 60 years old (PcAD stage).

Westman *et al.* (22) in a recent study compared the performance of visual scales of temporal atrophy, with multivariate evaluation Magnetic Resonance Imaging (MRI) system and manual measurement of hippocampal volume in order to distinguish 75 AD compared with healthy controls and predictive value for conversion of 101 MCI to AD. They found accuracies to distinguish AD from healthy controls of 83% for the multivariable system based on MRI, 81% for visual scale temporal atrophy and 89% for manual measurement of the hippocampus. All three methods show similar accuracy in estimating the conversion of MCI into AD in track a year.

Recently, Duara *et al.* (143) and previously, Wahlund *et al.* (21) have contributed with their studies to endorse the clinical validity of the temporal lobe scale.

Cavallin *et al.* (13) compared the scales of temporal atrophy with volumetric measurements in a cohort healthy subjects between 60 and 84 years getting a significantly high correlation, for healthy subjects and 70 years degrees 0 and 1 are considered normal grade 2 between 70 and 80 years and grade 3 over 80 years. To our knowledge there are no published studies of application of scales of temporal atrophy in cohorts of healthy subjects younger than 60 years (cohort PGA). A recent publication by Kim *et al.* (144) developed a rating scale of temporal atrophy in axial plane (including valuation of peritroncular tank) and compares it to the performance of the coronal temporary visual scale with good results.

(b) Parietal atrophy scale (Koedam).

The visual rating scale proposed by parietal atrophy Lehemann *et al.* (145) (in EA early and late debut and young and elderly controls) and its validation by Moller *et al.* (26) (in subjects with subjective memory complaints against DCL) has been more recent. However its development is based on the same reasons that support the use of the time scale in clinical practice. Atrophy parietal scale

has four degrees (0 to 3) **(Table 11, Figure 26)** values in three planes sulci dimensions of postero-superior cingulated sulcus, lateral parietal and occipital parietal sulcus. The inferior parietal sulcus is which best discriminated between degrees.

Table 11- Characteristics of parietal scales scores

Koedam score for Parietal Atrophy

Grade 0	no cortical atrophy	closed sulci of parietal lobes and cuneus
Grade 1	mild parietal cortical atrophy	mild widening of posterior cingulate and parieto-occipital sulci
Grade 2	substantial parietal atrophy	substantial widening of the sulci
Grade 3	end-stage "knife-Blade" atrophy	extreme widening of the posterior cingulate and parieto-occipital sulci

F Barkhof, M Hazewinkel, M Binnewijzend and R Smithuis. 2012
http://www.radiologyassistant.nl/en/p43dbf6d16f98d/dementia-role-of-mri.html
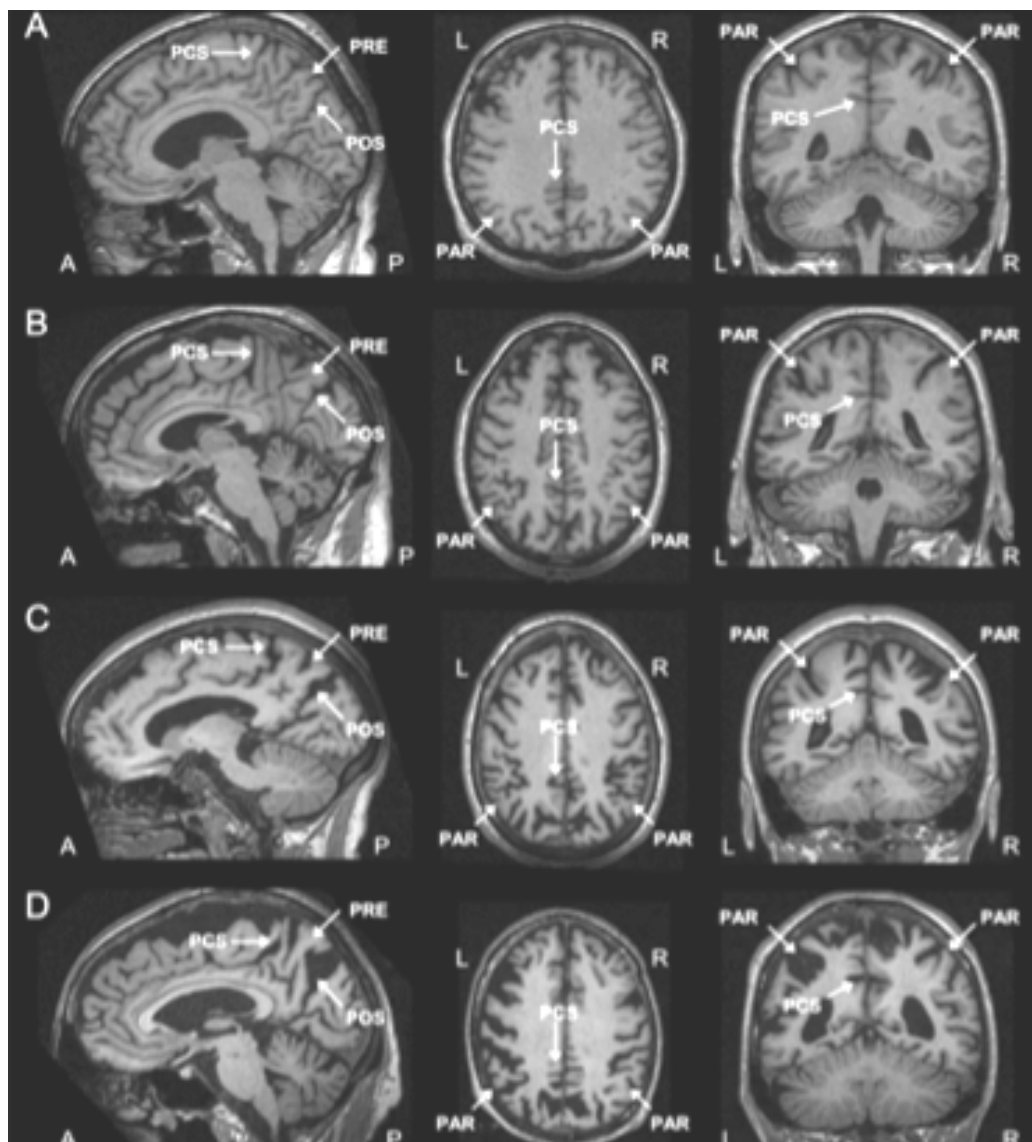
Figure 26- Examples of Parietal scales scores (159).

To our knowledge there are no published studies of application of parietal atrophy scales to a cohort of healthy subjects younger than 60 years (cohort PGA).

(2) Cortical thickness of AD signature regions (included hippocampus) decreases in preclinical AD.

Wang *et al.* (161) try to determine whether an MRI-based AD signature biomarker can detect tau-related neurodegeneration in preclinical AD, and to assess whether AD signature cortical thinning is associated with cognitive changes in cognitively normal (CN) older individuals.

This study consist of a large cohort of CN individuals (n=188), we measured the hippocampal volume and cortical thickness within independently defined AD signature regions.

We cross-sectionally assessed the associations between AD signature cortical thinning or hippocampal atrophy with CSF biomarkers of tau (increased tau) and b-amyloid (Ab) (decreased Ab42). We also examined the impact of AD signature cortical thinning or other biomarker changes (i.e., hippocampal atrophy, reduced CSF Ab42, or increased CSF tau) on cognitive performance in CN individuals. The results obtained shows that elevated CSF tau was associated with AD signature cortical thinning but not hippocampal atrophy. In contrast, decreased CSF Ab42 was associated with hippocampal loss but not AD signature cortical thinning. In addition, AD signature cortical thinning was associated with lower visuospatial performance. Reduced CSF Ab42 was related to poorer performance on episodic memory. In conclusion spatially distinct neurodegeneration is associated with Ab and tau pathology in preclinical AD. Ab deposition and AD signature cortical atrophy independently affect cognition in CN older individuals.

(a) How detect radiologically through structural MRI this cortical thickness decrease of Alzheimer's disease signature regions.

This thesis is based on the subtle changes at the anterior portion of the hippocampus body (around fimbria)(47) that can be observe through the progressive increases of the identifiable dilated choroid fissure first, followed after by the same phenomena with the temporal horn (that constitute grade 1 scheltens medial temporal lobe atrophy scale) just until the time in which this temporal horn just begins to dilated (early grade 2 scheltens medial temporal lobe atrophy scale). These subtle changes qualitatively (radiologically) identifiable by anatomical landmarks (almost used by Scheltens medial temporal lobe atrophy scale) constitute a new medial temporal lobe early atrophy scale that could also be quantitatively (VBM techniques) demonstrated.

(3) Consequences of the application of this sensitive new medial temporal lobe early atrophy scale in combination with CSF biomarkers.

The application of this sensitive new medial temporal lobe early atrophy scale in combination with CSF biomarkers could allow us to identify the preclinical AD late states subjects in whose neurodegeneration had already began (demonstrated by CSF biomarkers- decrease Aβ $_{1-42}$

together with increase T-tau or P-tau) without cognitive impairment but with low performance in memory cognitive tests and accompanied by cortical thickness decreases of hippocampus.

ii) DTI studies in Alzheimer's disease.

Several works have been performed multiple studies comparing diffusion tensor imaging (DTI) with volumetric measures, some like Clerx *et al.* (146) centered in the medial temporal lobe (LTM) performing a meta-analysis evaluated the diagnostic value of the diffusion tensor imaging (DTI) in early AD compared to commonly accepted measures of atrophy of the medial temporal lobe. Seventy-six studies about LTM atrophy measures including 8122 subjects and 55 DTI studies including 2791 subjects are reviewed. Volumetric studies (effective size expressed as Hedge index) differed between AD and controls (ES 1.32–1.98)) and MCI and controls (ES 0.61 - .146). In studies of DTI fraction anisotropy (FA) of the total cingulate was the index that best differentiated AD controls (ES =1.73) and FA parahippocampal gyrus, which did between MCI and controls (ES = 0.97). Moreover, the mean diffusivity (MD) of the hippocampus allowed differentiating AD vs. controls (ES = -1.17) and DCL controls (ES = -1 .00). As a general conclusion LTM volumetric measurements showed the same performance as the DTI.

However in the comparison between controls and MCI, ES measures DCL to MD exceeded those ES measured hippocampal volume. MD values seem to have greater discriminatory power than the FA with higher values of ES in frontal, parietal, temporal and occipital lobes. Other jobs with the same approach (comparing DTI and VBM) include all brain regions in their area (not just the medial temporal lobe) as the study of Wang *et al.* (147) compared the grey matter integrity and tracts white matter (DTI) of 10 subjects with MCI and 10 controls. They are analysed in group's cortical thickness, fraction anisotropy (FA) and apparent diffusion coefficient (ADC). MCI patients showed decreased FA and increased ADC in frontal region, temporal and corpus callosum. MCI cortical thickness resulted in decreased frontal, temporal and parietal regions.

Changes in white matter pathways and cortical thickness were more pronounced in left hemisphere. In conclusion both DTI as cortical thickness are effective methods to differentiate

controls vs. MCI patients, improving the combination of the two the diagnostic accuracy. Other studies link patterns focal cerebral atrophy with the integrity of white matter pathways that connect them and their metabolism and the study of Firbank *et al.* (148) of the foreknowledge that hippocampal atrophy and hypometabolism of the posterior cingulate phenomena are often found in AD and dementia with Lewy bodies body (LBCD).

These regions also show a correlation of activity at rest as parts of the default neural network (DMN) connected by the cingulus as large white matter tract. Their study hypothesized that hippocampal atrophy associated with disruption of the cingulus, which can be measured by techniques DTI. 5 AD study, 5 healthy volunteers and 5 LBCD. Hippocampal volume and cingulate FA is calculated. Multivariable analysis correlating FA cingulate against hippocampal volume, overall atrophy and Group (AD, LBCD or control) is performed. The results suggest that the progression of dementia is associated with increased measures of global atrophy and disruption of the posterior cingulate and white matter pathways that connect this with the lateral parietal. The study concludes that in addition to these hypo metabolism areas which are described in AD and LBCD seems to be a disruption of white matter pathways that connect them. Finally there are jobs like Canu *et al* (149) which studied the integrity of white matter pathways from the perspective of volume, so this paper studies the ways of white matter in 18 AD early onset (EO) 24 AD Late onset (LO) and 4 controls, exploring the volume of white matter pathways and correlating the measures with the terms of the genotype of apolipoprotein (APOE). VBM studies are performed to estimate the volume of white matter.

Compared with control patients LO showed selective loss of volume of the parahippocampal white matter, while the EO showed a more diffuse pattern with involvement of posterior structures. The different distribution pattern of white matter atrophy in turn reflects the grey matter one. The highest risk was associated with increased ApoE atrophy of the parahippocampal white matter in both groups. Atrophy values were higher in white matter in EO than in LO which gives an idea of the greater aggressiveness of this type of disease.

iii) fMRi studies in Alzheimer's disease.

Functional studies are based on the sampling of neural networks that have an anatomical basis recognized by the white matter pathways that connect them (149). Thus the study of He

et al. (150) focuses on the investigation of a large-scale network of connections between different brain regions on the basis of studies of cortical thickness. Two areas that are considered anatomically connected when they show statistically significant correlations between its cortical thicknesses thus constituting a network of cortical connections from 124 brains of the database of the international consortium of the human brain mapping. Connections significant short and long range found within each hemisphere and between brain hemispheres, many of which coincide with known white matter tracts measured by DTI techniques. The study concludes that the human brain has a structure robust network connection to a pattern of "small world" with robust neighbourly relations alternating with relations between distant areas. These results support the functional studies of known neural networks.

The DMN default neural network has focused the attention of many studies in healthy population and served as the basis for the AD. So Damoiseaux *et al.* (151) focused their study on aging that is associated with impairment of cognitive functions without disease. Attention, information processing and memory are affected. Based on the observations of disruption of white matter pathways OSullivan *et al.* (152) the theory that starts off with normal aging affects neural networks as the default neural network (DMN) whose condition can be tested by studies functional fMRI. This work studied 10 young and 22 elderly subjects with functional studies in waking state, at rest and with open eyes (resting-state Studies). The study concludes that DMN components that are affected by aging are the superior and middle frontal gyrus, the second cinguloposterior and third the medial parietal and superior temporal gyrus.

When first decreases activity any of these neural networks has less executive ability. Davis *et al.* (153) summarized in his study that changes with aging (with greater difficulty completing tasks) are given in the DMN to translate a compensation mechanism (the occipital activity is reduced and increased frontal activity) reflected in the medial posterior cortex activation which is reduced and increases medial frontal cortex. Sorg *et al.* (154) in their work hypothesizes that the EA components DMN reduced functional connectivity and atrophy. Studied 16 healthy volunteers for this year and 24 subjects with amnestic MCI by resting-state fMRI. The object of the work was to identify if there was any neural network study resting-state fMRI (RNs) that affect the MCI and whether these alterations of functional connectivity

changes were associated with atrophy. Eight networks RNs were identified, of which only DMN and executive attention network were affected in MCI. Volumetric studies meanwhile reflected lost volume of medial temporal lobes. Functional connectivity between medial temporal lobes and the posterior cingulated was lost in MCI, being preserved in controls. The study concludes that in MCI deterioration of a group of neural networks represented a process of neurodegeneration is proved.

Meanwhile Binnewijzend *et al.* (155) studied the functional regional connectivity in 9 AD and MCI and 4 healthy controls using resting-state fMRI. The study tracked 2.8 years (sd 1.9 years) with 7 MCI converted to AD and 4 stable MCI. AD patients showed changes in functional connectivity in cinguloposterior precuneus versus controls (regardless of cortical thickness). Values of functional connectivity of the MCI were between the controls and AD, although only AD and MCI stable showed statistically significant differences. The study concludes that the deterioration of functional connectivity in the DMN in AD is shown.

Finally Buckner *et al.* (156) indicate that the target age changes focus on posterior cortical regions including the posterior cingulate, the splenium of the CC and lateral parietal regions involved in DMN in young adults and show amyloid deposition in elderly adults and AD. In the initial AD atrophy and metabolic decrease was observed in these posterior cortical regions and medial temporal lobe. These regions are involved in retrieving memories in young and subsequently undergo changes with age own AD (amyloid deposits, metabolic disorder and atrophy). These regions of the medial temporal lobe part of a neural network whose disruption contributes to the deterioration of memory (DMN)

iv) Metabolic imaging studies in Alzheimer's disease (PET / SPECT / MRI-ASL).

Metabolic imaging studies in AD are based on the application of techniques of positron emission tomography (PET), positron single photon emission (SPECT) and magnetic resonance flow technique spin labeling (ASL).

PET studies in the context of the AD use the longitudinal sensitive markers to study this technique. Ossenkoppele *et al.* (157) evaluates changes in the longitudinal PET markers

pathological changes of AD [^{11}C] PIB y [^{18F}) FDDNP and cerebral metabolic activity ^{18}F] FDG in patients with AD, MCI and healthy volunteers. The study focuses on controls, patients MCI and AD. The interval between the baseline and follow-up study was 2.5 years (2-4 years). Parametric maps for each path are generated and the uptake ratio (SUVR) is measured. An overall significant increase cortical global [^{11}C] PIB, [^{18F}) FDDNP was found in subjects with MCI, but no changes were observed in AD and controls. Regional analysis revealed that the increase of PIB was produced in lateral temporal lobe. The uptake of [^{18}F] FDG was reduced by tracking AD in frontal, parietal and lateral temporal regions. Correlation between overall minimental test and overall PIB deposit and FDG uptake in the posterior cingulate was established. It is concluded that increased amyloid burden in MCI patients and progressive metabolic deterioration in AD is credited.

Regarding SPECT studies as the work of Lee *et al.* (158) focus on applying techniques of positron emission single photon (SPECT) using technetium-99m as a marker 99mTc-HMPAO). The study is based on 20 patients with mild AD, 20 with moderate AD and 20 controls. The images obtained were transformed into an anatomic space transformations reference based on the voxel to voxel image. Hypoperfusion in the left parietal lobe was found in patients with mild AD, the AD moderate hypoperfusion affect both parietal-temporal regions rear, front occipital lobes contiguous region of the posterior cingulate and frontal lobes with less intensity.

ASL techniques as the work of Alsop *et al.* (159) studied the cerebral flow in this study in 18 patients and 11 controls. Sixteen slices of 5mm were made. Flow images transformed to an anatomical reference space based on transformations of the voxel image voxel. The analysis showed significant decrease in flow relative to controls in temporal, parietal, frontal and posterior cingulate region. Correlations between degrees of more severe involvement of the minimental test with the posterior parietal lobe, posterior cingulate region were obtained, but not the temporal lobe. Tosun *et al.* (160) perform a combination study based on identifying structural atrophy using MRI techniques, alterations of cerebral blood flow (CBF) by ASL techniques as the best predictors of expansion measured by amyloid deposition techniques [8F]-AV45-PET in patients with MCI. Also evaluate the relative importance of the methods to classify subjects with initialMCI as AB + and AB-. Sixty-seven patients ADNI-GO / 2 with initial MCI are studied. The [8F]-AV45-PET positive initial MCI posted a return on the classification of

these subjects 83% accuracy, 78% positive predictive value and 84% negative predictive value using a multidisciplinary classifier that took into account demographic, APOE4 and multimodal MRI analysis based on the categorization AB. We conclude that multimodal MRI can predict the state of deposit of amyloid in patients with initial MCI.

v) Early onset _vs_ late onset Alzheimer's disease patterns.

Alzheimer´s disease is the most common form of degenerative dementia with debut either early age (EO) or late age (LO) (arbitrarily defined as less than or greater than 65 years respectively). The clinical presentation is dominant form of anterograde episodic memory deficit. However, there are an increasing number of evidence pointing to a clinic inhomogeneity in the EA forms of clinical predominance memory impairment (LO) and others with greater involvement of nonamnesic functions (visual, spatial, praxis, language disorders and executive dysfunction) that focuses on the EO forms. The latter forms of no amnesic functions impairment debut have been less studied. Early diagnosis of AD depends heavily on detailed study of the distinguishing features between the two clinical presentations.

Using MR imaging techniques, this thesis focuses on exploring the structural differences and metabolic between EA (EO vs LO) in the rostral and caudal parts of the DMN, particularly those differentials preclinical stage of the disease having as one of its objectives to develop a quantitative scale of structural changes in defining the preclinical stage of AD (EO vs LO) so far not developed (161). It is possible to detect early structural changes in the DMN during the preclinical phase of AD through the structural impact of the early accumulation of b-amyloid by DWI (microstructure) and MRI (macrostructure) studies (162-164). We can analyse the metabolic changes associated with structural ones, particularly cerebral blood flow changes (ASL) in the DMN (165) **(Table 12).**

Table 12- impact of the early accumulation of β-amyloid by DWI (microstructure), MRI (macrostructure) and blood flow changes (ASL) in the rostral DMN (MTL).

			Art. Blood flow	Microstructure	Macrostructure		
			Perfusion	Diffusivity	Cortical Thickness	Tractography	
Risk level	Cognition	CSF	ASL	DWI	sMRI	DTI	
Low Risk (LR)	(-) normal	βA (-) Tau (-)	normal DMN	normal DMN	normal DMN	normal DMN	**control**
High Risk (HR)	(-) normal	βA ↓ Tau (-)	normal MTL	MTL ↑	MTL (atrophy)	normal DMN	**preclinical**
	(+) early symptoms	βA ↓ Tau ↑	MTL ↑	MTL ↑	MTL (atrophy)	normal MTL	**Prodromal / MCI**

2- HYPOTHESIS and OBJECTIVES

a) Basics for Hypothesis and Objectives (Hypothesis's arcade).

The hypothesis of this thesis affirm that it is possible to define a new MRI structural medial temporal lobe atrophy scale (EMTA), whose last fourth of fourth stages (corresponding with early stage 2 of MTLA (5)) is able to identify subjects at late stages of preclinical AD (with decrease $A\beta_{1-42}$ together with increase T-tau or P-tau in CSF but no cognitive deficit only low performance at verbal memory test-TAVEC – Spanish version of CVLT test) as has been defined by NIAA-AA criteria (1, 2, 15, 16).

Identify subjects at late stages of preclinical AD through a new MRI structural medial temporal lobe atrophy scale (EMTA) is important because it only requires neuroradiological trained expertise, commonly present in radiology departments of hospitals, resulting in a quick and inexpensive method to detect those subjects who could benefit from the new therapies now on trial II & III phases (17, 18).

b) Hypothesis

i)   There is atrophy in MTL before it becomes detectable within the range described by the currently available radiological atrophy scales used for diagnoses.

ii) This atrophy is different in terms of magnitude from ageing effects and could correspond to the early stages of AD prior to cognitive deficits leading to clinical diagnosis of AD.

iii) It is possible to detect this low-grade MTL atrophy by means of a radiological atrophy scale based on well-defined anatomical criteria.

iv) The low-grade MTL atrophy can be measured quantitatively and the volumetric changes measured correspond to the anatomically defined changes and proposed radiological atrophy stages.

v)   Together with other early-AD biomarkers, the new low-grade MTL atrophy scale might prove of great value to detect the first phase of the neurodegenerative process leading to AD.

_____

c) Objectives

i) Define and validate a new MRI structural medial temporal lobe atrophy scale (EMTA) to identify the preclinical stages of AD subjects (PcAD).

ii) Test the reproducibility of the anatomically based criteria for low-grade atrophy by qualified independent radiologists.

iii) Volumetrically quantify early MTL atrophy and compare with the previously identified anatomically based atrophy criteria of the atrophy scale.

iv) Identify other non-MRI biomarkers of AD (CSF and cognitive biomarkers) in the same population under study and compare with the low-grade MTL atrophy scale in order to confirm the status of possible late stages of preclinical AD related to low-grade MTL atrophy.

3- MATERIAL AND METHODS

a) GAP Cohort

i) Design

Transversal study in a cognitively healthy adults cohort of subjects enrolled in the GAP (Guipúzcoa Alzheimer Project), men and women without dementia aged between 39 and 79 years (both inclusive) and with and without history of AD in first-degree relatives. Subjects were recruited between June 2011 and January 2013 via advertisements in the local media and presentations at the local Alzheimer Family Association.

ii) Study subjects

(1) Inclusion criteria

The local Ethics Committee approved the study protocol and all subjects gave written informed consent consisted of general consent of the study, collection and storage of biological and genetic samples and consent to MRI. All participants were invited for lumbar puncture and cerebrospinal fluid (CSF) sample donation. Those subjects who chose not to participate in this procedure not have been excluded. A 50% of the samples are people with a history of dementia by EA in first-degree relative (father and / or mother and / or sister). Other 50% of the samples will no history of EA in the family (both parents have reached the age of 70 years without developing symptoms of AD). There were availability of companion / reporting people.

(2) Exclusion Criteria

Criteria mild, moderate or severe dementia according to DSM-IV criteria and stadium CDR people ≥ 1. Background of significant neurological disease of any kind that might cause cognitive impairment dementia. The history of symptomatic stroke that has left no significant cognitive sequelae (e.g. aphasia) is not an exclusion criterion. Background of diagnosed psychiatric illness that could cause dementia cognitive impairment. No people with mild

psychiatric symptoms (anxiety, depression) that do not constitute a specific diagnosis are excluded. Severe or uncontrolled systemic-disease that can cause cognitive impairment or dementia may restrict participation. Sensory longitudinal follow limitation, blindness or deafness, any significant limitation (severe aphasia, excessive anxiety, lack of fluency study / sufficient understanding in basque or castilian) for the administration of cognitive tests. Contraindication for MRI study: pacemakers, other metallic stents contraindicated, shrapnel, claustrophobia, and extensive tattoos. Negative to sign the informed consent.

iii) Study variables **(Table 13).**

(1) Clinical data.

(2) Neurocognitive data

(3) Neuroimaging data

(4) Genetic and epigenetic data

(5) CSF data

iv) Blood, plasma and serum data.

Table 13- Study variables

Study Variables
Clinical Data

Demographic variables
 	
     1. Age (years)
     2. Sex (Male/Female)
     3. Education level
     4. Years of schooling
     5. Profession exercised
     6. Index of Social Position Hollinghead

Vascular Risk Factors (structured interview).   1. Hypertension (criteria of the guidelines of the European

_____

Society of Hypertension, 2005)
2. Hypercholesterolemia (NIH criteria-National Heart, Lung, and Blood Institute, 2001)
3. Diabetes and pre-diabetes (type and type criteria of the American Diabetes Association, 2010).
4. Alcohol consumption (measured by survey methodology National Health)
5. Snuff consumption (measured according to the methodology of the national health survey)
6. Heart disease (ischemic, heart insufficiency, valve disease, arrhythmia, cardiac surgery and type)
7. Peripheral arterial disease (ankle-brachial index)
8. Syncope

Personal and family medical history (structured interview).
1) Neurological
2) Psychiatric
3) Nephro-urological
4) Digestive
5) Trauma
6) Rheumatic or autoimmune
7) Respiratory
8) Infectious (including banal infections, with particular emphasis on herpes).

Family history (structured interview)
1) Dementia (dementia type, age of onset) Psychiatric
2) Current symptoms (structured interview) Dementia (dementia type, age of onset) Psychiatric
Neurocognitive data
1. General: Mini-Mental State Examination (MMSE)
2. Vocabulary test (WAIS-III)
3. Verbal memory

4. Visual memory
5. Language
6. Visual perceptive skills capacity
7. Visual constructional ability
8. Attention and executive functions
9. Semantic verbal fluency
10. Phonetic verbal fluency
11. Tracking test (trail making) A and B;
12. Test key numbers (WAIS-III)
13. Stroop test
14. Zoo test
15. Plane (behavioural assessment of the dysexecutive syndrome, BADS)
16. Praxias (apraxia subscale of the WAB).

Neuroimaging data	
	(1) Voxels based morphometry (atrophy)
	(2) "Cortical Mapping / Cortical thickness" (regional study the thickness of the cerebral cortex

Genetic data	
	(1) APOE polymorphism

CSF data	
	(2) Levels of amyloid Aβ 1-42 (INNOTEST® ß-AMYLOID (1 -42)
	(3) Total tau protein levels (INNOTEST® htau Ag)
	(4) Phosphorylated tau protein levels (INNOTEST® PHOSPHO-TAU P)

Blood, plasma and serum data	
	(1) Cholesterol; HDL
	(2) LDL
	(3) Fasting glucose, Glycosylated hemoglobin
	(4) Insulin
	(5) β-amiloide 1-40(ABTest® Araclon-Biotech)

(6)   β-amiloide 1-42 and plasma (ABTest® Araclon-Biotech)

(7)   C reactive protein

(8)   Homocysteine

(9)   Folic acid,

(10)   Vitamin B12

b) MRI

i) Acquisition protocol

Whole-brain scans were obtained using a 3 T scanner (Siemens Magnetom Tim Trio) using a 32-channel head coil. Isotropic structural 3D T1-weighted images were acquired using a sagittal magnetization prepared rapid acquisition gradient echo (MPRAGE) sequence (1.25 mm x 1.25 mm x 1.25 mm voxels, repetition time (TR) = 2300 ms, echo time (TE) = 2.86 ms, inversion time (TI) = 900 ms, flip angle = 9 degrees), which were used for VBM analysis. A 2D fat-saturated FLAIR sequence (0.9 mm x 0.9 mm x 3 mm voxels, TR = 9000 ms, TE=79 ms, TI = 2500 ms) was acquired for the visual rating of white matter hyperintensities (WMH).

ii) Temporal (Scheltens-MTA) and parietal (PA-Koedam) scale atrophy

We use the isotropic structural 3D T1-weighted images were acquired using a sagittal magnetization prepared rapid acquisition gradient echo (MPRAGE) reformatted to the coronal plane through OsiriX: An open-source software for navigating in multidimensional DICOM images (166). The coronal plane perpendicular to the long hippocampus axis has been advocated as the best one to study the temporal lobe, although some authors have proposed the axial plane to the same purpose (7, 8). The Scheltens scale of medial temporal lobe atrophy was defined (5) using a coronal plane planned parallel to the brainstem axis that is the one we have used in our reading of images. Nevertheless, Hasboun *et al.* (7) tested three different volume-calculation protocols: (a) on sections from a coronal 3D acquisition not perpendicular to the axis of the

hippocampal formation (NOPERP protocol), (b) on sections obtained with the same acquisition but reformatted perpendicular to the axis of the hippocampal formation (REFOR protocol), and (c) on sections from a coronal 3D acquisition perpendicular to the axis of the hippocampal formation (PERP protocol), obtained with the patient's head tilted backward to obtain measurements of the volume of the hippocampal formations, an accurate 3D processing technique was used to segment the hippocampus. In all subjects, two hippocampal formation right-left asymmetry indexes were calculated by using each of the three protocols. They concluded that with the use of 3D acquisitions in the study of hippocampal formation biometry, different procedures lead to significant variations in the absolute values of the volume of the hippocampal formation. However, there is a strong correlation between the results obtained by each method (7). PA was scored on T1-weighted images viewed in the sagittal, axial and coronal planes (145).

iii) VBM postprocessing

(1) FIRST-Vertex

FIRST was used to segment the amygdala, hippocampus, from the in-painted T1. The reproducibility of FIRST has been previously reported (167-169). Voxel-wise statistics were conducted with randomise (170) function (FSL v5.0.5). Permutation-based nonparametric F-tests were performed within the framework of the general linear model (GLM) with TFCE (threshold-free cluster enhancement) (185, 186) and 5000 permutations. The resulting statistical maps, corrected for multiple comparisons with family wise error (FWE), where threshold at $p < 0.05$ and clusters of less than 100 voxels were excluded from the results.

(2) SPM

The structural 3D T1 images were segmented using the VBM8 toolbox (Gaser, Department of Psychiatry, University of Jena, Germany) as implemented in Statistical Parametric Mapping (SPM8; Welcome Department of Cognitive Neurology, London, UK) running in MATLAB 2011a (MathWorks Inc., Natick, MA, USA). Default parameters of VBM8 were used unless specified otherwise. The VBM8 toolbox provides an integrated pre-

processing pipeline for image segmentation including nonlinear DARTEL warping to Montreal Neurological Institute (MNI) space (171). Resulting grey matter (GM) images (1.5 mm^3 voxels) were modulated for non-linear effects only, compensating for volume changes during normalization while correcting for brain size. Images were smoothed using an isotropic Gaussian filter of 8mm full-width at half-maximum (FWHM). To limit the analysis to areas of GM, absolute threshold masking with a threshold of 0.2 was used. After processing, the quality of the segmentations was visually checked and none had to be excluded. Total GM, white matter (WM) and total intracranial volumes (TIV, i.e. GM + WM + CSF) were derived from segmented images in native space.

WMH were rated on FLAIR images using the three-point Fazekas scale ranging from 0 (no WMH) to 3 (large confluent areas of WMH). Severe WMH are (172) associated with increased brain atrophy (173) and can be a separate risk factor for dementia (174). Hence, Fazekas score was included as a covariate in the analysis (175).

(3) Free Surfer

Cortical reconstruction and volumetric segmentation was performed with the Free Surfer image analysis suite, which is documented and freely available for download online (http://surfer.nmr.mgh.harvard.edu/). Briefly, this processing includes motion correction and averaging (176) of multiple volumetric T1 weighted images (when more than one is available), removal of non-brain tissue using a hybrid watershed/surface deformation procedure (177) automated Talairach transformation, segmentation of the subcortical WM and deep GM volumetric structures (including hippocampus, amygdala, caudate, putamen, ventricles) (178, 179) intensity normalization (180), tessellation of the GM WM boundary, automated topology correction (181, 182), and surface deformation following intensity gradients to optimally place the grey/white and grey/cerebrospinal fluid borders at the location where the greatest shift in intensity defines the transition to the other tissue class (175, 183-185). Nowadays is common specialized software used when cortical thickness and volumetric measurements are required (186).

c) Laboratory

i) CSF biomarkers

We performed $A\beta_{1-42}$ (Innotest®), *tau* (Innotest®),*p-tau* (Innotest®) analysis at the Laboratory of Neurosciences of Hospital Sant Pau, Barcelona. Dr. Alberto Lleó (participates in the Alzhemimer's Association/JPNd quality control / standardization program of CSF biomarkers). The Innotest® $A\beta_{1-42}$ is a solid-phase enzyme immunoassay for the quantitative determination of β-amyloid$_{(1-42)}$ in human CSF. The combined use of CSF-Tau and CSF-β-amyloid$_{(1-42)}$ marker concentrations allows differentiation between AD and normal aging or other neurological diseases such as depression (175, 187-191). The cut-off value used to classify subjects as positive or negative regarding CSF beta-amyloid levels is 580pg/ml (values below this cut-off are positive).

ii) APOE

*APOE*4 genotype was determined using one-stage PCR as previously described (175, 192), and dichotomized as no *APOE*4 allele (*APOE*4-) or at least one *APOE*4 allele (*APOE*4+).

d) Cognitive test

In order to check that the distribution of scores is approximately normal, the Kolmogorov-Smirnov test was applied. If the Kolmogorov-Smirnov test was significant, three groups were compared with the Kruskal-Wallis test. If not, they were compared with ANOVA. These results are non adjusted for multiple comparisons (due to the fact of being exploratory analyses) (175). Several domains have been analysed:

i) Memory

(1) Verbal: TAVEC-CVLTT Spanish version (193)

(2) Visual-Rey complex figure (194-196)

(3) Semantic: Vocabulary WAIS-III, memory alteration test (197).

ii) Language

   (1) Boston naming test (198-200)

iii) Visual perception and praxis

   (1) Rey complex figure (194-196)

   (2) Judgement line orientation (201-203)

   (3) Poppelreuter (The 15-object test) (20)

iv) Attention and executive Functions

   (1) Verbal fluency test (204-206)

   (2) Digital span (WAIS-III) (207-209)

   (3) Stroop test (210-212)

   (4) Trail making test (208, 209)

   (5) Zoo map test (BADS)(213)

   (6) Symbol digit-coding (WAIS-III)(207).

v) General

   (1) MMSE (214)

   (2) CDR (215)

4- RESULTS

a) GAP epidemiological variables analysis.

The GAP cohort population consisted of 482 healthy volunteers between 39 and 79 years were recruited between June 2011 and January 2013 via advertisements in the local media and presentations at the local Alzheimer Family Association. Seventy two subjects moved off GAP voluntarily, 6 were excluded for performing a MMSE>26 and additional 44 more for having a low quality 3D T1-MPRAGE study (due to low signal to noise ratio or movement artefacts). The final total amounts of healthy volunteers whose structural MR studies are acceptable for analysis are 360. Three hundred thirty five out of 360 showed dexterity, 8 were left-handed, 12 ambidextrous, 5 left-handed corrected. Bearing in mind the GAP volunteers who accepted the CSF lumbar puncture we obtained 213 healthy volunteers with MMSE>26, 199 of whom showed CDR of 0.

Table 14- MMSE the subjects might perform

MMSE	30-27 without impairment
	25-26 possible impairment
	24-10 mild-moderate AD
	9-6 moderate-severe AD
	<6 severe AD

Table 15- CDR the subjects might perform

	0 without risk
	0,5 MCI
	1 mild AD
	2 moderate AD
	3 severe AD

Finally studied by their APOe genes expression they displayed the following distribution **(Table 16):**

Table 16- APOe genes expression the subjects show

Risk Levels	APOe	Female	Male
Normal risk	3/3	142	99
Increase risk	3/4	454	40
High risk	4/4	4	1
Low risk	2/3	15	12
No data		2	
Total			**360**

b) First analysis temporal and parietal scale vs. high / low APOe risk

The first analysis we performed was to test if the Scheltens (MTLA-scale) or the parietal atrophy scale (Koedam) applied to the GAP cohort were able to classified the healthy volunteers by their APOe gene expression AD risk levels.

As it is shown at **Tables 17-18** the vast majority of the GAP subjects were graded G0 & G1 in both scales

Table 17- Distribution displayed by the GAP cohort classified following Scheltens (MTLA-scale)

Sheltens MTA	G0	G1	G2	G3	G4
Left	198	154	6	1	1
Right	150	205	5	0	0

Table 18- Distribution displayed by the GAP cohort classified following parietal atrophy scale (Koedam)

Koedam Parietal	G0	G1	G2	G3
Left	190	141	28	1
Right	202	128	26	4

The next analysis we performed was to identify covariates (besides APOe genes expression) to take into account in our analysis. With this aim we performed a T-Test **(Tables 19-23).**

Table 19- Covariate Age statistical significance

AGE	Mean	St-dev	Lower	Upper	Sig (2t)
APOe 3/3 N=214	57,27	7,097	56,41	58,25	
APOe 3/4 N=85	55,91	6,900	54,43	57,47	
Total N=326					0.123

Table 20- Covariate Sex statistical significance

Sex	Mean	St-dev	Lower	Upper	Sig (2t)
APOe 3/3 N=214	0,59	0,493	0,53	0,65	
APOe 3/4 N=85	0,53	0,502	0,42	0,63	
Total N=326					0.344

Table 21- Covariate Educational level statistical significance

Edu-level	Mean	St-dev	Lower	Upper	Sig (2t)
APOe 3/3 N=214	13,95	3,578	13,54	14,40	
APOe 3/4 N=85	13,89	3,745	13,06	14,72	
Total N=326					0.898

Table 22- Covariate MMSE statistical significance

MMSE	Mean	St-dev	Lower	Upper	Sig (2t)
APOe 3/3 N=214	28,63	1,155	28,47	28,78	
APOe 3/4 N=85	28,88	1,085	28,66	29,11	
Total N=326					0.073

Table 23- Sum up covariate statistical significance

Apoe	Age	Sex	Edu	MMSE
Sig (2t)	0,123	0,344	0,898	0,073

As it is shown at **Tables 19,20,21,22 & 23 there** were no statistical significance correlation of covariates of Age, Sex, Educational level and MMSE with respect to the Apoe risk expressions

The following analysis we performed was a Chi^2 analysis for studying the distribution of the normal APOe risk volunteers (3/3) vs increase APOe risk volunteers (3/4) into the different Scheltens (MTA-scale) or the parietal atrophy scale (Koedam) grades **(Tables 24-28).**

Table 24- Chi^2 analysis for studying the distribution of the normal APOe risk volunteers (3/3) vs increase APOe risk volunteers (3/4) into the different left parietal atrophy scale (Koedam) grades.

Left Parietal	0	1	2	3	Sig (2t)
APOe 3/3 N=214	124 (57,9%)	95 (44,3%)	21 (9,8%)	1 (0,4%)	
APOe 3/4 N=85	48 (56,4%)	31 (36,4%)	6 (7%)	0 (0%)	0.801
Total N=326	172	126	27	1	

Table 25- Chi² analysis for studying the distribution of the normal APOe risk volunteers (3/3) vs increase APOe risk volunteers (3/4) into the different right parietal atrophy scale (Koedam) grades

Right Parietal	0	1	2	3	Sig (2t)
APOe 3/3 N=214	130 (60,7%)	84 (39,2%)	23 (10,7%)	4 (1,8%)	
APOe 3/4 N=85	49 (57,6%)	34 (40%)	2 (2,3%)	0 (0%)	0.801
Total N=326	179	118	25	4	

Table 26- Chi² analysis for studying the distribution of the normal APOe risk volunteers (3/3) vs increase APOe risk volunteers (3/4) into the different left Scheltens (MTLA-scale)

Left Temporal	0	1	2	3	4	Sig (2t)
APOe 3/3 N=214	124 (57,9%)	109 (50,9%)	6 (2,8%)	1 (0,4%)	1 (0,4%)	
APOe 3/4 N=85	58 (68,2%)	27 (31,7%)	0 (0%)	0 (0%)	0 (0%)	0.068
Total N=326	182	136	6	1	1	

Table 27- Chi² analysis for studying the distribution of the normal APOe risk volunteers (3/3) vs increase APOe risk volunteers (3/4) into the different right Scheltens (MTLA-scale)

Right Temporal	0	1	2	3	4	Sig (2t)
APOe 3/3 N=214	104 (48,5%)	132 (61,6%)	5 (2,3%)	0 (0%)	0 (0%)	
APOe 3/4 N=85	33 (38,%)	52 (61,1%)	0 (0%)	0 (0%)	0 (0%)	0.286
Total N=326	137	184	5	0		

Table 28- Sum up of statistical significance obtained performing a Chi² analysis for studying the distribution of the normal APOe risk volunteers (3/3) vs increase APOe risk volunteers (3/4) into the different Scheltens (MTLA-scale) or the parietal atrophy scale (Koedam) grades both sides (right and left).

APOe 3/3 vs APOe 3/4	Scheltens Left temporal	Koedam Right parietal
Sig(2t)	0,068	0,099

As it is shown at **Tables 24-28** there were no statistical significance correlation of a Chi² analysis for studying the distribution of the normal APOe risk volunteers (3/3) vs increase

APOe risk volunteers (3/4) into the different Scheltens (MTLA-scale) or the parietal atrophy scale (Koedam) grades.

The last analysis we performed was an ANCOVA (analysis of covariance) for studying the multiple variable effects of MMSE and APOe in left Scheltens (MTLA-scale) and the right parietal atrophy scale (Koedam) grades **(Tables 29a and 29b).**

Table 29a- ANCOVA-analysis-dependent variable: Right parietal

Source	Type III Sum of Squares	df	Mean Square	F	Sig.
Corrected Model	3,206[a]	4	,802	1,747	,139
Intercept	,021	1	,021	,045	,832
MMSE total	,217	1	,217	,474	,492
APOEcode_partic	3,008	3	1,003	2,186	,089
Error	161,956	353	,459		
Total	266,000	358			
Corrected Total	165,162	357			

Table 29b- ANCOVA-analysis-dependent variable: Left temporal

Source	Type III Sum of Squares	df	Mean Square	F	Sig.
Corrected Model	3,254[a]	4	,814	2,473	,044
Intercept	,208	1	,208	,633	,427
MMSE total	,014	1	,014	,041	,840
APOEcode_partic	3,150	3	1,050	3,191	,024
Error	116,145	353	,329		
Total	203,000	358			
Corrected Total	119,399	357			

This last analysis reflects no effects demonstrated in terms of MMSE and APOE for the right parietal Koedam grades, but effects in terms of APOE for the left temporal.

c) Vertex analysis of GAP classified by Scheltens (MTA-scale).

A number of cases representative for the main Scheltens´grades were selected as reference. Due to the characteristics of the sample under study, the majority of the cases were classified as grades 0 and 1. Only a few cases belonged to grade 2 (n=5 for the right temporal, n=6 for the left temporal); grade 3 (n=1 for the left temporal) and grade 4 (n=1 for the left temporal) were only present in one case each grade that were pathological.

We analysed GAP subjects classified by Scheltens (MTA-scale) as grade 0 and grade 1 through Vertex analysis.

Three of subjects were removed from the original sample due to bad 3D T1 structural MRI in one case, being acquired with a different protocol in other case and a third case in which the process of segmentation was unsatisfactory. Five cases were removed for the Scheltens scale analysis for the right temporal (due to be graded 2 n=5) and 11 for the left temporal (due to be graded 2 n=6, graded 3 n=1, graded 4, n=1 and 3 in which the process of segmentation was unsatisfactory). The final number of subjects included in the analysis of the Scheltens MTA scale was 352 for the right temporal and 349 for the left temporal **(Table 30).**

Table 30- Scheltens MTA scale distribution right and left temporal

Scheltens (MTA-scale)	MTA 0 RT n=149, LT n=196	MTA 1 RT n=203, LT n=153
		MTA2 RT n=5, LT n=6
		MTA 3 LT n=1
		MTA 4 LT n=1

We found statistically significant clusters of voxels differentiating Scheltens (MTA-scale) grade 0 and grade 1 for the right and left hippocampus **(Tables 31 and 32), and (Figure-33).**

Table 31- Statistically significant clusters of voxels grade 0 vs grade 1 for right temporal

MTA-Shelten's Right Hippocampus, AGE-SEX Corrected	(941) 27, -10, -30 P=0,001	85% GM Hippocampus entorhinal cortex RH 67% GM Hippocampus subiculum RH 16% GM Hippocampus cornu ammonis RH

Table 32- Statistically significant clusters of voxels grade 0 vs grade 1 for left temporal

MTA-Shelten's Left Hippocampus, AGE-SEX Corrected	(705) -28, -7, -29 P=0,012	88% GM Amygdala_laterobasal group LH 48% GM Hippocampus subiculum LH 29% GM Hippocampus cornu ammonis LH
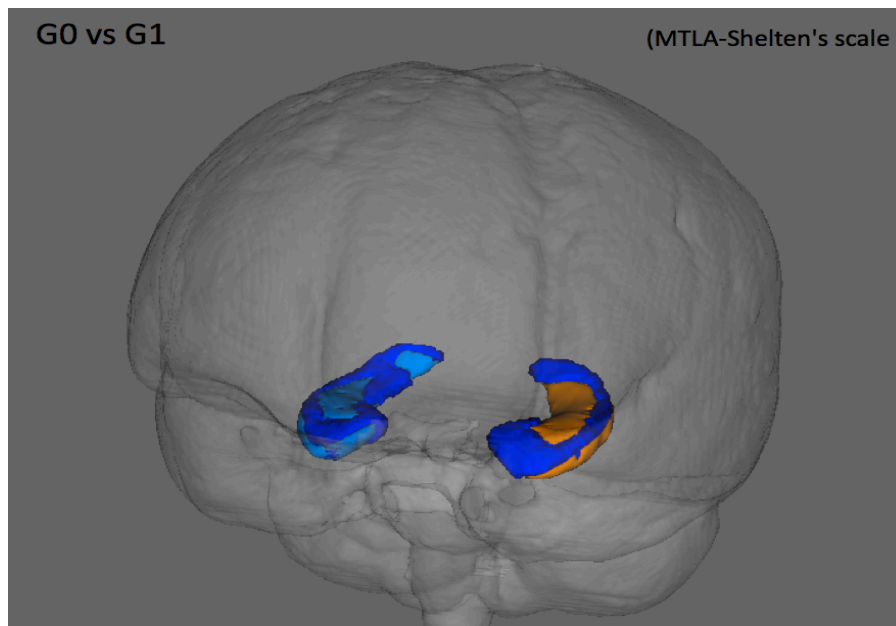
Figure 27- Statistically significant clusters of voxels grade 0 vs grade 1 both sides 3D model.

d) Early temporal lobe atrophy EMTA: Definition

Due to the fact that the Scheltens (MTA-scale) or the parietal atrophy scale (Koedam) applied to the GAP cohort were not able to classified succesfully the healthy volunteers by their APOe gene expression AD risk levels (only the ANCOVA analysis shows statistically significant results). And based on our observation on anatomical landmarks that surrounds the body of the hippocampus in grade 0 of Scheltens (MTA-scale) subjects (fimbria, choroidal fissure, lateral temporal horn and peritroncular fissure **(Figure 11, pp 66),** we proposed a new medial temporal lobe atrophy EMTA describing the variety of appearances of theses referred structures observed in GAP healthy cohort subjects **(Figure 28).** We establish besides the concordance between Scheltens (MTLA-scale) and the new new medial temporal lobe atrophy EMTA stages **(Figure 28).**
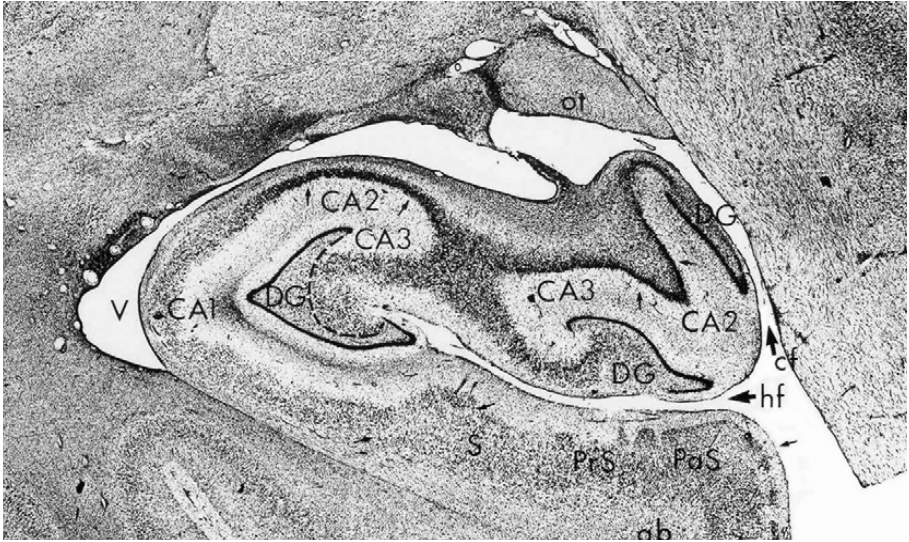
Figure 11-Anatomical landmarks that surrounds the body of the hippocampus (9).
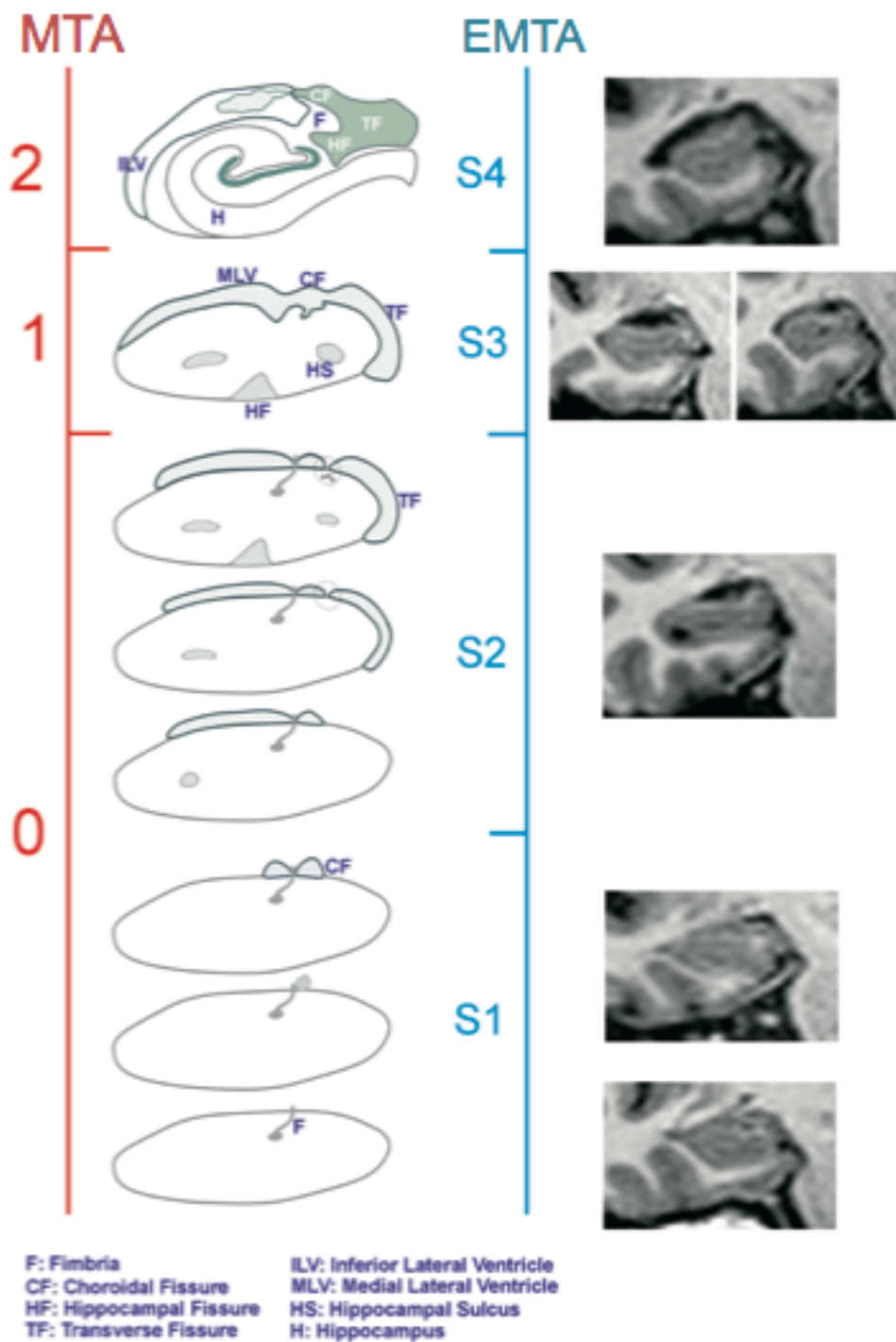
Figure 28-New medial temporal lobe atrophy EMTA describing the variety of appearances of these structures that surrounds the body of the hippocampus observed in GAP healthy cohort subject.

The description of the new medial temporal lobe atrophy **EMTA** based on strict anatomical criteria is as follows in **Figures- 29-34.**

S1 there is no dilation of the choroidal fissure or the temporal horn.
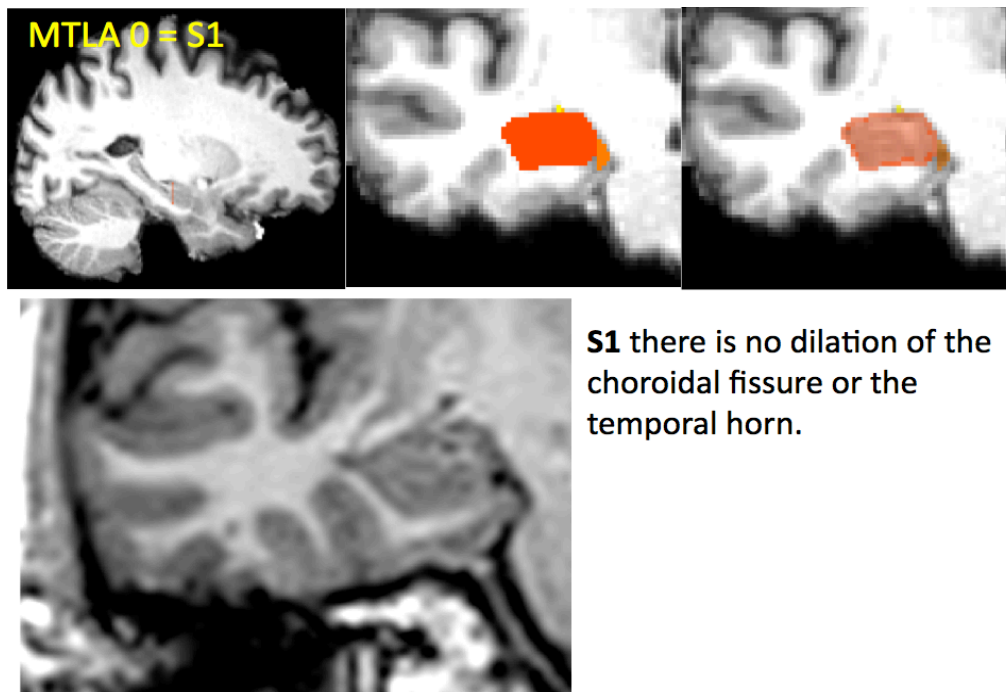
Figure 29- Description of the new medial temporal lobe atrophy EMTA stage S1.

S2 a focal dilation of the choroidal fissure medial to fimbria can be detected.
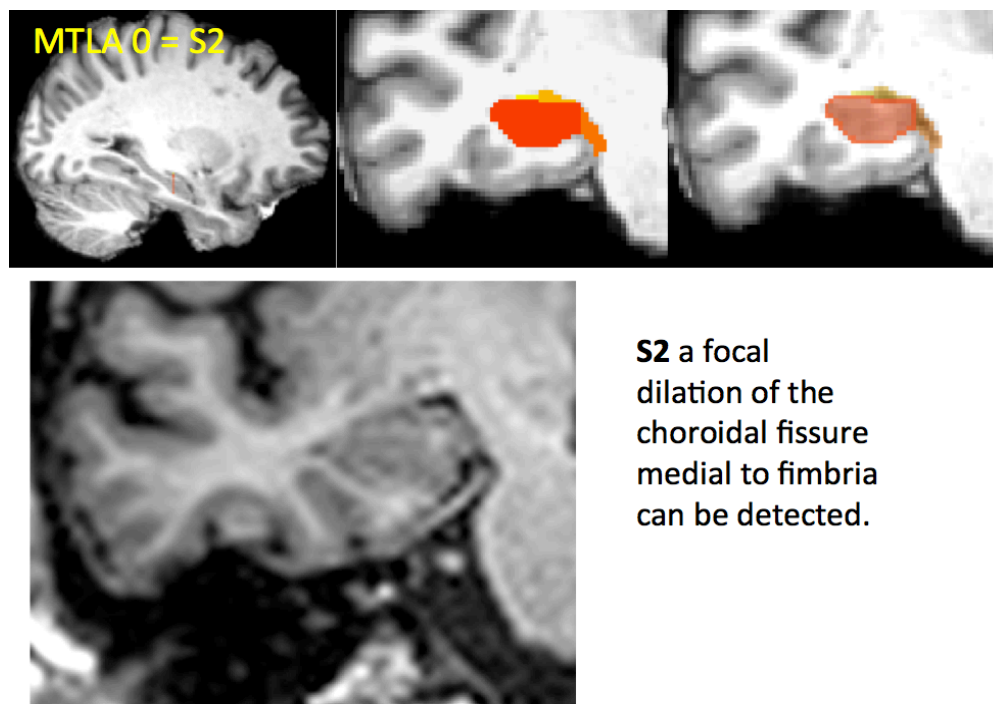
Figure 30- Description of the new medial temporal lobe atrophy EMTA stage S2.

S3 there is a focal dilation of the choroidal fissure and the medial temporal horn at both sides of fimbria that divide the CSF space above Hippocampus.
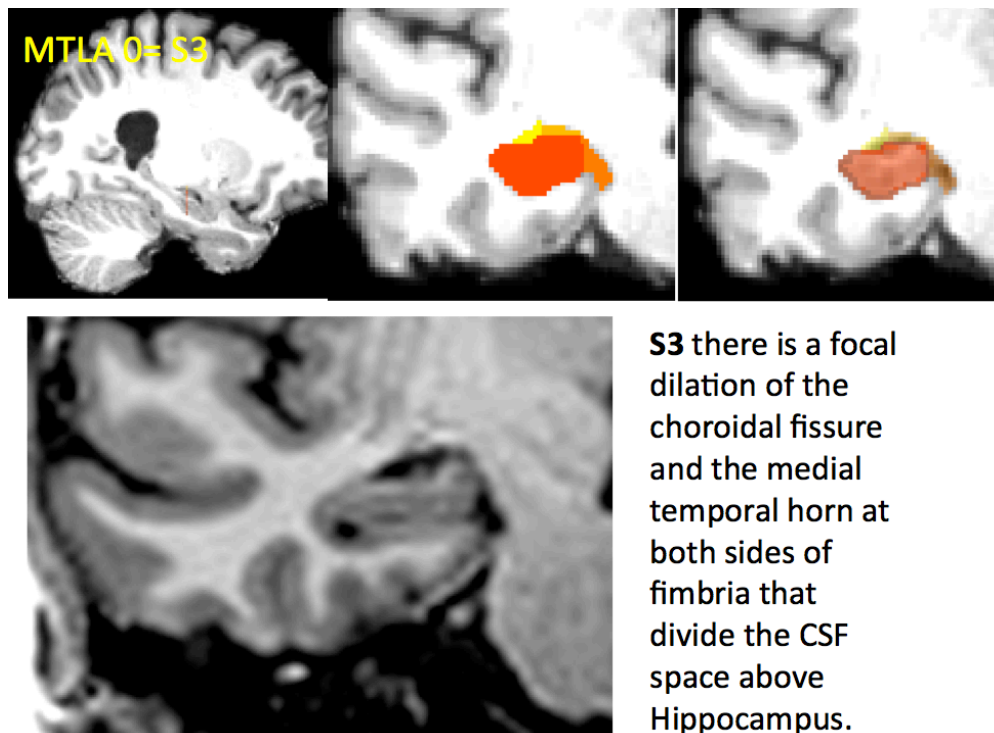
Figure 31- Description of the new medial temporal lobe atrophy EMTA stage S3.

S4 A There is a global dilation of the medial temporal horn. The choroidal fissure is placed medially. The SCF appear to represent one continuous space
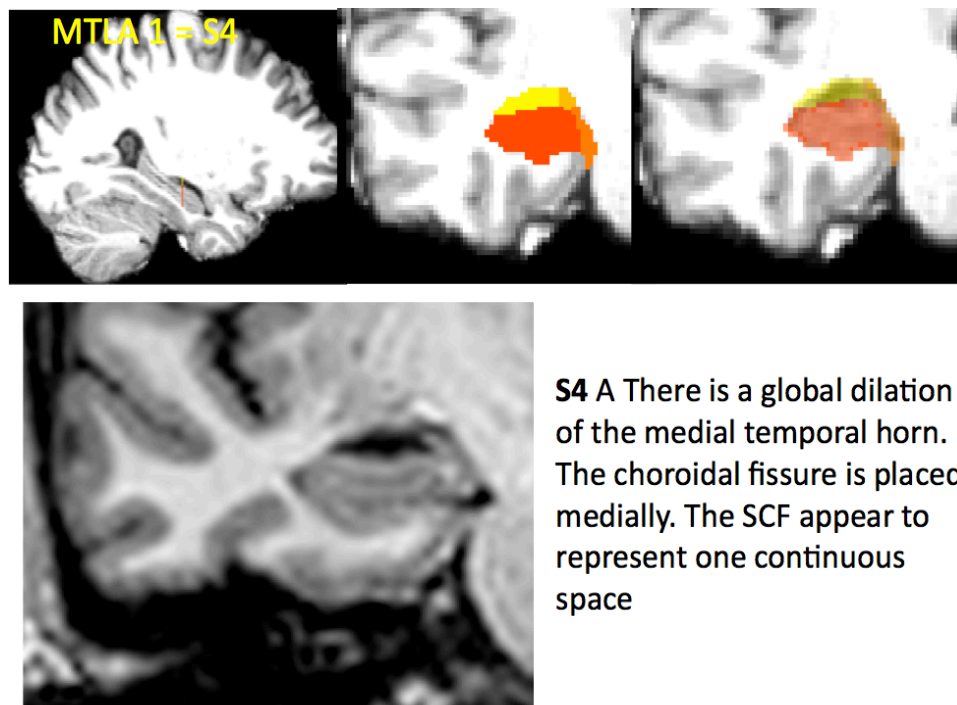
Figure 32- Description of the new medial temporal lobe atrophy EMTA stage S4.
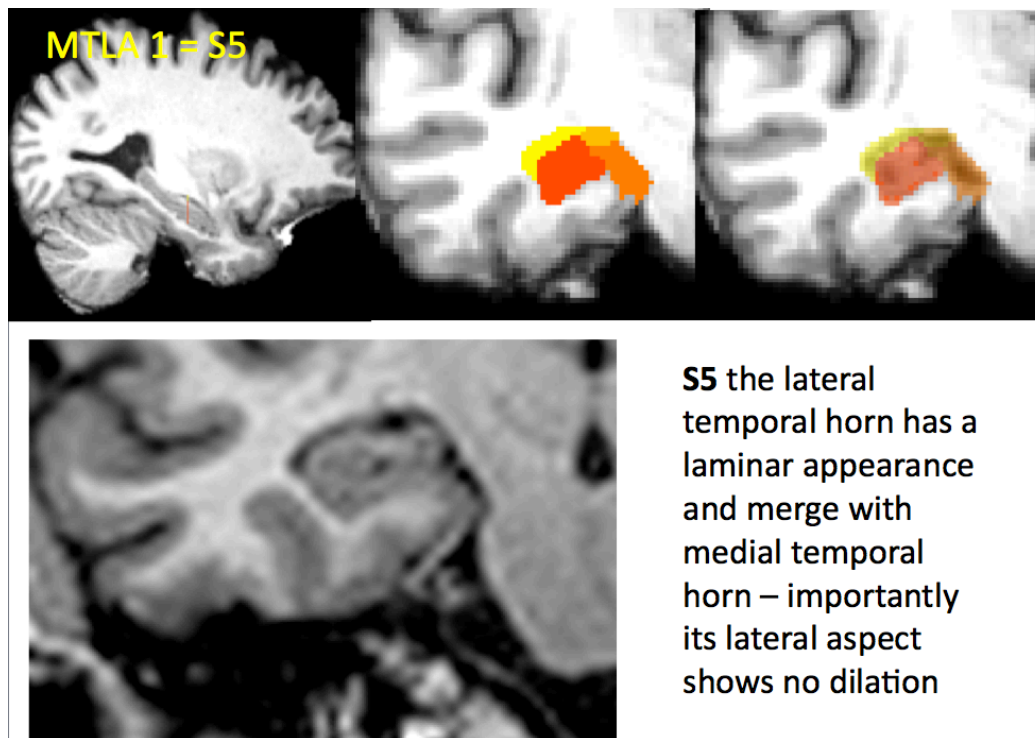
Figure 33- Description of the new medial temporal lobe atrophy EMTA stage S5.
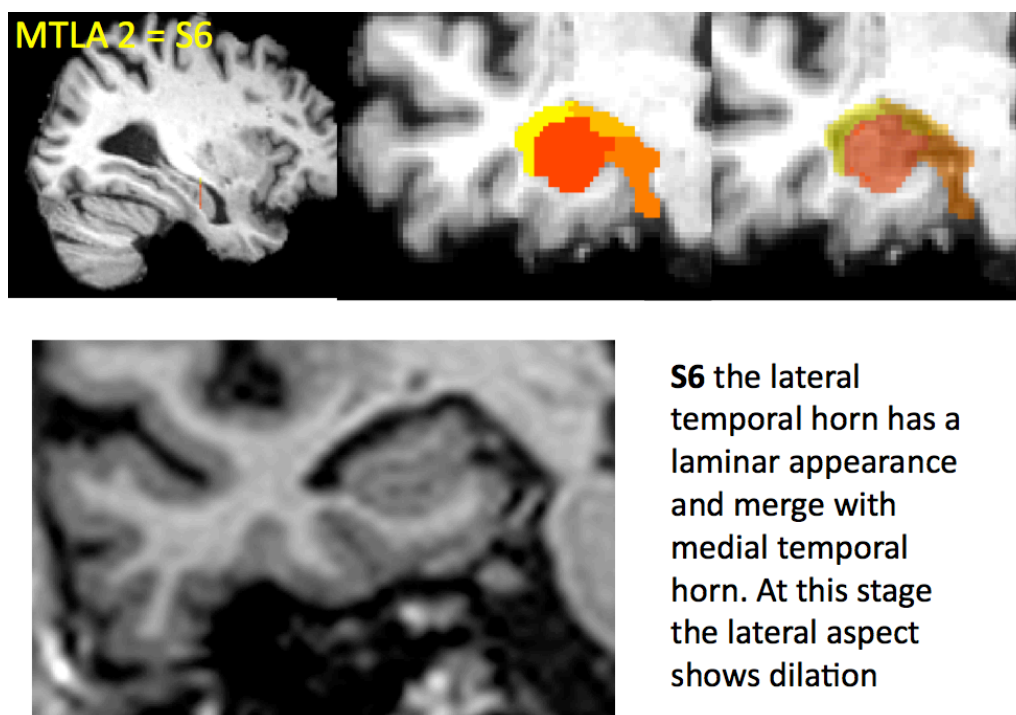
Figure 34- Description of the new medial temporal lobe atrophy EMTA stage S6.

e) Development of new EMTA$_6$ scale.

i) First step: Definition of stages EMTA$_6$ and its correlation with Scheltens MTA **(Figure-35)**.
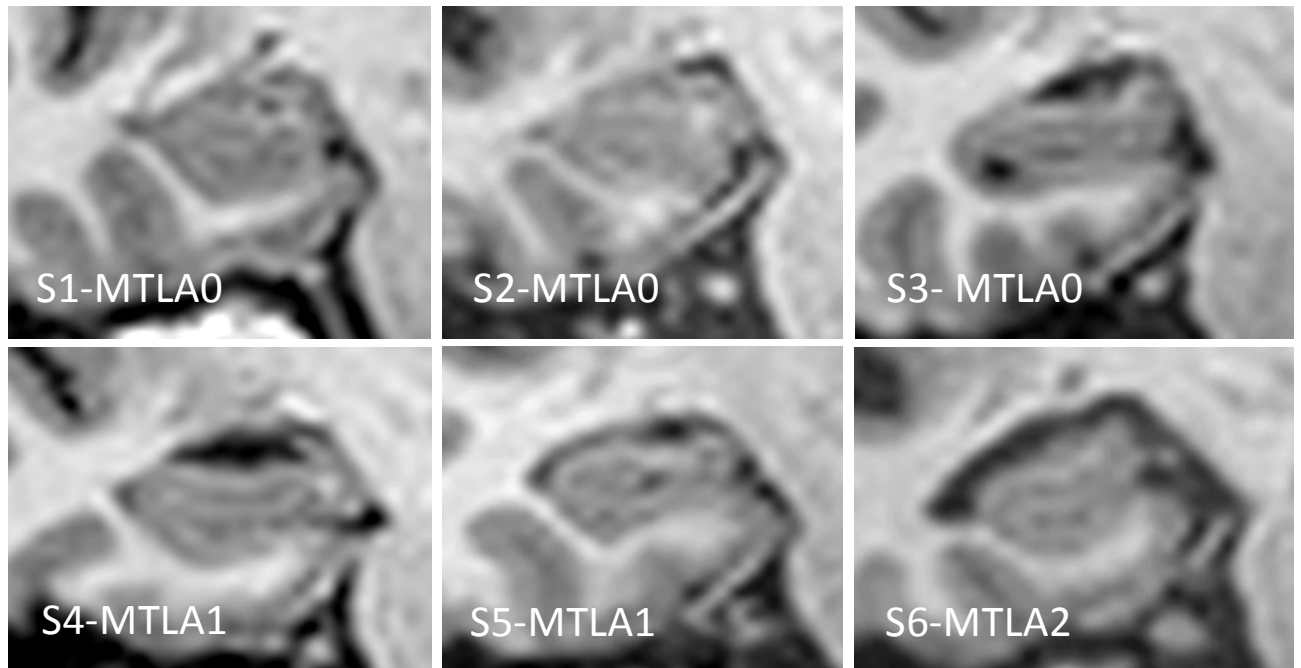
S1(no dilation Choroidal Fissure), S2 (focal dilation of Choroidal Fissure), S3 (focal dilation of Choroidal Fissure and medial temporal horn) all of them corresponding to Sheltens MTA 0. S4 (global dilation of the medial temporal horn over the body of the hippocampus) and S5 (Laminar apprearance of the lateral temporal horn with no dilation that merges with medial temporal horn) these stages correspond to MTLA 1. Finally S6 (Dilation of the lateral temporal horns that merges with medial temporal horn)

Figure 35- Definition of stages EMTA $_6$

After discussing on strict anatomical criteria the definitions of the new EMTA stages, we read again the former MTA ratings in the GAP cohort of healthy volunteers **(Table 33)**.

Table 33- Distribution of scores MTLA and EMTA S1-S6, and their correlation

MTLA	**MTLA** 0 RT n=149 LT n=196			**MTLA** 1 RT n=192 LT n=130	**MTLA 2*** RT n=10 LT n=18	**MTLA 3** LT n=1 **MTLA 4** LT n=1
EMTA	**S1** RT N=103 LT N=130	**S2** RT N=46 LT N=79	**S3** RT N=121 LT N=43	**S4** RT N=31 LT N=4	**S5** RT N=46 LT N=75	**S6** RT N=11 LT N=24

* MTLA ratings read again (former MTLA 1) after discussion on strict anatomical definitions (Amsterdam, March 2015).

Now we proceeded to validate by VBM-SPM8-tool-box analysis the 6 EMTA stages as we have defined them in **Table 34**.

Table 34- VBM EMTA$_6$ analysis characteristics

Separately for the right and left temporal lobe
• Full factorial design: 　1. One factor scale – 6 levels 　2. No covariates 　3. Inclusive mask temporal lobe 　4. Threshold for significance FEW<0,05

We began with the right temporal lobe **(Table 35).**

Table 35- VBM matrix and stage contrast applied in the EMTA $_6$ right temporal lobe analysis.

S1 n=103	S2 n=46	S3 n=121	S4 n=31	S5 n=47	S6 n=9	Contrast
1	-1					F contrast: overall effect of scale
	1	-1				
		1	-1			
			1	-1		
				1	-1	
1	-1					T contrast: S1 > S2
	1	-1				T contrast: S2 > S3
		1	-1			T contrast: S3 > S4
			1	-1		T contrast: S4 > S5
				1	-1	T contrast: S5 > S6

First, we studied the overall effect of the scale on the right temporal lobe **(Figure 36).**
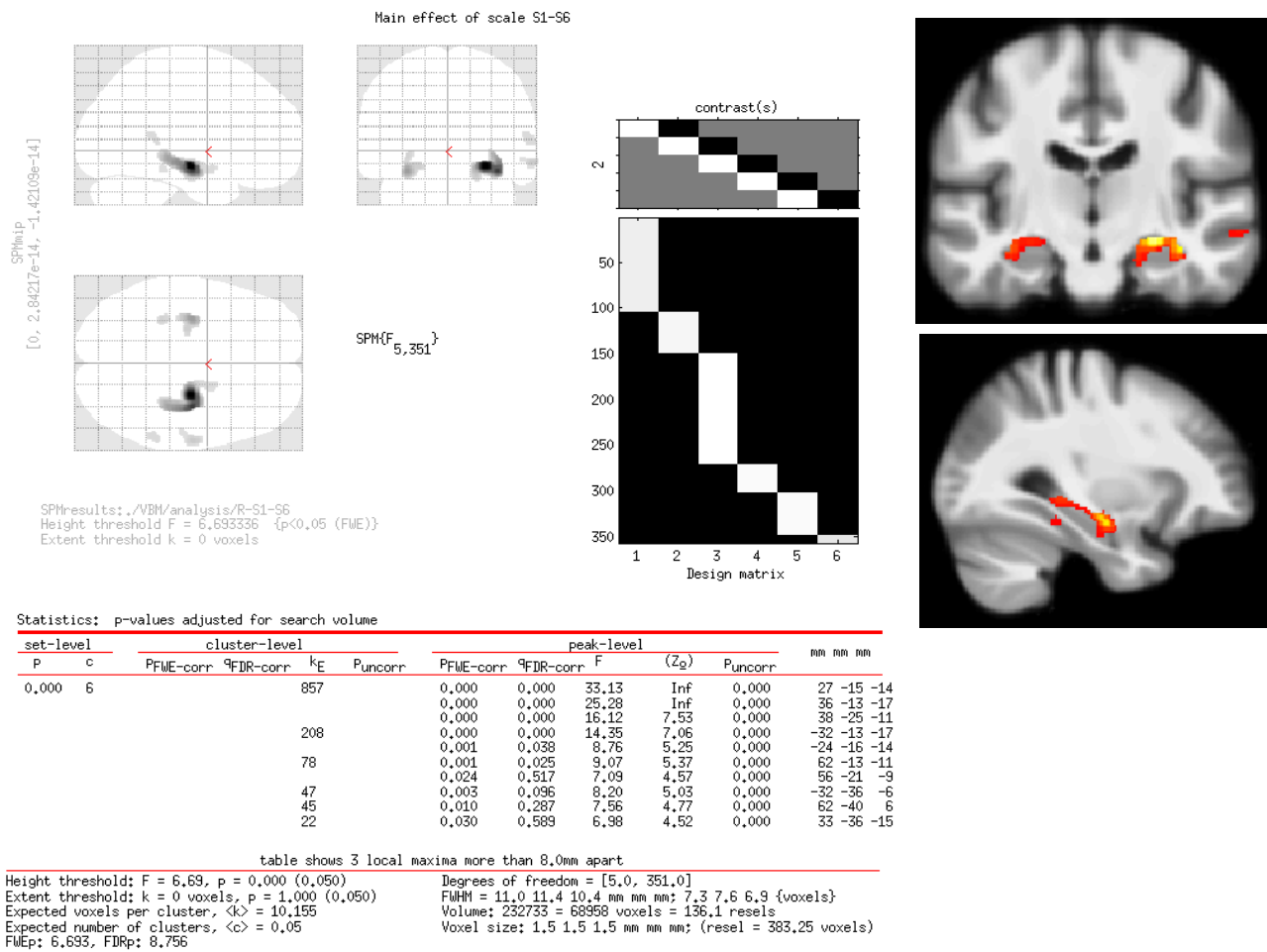
Figure 36- VBM the overall effect analysis of the EMTA $_6$ scale on the right temporal lobe. Area: cf,f mth,ilth and lth. Coordinates 27-15-11. Cluster Size 957. Pvalue (FEW, peak value) p<0,000. Z-value 7.53.

Secondly, we studied the differences on GM volume on the right temporal lobe among S1, S2, S3, S4, S5 and S6 EMTA stages **(Figure37).** The GM volume of stages S1, S2 and S2, S3 did not show statistically significant differences in terms of GM volume. On the other hand, the GM volume of stage S3 was greater than the one corresponding to stage S4 (mth, 27-15-14,80,p<0,001,7.08), the GM volume of stage S4 was greater than the one corresponding to stage S5 (ilth, 36-13-18,27,p<0,001,5.28), and finally the GM volume of stage S5 was greater than the one corresponding to stage S6 (lth, 34-12-17,68,p<0,001,5.79) **(Figure 37).**
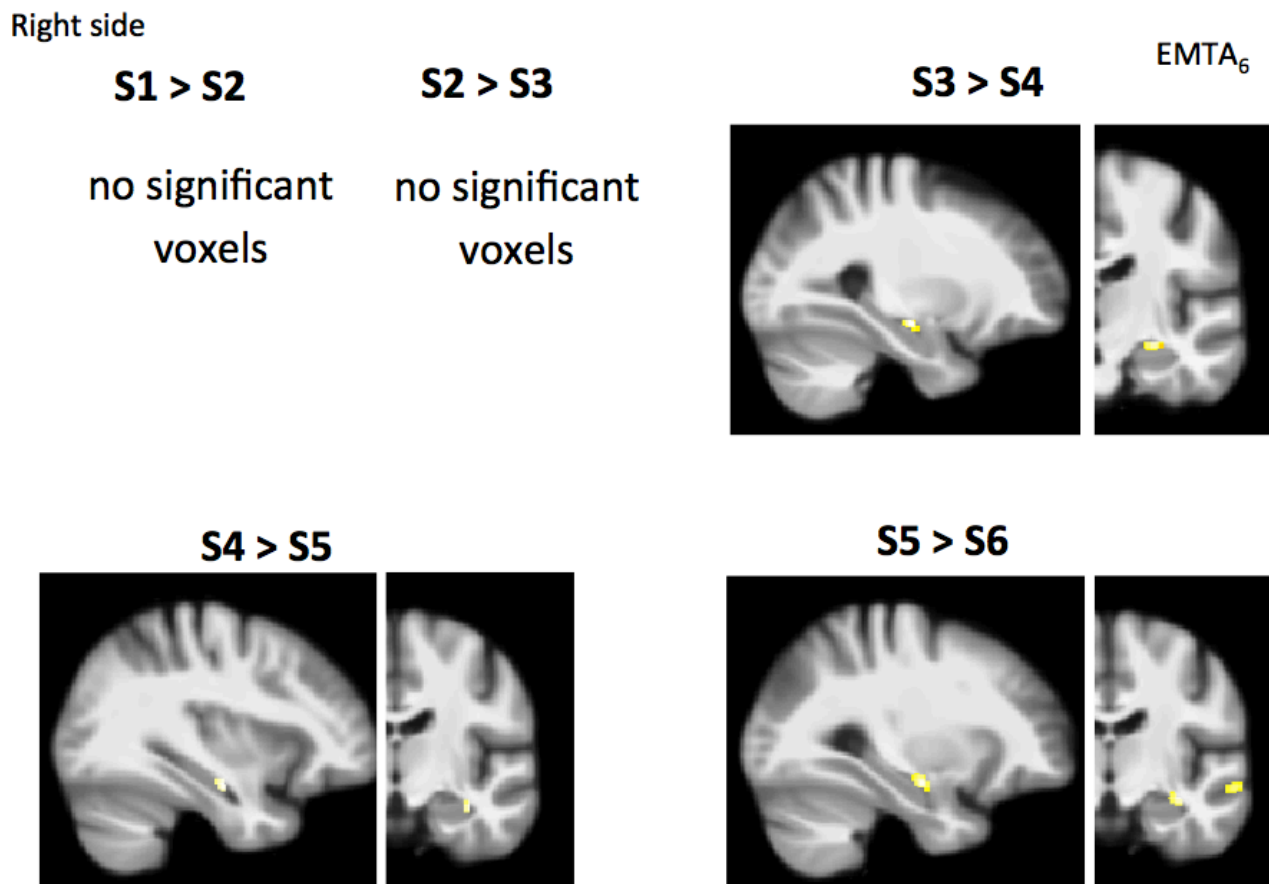
Figure 37- VBM differences on Grey Matter (GM) volume on the right temporal lobe among S1, S2, S3, S4, S5 and S6 EMTA$_6$ stages

Now we proceeded to validate by Free Surfer analysis the results obtained by SPM8-tool box EMTA$_6$ stages as we have defined them. Statistically significant differences were demonstrated between S1 and S3, S4, S5 and S6 (p<0,001); S2 and S3, S4, S5 and S6, (p<0,001); between S3 and S4 and S6 (p<0,001) and not significant between S3 and S5 (p<0,09); in terms of inferior lateral ventricle (temporal horn) volume. Statistically significant differences were demonstrated between S6 *vs.* S1, S2, S3, S4, and S5 in terms of hippocampus volume (p<0,001) **(Figure 38).**

Free surfer - right side
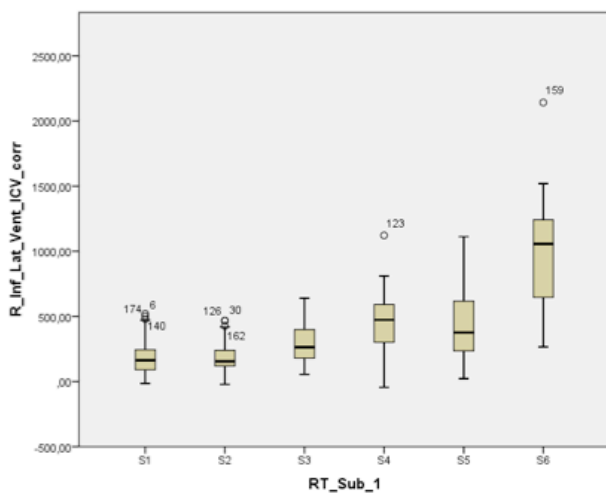
Inferior lateral ventricle   ## Hippocampal volume
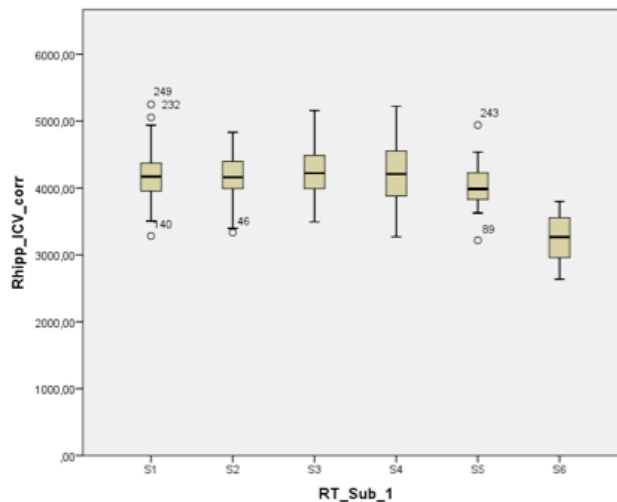
Figure 38- Free-Surfer differences on inferior lateral ventricle (temporal horn) volume and hippocampus volume on the right temporal lobe among S1, S2, S3, S4, S5 and S6 EMTA$_6$ stages

As a conclusion for this first step, the definitions of stages EMTA6 are summarized in **Table 36.**

Table 36- Definition of stages EMTA$_6$

Conclusions EMTA$_6$ right side
• **No significative statistical differences between S1 and S2 on VBM Grey matter analyses**
• **No significative statistical differences between S1 and S2 on inferior lateral ventricular and hippocampus volumes**

- **We decide to collapse S1 and S2 into a single stay that leads to new McTA$_5$**

ii) Second step: Volumetric biomarkers study of new EMTA$_5$ right sided.

After EMTA$_6$ analysis we decided to collapse the former S1-S2 stages giving as a result the new EMTA$_5$ scale **(Figure 39).**
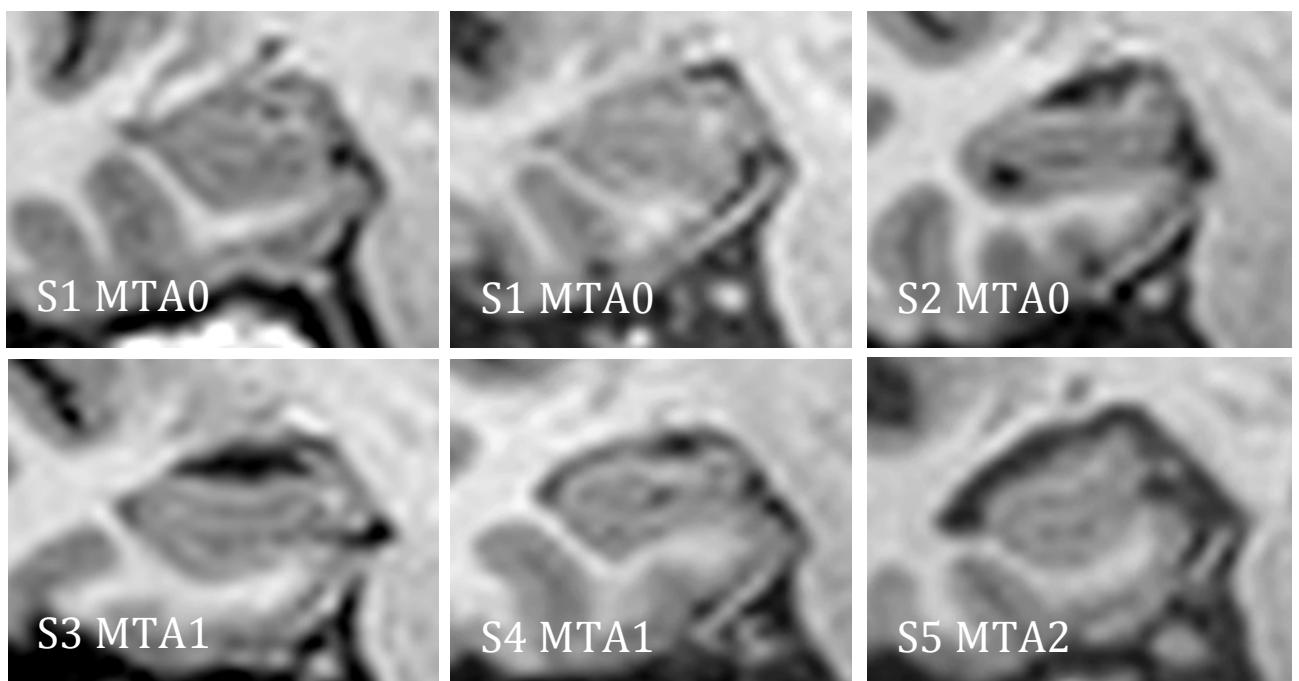
Figure 39- Definition of stages EMTA$_5$

We began with the right side **(Table 36)** volumetric studies. We proceed to validate by VBM-SPM8-tool-box analysis the 5 remaining EMTA$_5$ stages for the right side (after collapsing former S1 and S2) **(Table 37).**

Table 37- VBM matrix and stage contrast applied in the EMTA$_5$ rigth side analysis

S1& S2 n=149	S3 n=121	S4 n=31	S5 n=47	S6 n=9	Contrast Right Side
1	-1				F contrast: overall effect of scale
	1	-1			
		1	-1		
			1	-1	
1	-1				T contrast: S1&S2> S3
	1	-1			T contrast: S3 > S4
		1	-1		T contrast: S4 > S5
			1	-1	T contrast: S5 > S6

Firstly, we studied the overall effect of the EMTA$_5$ scale on the right temporal lobe that shows a huge number of voxel cluster illustrating the differences introduces by this new scale **(Figure 40).**

Figure 40- VBM the overall effect analysis of the EMTA₅ scale on the right temporal lobe. Area: cf,f mth,ilth and lth. Coordinates 27-13-14. Cluster Size 1105. Pvalue (FEW, peak value) p<0,000. Z-value 7.65

Secondly, we studied the differences on GM volume corresponding to the right temporal lobe among S1 & S2 vs, S3, S3 vs S4, S4 vs S5 and S5 vs S6 EMTA₅ stages **(Figures 41 and 42).** The GM volume of stages S1 and S2 collapsed was statistically significative greater than the GM volume of stage S3 (f, 27-15-14,41,p<0,001,5.89). The GM volume of stage S3 was also greater than the one corresponding to stage S4 (f-cf, 27-15-14,81,p<0,001,7.04). **(Figure 41).**

_____

Right side

GM S1&2 > S3

GM S3 > S4
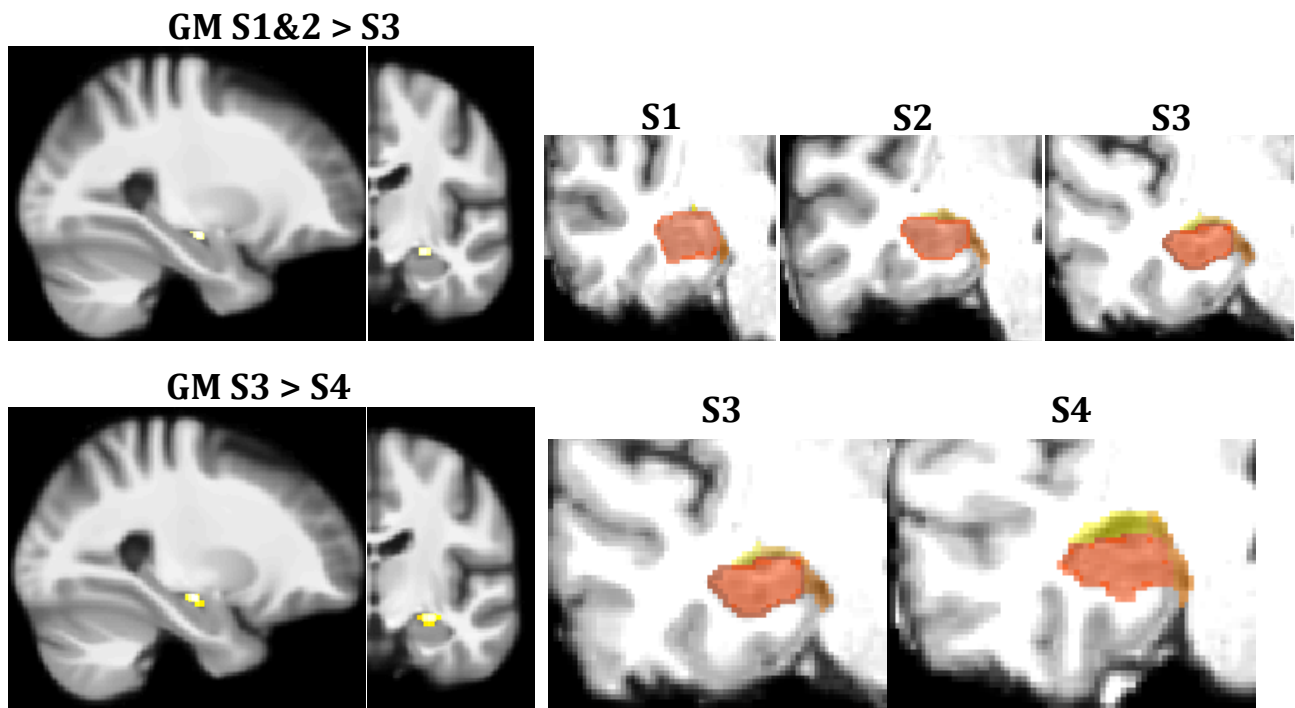
Figure 41- VBM differences on Grey Matter (GM) volume on the right temporal lobe among S1, S2 vs. S3, and S3 *vs.* S4 EMTA$_5$ stages

The GM volume of stage S4 collapsed was statistically significant greater than the GM volume of stage S5 (ilth, 36-13-18,27,p<0,001,5.29). The GM volume of stage S5 was also greater than the one corresponding to stage S6 (mth, 34-12-17,68,p<0,001,5.66) **(Figure 42).**

Right side
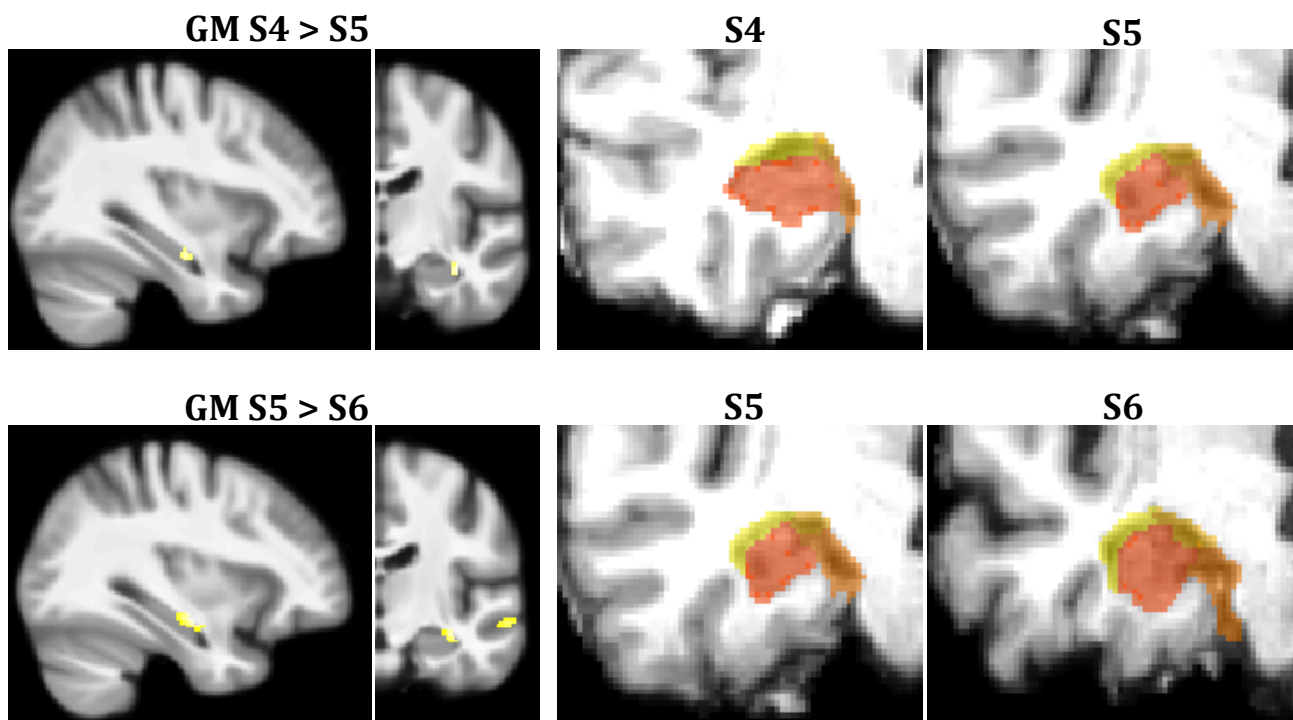
Figure 42- VBM differences on Grey Matter (GM) volume on the right temporal lobe among S4 vs. S5, and S5 *vs.* S6 EMTA$_5$ stages.

Now we proceed to validate by Free Surfer analysis the results obtained by SPM8-tool-box EMTA$_5$ stages as we have defined them **(Figure 39).** Statistically significant differences were demonstrated between S1 and S2 (collapsed) and S3, S4, S5, S6 (p<0,001), between S3 and S4, S5, S6 (p<0,001) and not significant between S3 and S4 (p<0,09) in terms of inferior lateral ventricle (temporal horn) volume. Statistically significant differences were demonstrated between S6 *vs.* S1, S2, S3, S4 and S5 (p<0,001) in terms of hippocampus volume **(Figure 43).**

_____

Free Surfer - right side

Inferior lateral ventricle   **Hippocampal volume**
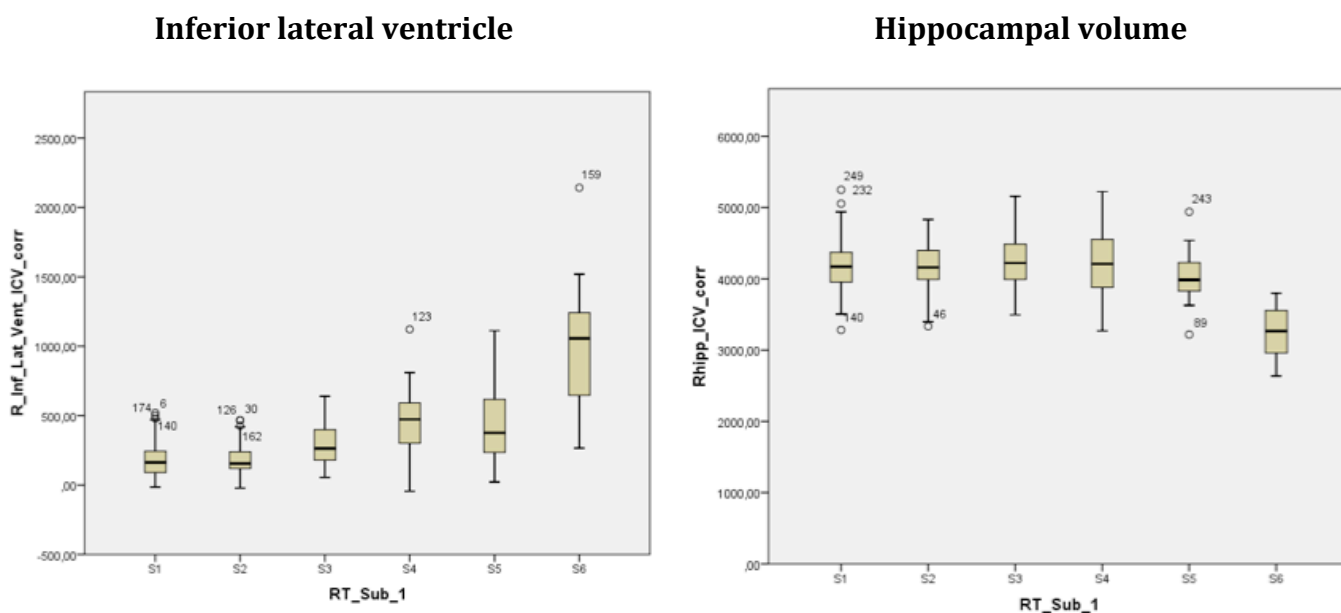
Figure 43- Free Surfer differences on the right temporal lobe between S1 and S2 (collapsed) and S3, S4, S5, S6 and between S3 and S4, S5, S6 in terms of inferior lateral ventricle (temporal horn) volume.

Analysed S4 and S5 stages of EMTA$_6$**,** we realised that there were clusters of voxels indicating GM volume S4 is greater than S5 (ilth, 36-13-18,27,p<0,001,5.29) and others clusters of voxels showing the contrary (fimbria 28-15-12,7,p<0,01,4.73) (**Figure 44).** In addition to the fact that inferior lateral ventricular volume and hippocampus volume were in reality almost the same between S4 and S5 of EMTA$_6$. So one question come out: Are S4 and S5 consecutive stages or parallel paths from S3 to S6?. Additionally there were no significante clusters that indicates S6 > S5 and S4 > S3.

Figure 44- S4 and S5 right side EMTA $_6$

GM S4 > S5   **GM S5 > S4**
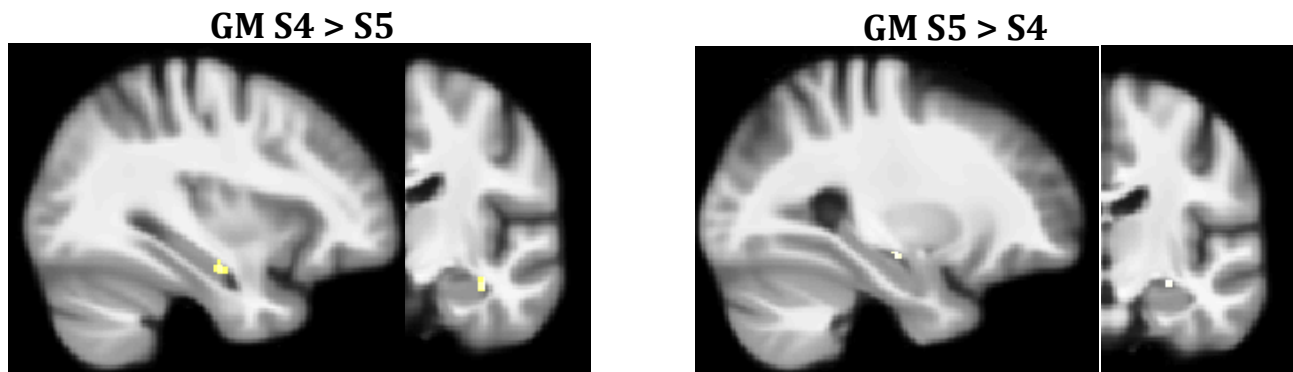
When we tried to validate by VBM-SPM8-tool-box analysis the 6 $EMTA_6$ stages for the left side **(Table 38)** we found that no analysis was possible for subgroup S4. Otherwise other VBM results were comparable to that obtained for the right side.

Table 38- VBM matrix and stage contrast that it can be applied in the $EMTA_6$ left temporal lobe analysis.

S1 n=130	S2 n=79	S3 n=46	S4 n=3	S5 n=75	S6 n=24	Contrast
1	-1					F contrast: overall effect of scale
	1	-1				
		1	-1			
			1	-1		
				1	-1	
1	-1					T contrast: S1 > S2
	1	-1				T contrast: S2 > S3
		1	-1			T contrast: S3 > S4
			1	-1		T contrast: S4 > S5
				1	-1	T contrast: S5 > S6

➹No analysis possible for subgroup S4. Other VBM results comparable to right side

As its shown at **Table 38** Left $EMTA_6$ no leads to Left $EMTA_5$ due to the small number of S4 subjects found n=3

As a conclusion for this second step, the definition of stages $EMTA_4$ is summarized in **Table 39.**

Table 39- Definition of stages EMTA₄

Conclusions EMTA₅ right side
Should we further collapse the scale (S4 and S5)? Yes
How do S4 and S5 relate each other?   **Why? Because VBM shows significant clusters both ways. Inferior lateral ventricular volume and hippocampal volume same in S4 and S5. Collapse**
How to deal with CSF and neuropsychological comparisons for left side EMTA₆ with (S4 N=3)? Collapse

iii) Third and final step: Comparison of CSF and cognitive biomarkers: Study of the new EMTA ₄: A suitability study.

After $EMTA_5$ analysis we decided to collapse the former S4-S5 stages giving as a result the new EMTA ₄ scale **(Figure 45)**.
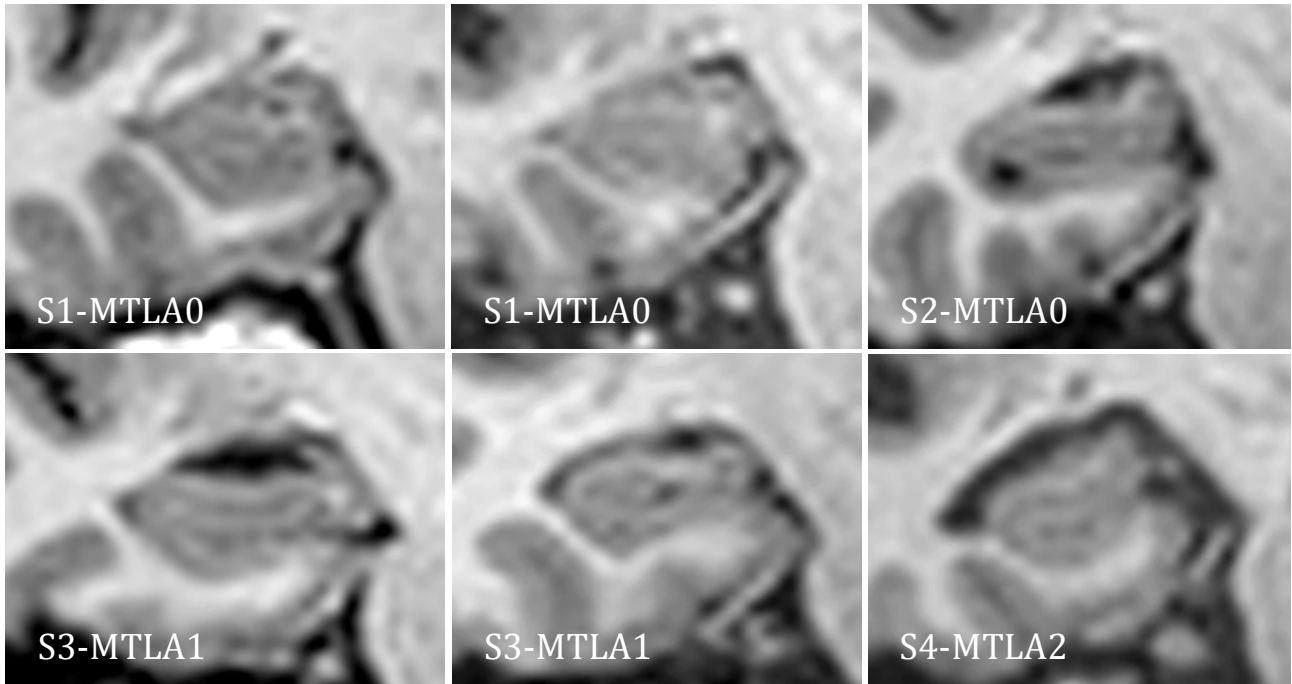
Figure 45- Definition of stages EMTA$_4$

We began making an exploratory comparative analysis of the CSF biomarkers with the stages corresponding to the EMTA$_4$ scale at the right side **(Table 40).** We could observe how there was a statistically significant difference related to the mean age between S4 and S1, S2 and S3 groups. Moreover, there were statistically significant differences in CSF A$\beta_{1\text{-}42}$/tau biomarker between all groups (p<0,001) and also between S1 vs. S4 (p<0,002), S2 vs. S4 (p<0,012) and S3 vs. S4 (p<0,016). When we studied the CSF A$\beta_{1\text{-}42}$/p-tau biomarker there were a statistically significant differences between all groups (p<0,0245) and between to S1 and S4 (p<0,0017) **(Table 40).**

Table 40-Exploratory comparative analysis of the CSF biomarkers with the stages corresponding to the EMTA $_4$ scale at the right side

	S1		S2		S3		S4	
n	92		73		40		8	
	mean	**SD**	**mean**	**SD**	**mean**	**SD**	**mean**	**SD**
Age	56,5	6,7	57,2	6,6	57,8	6,7	68,1*	7,0
CSF Aβ$_{1-42}$	837,1	204,5	838,4	229,5	814,0	207,1	663,6	317,5
CSF Tau	211,4	82,4	234,2	98,4	212,5	79,5	290,8	125,0
CSF p-tau	40,9	13,0	45,2	16,2	42,1	12,8	50,1	15,6
CSF Aβ$_{1-42}$/tau	4,4	1,3	4,1	1,5	4,1	1,2	2,5$^\&$	1,1
CSF Aβ$_{1-42}$/p-tau	21,8	6,3	20,7	7,4	20,5	5,9	14,4$^\$$	7,4

(*) p<0.001 vs. S1, S2, S3, S4, S5

(&) Between all groups p< 0.0049, p< 0.002 S4 vs. S1; p<0.012 S4 vs. S2, p<0.016 S4 vs. S3

($) Between all groups p< 0.0245, p< 0.017 S4 vs. S1.

Then we studied the percentage CSF Aβ$_{1-42}$ positive biomarker for each EMTA $_4$ at the right side **(Table 41).** We found that there was a statistically significant difference related to the percentage CSF Aβ$_{1-42}$ positive biomarker between S4 and S1, S2 and S3 groups (p<0,000).

Table 41- Percentage CSF Aβ$_{1-42}$ positive biomarker for each EMTA $_4$ at the right side

	NEGATIVE	POSITIVE
S1	90,2%	9,8%
S2	86,3%	13,70%
S3	82,5%	17,5%
S4	25,0%	75,0%
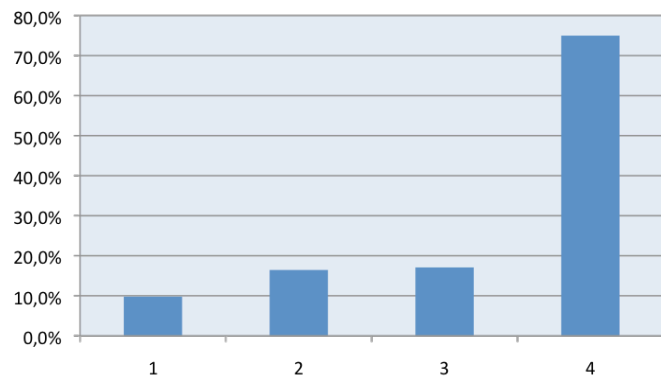
Chi-Squared Test			
	Value	df	Asymp. Sig. (2-sided)
Pearson´s Chi-Squared	23,544a	3	,000
Likelihood Ratio	16,732	3	,001
Linear-by-Linear Association	11,323	1	,001
N of Valid Cases	213		

Afterwards we continued making an exploratory comparative analysis of the CSF biomarkers with the stages corresponding to the EMTA$_4$ scale at the left side **(Table 42).** We could observe how there was a statistically significant differences related to the mean age between S4 and S1 groups (p<0,005). Moreover there were no statistically significant differences in CSF Aβ$_{1-42}$/tau or CSF Aβ$_{1-42}$/p-tau biomarkers at EMTA $_4$ scale **(Table 42).**

_____

Table 42- Exploratory comparative analysis of the CSF biomarkers with the stages corresponding to the EMTA$_4$ scale at the left side

	S1		S2		S3		S4	
n	**128**		**29**		**40**		**16**	
	mean	**SD**	**mean**	**SD**	**mean**	**SD**	**mean**	**SD**
Age	56,5	6,7	57,4	6,5	57,8	6,8	61,8*	8,8
CSF Aβ$_{1-42}$	838,3	212,3	893,5	225,1	754,4	207,4	797,5	261,5
CSF Tau	220,9	85,1	239,9	98,9	213,4	101,2	225,8	92,1
CSF p-tau	42,9	13,6	46,6	14,9	41,5	16,0	40,6	15,3
CSF Aβ$_{1-42}$/tau	4,2	1,3	4,2	1,4	4,1	1,6	3,9	1,5
CSF Aβ$_{1-42}$/p-tau	21,1	6,5	20,6	5,9	20,5	8,0	21,0	7,2

(*) $p < 0.005$ vs. S1

Then we studied the percentage CSF Aβ$_{1-42}$ positive biomarker for each EMTA$_4$ at the left side **(Table 43).** We found that there were no statistically significant differences related to the percentage CSF Aβ$_{1-42}$ positive biomarker between S4 and S1, S2 and S3 groups, much less pronounced than at the right side **(Table 43).**

Table 43- Percentage CSF Aβ$_{1-42}$ positive biomarker for each EMTA $_4$ at the left side

	NEGATIVE	POSITIVE
S1	86,7%	12,50%
S2	89,7%	10,34%
S3	80,5%	20%
S4	62,5%	31,25%
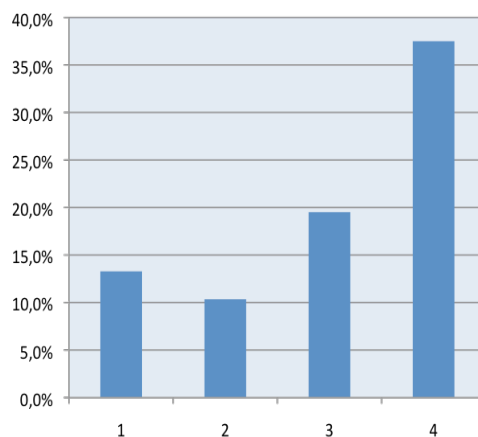
Chi-Squared Test			
	Value	df	Asymp. Sig. (2-sided)
Pearson´s Chi-Squared	7,313a	3	,157
Likelihood Ratio	6,173	3	,103
Linear-by-Linear Association	4,689	1	,030
N of Valid Cases	213		

Finally, we made an exploratory comparative analysis of all the neurocognitive biomarkers included in **Table 13** with the EMTA$_4$ stages showing only at **Table 43**, the ones that show a statistical significant difference. Therefore with respect to the right side we only found statistically significant difference between S4 and S1 in the memory alteration test. Nevertheless, for the left side we found significant

difference between S4 and S1 in: a) global memory composite, b) memory alteration test, c) TAVEC short delay free recall, d) TAVEC short delay cued recall and e) TAVEC long delay free recall. Between S1 and S3 for TAVEC immediate total trial. And, we found difference between S1, S2, S3 and S4 in short delay memory composite **(Table 44).**

Table 44-Exploratory comparative analysis of all the neurocognitive biomarkers included in Table 13 with the EMTA$_4$ stages showing only at Table 43, the ones that show a statistical significant difference

RT	S1 n=148	S2 N=121	S3 N=77	S4 n= 11	_p_
Memory Alteration Test, median (S1,S4	1.14 (0.53, 1.55)	0.94 (0.43, 1.35)	0.94 (0.33, 1.35)	0.33 (-0.49, 0.73)	.0054
LT	**S1 n=209**	**S2 N=44**	**S3 N=79**	**S4 n= 24**	**p**
Global memory composite, median (S1,S4)	0.40 (-0.19, 0.77)	0.17 (-0.35, 0.58)	0.28 (-0.29, 0.60)	-0.24 (-0.41, 0.32)	.0074
Short delay memory composite, median (S1,S2,S3,S4)	0.19 (-0.44, 0.70)	-0.01 (-0.47, 0.45)	0.05 (-0.43, 0.51)	-0.22 (-0.68, 0.13)	.044
Memory Alteration Test, median (S1,S4)	1.14 (0.53, 1.55)	0.94 (0.33, 1.35)	0.94 (0.33, 1.35)	0.53 (-0.08, 0.94)	.0074
TAVEC immediate total trial, median (S1,S3)	0.24 (-0.40, 0.82)	0.11 (-0.45, 0.76)	-0.10 (-0.72, 0.61)	-0.34 (-0.73, 0.33)	.0121
TAVEC short delay free recall, median (S1,S4)	0.15 (-0.56, 0.66)	-0.01 (-0.34, 0.64)	0.00 (-0.56, 0.66)	-0.56 (-0.92, 0.07)	.0484
TAVEC short delay cued recall, median (S1,S4)	0.06 (-0.69, 0.82)	-0.06 (-1.07, 0.46)	0.03 (-0.74, 0.51)	-0.95 (-1.38, 0.37)	.0474
TAVEC long delay free recall, median (S1,S4)	0.14 (-0.57, 0.94)	-0.07 (-0.68, 0.63)	-0.07 (-0.94, 0.63)	-0.68 (-1.13, 0.28)	.0464

- Non-parametric test: Kruskal-Wallis test.

- Age-adjusted Z scores. Mean=0.00, standard deviation=1.00.

- Years of education did not differ significantly between three groups (RT, p=.816; LT, p=.219).

No statistically significant differences were found in: a) Language: Boston Naming Test, Repetition and Comprehension (Boston), b) Visual Perception and Praxis: Rey Complex Figure, Judgment Line Orientation, Poppelreuter (the 15-objects test(20), and c) Attention and Executive Functions: Verbal Fluency Test, Digit Span (WAIS-III), Stroop Test, Trail Making Test, Zoo Map Test and (BADS) Symbol Digit-Coding (WAIS-III).

f) Intra e inter-observer variability.

Based on our observation on anatomical landmarks that surrounds the body of the hippocampus in grade 0 of Scheltens (MTA-scale) subjects (fimbria, choroidal fissure, lateral temporal horn and peritroncular fissure-**((47)-Figure 11)** we propose a new medial temporal lobe atrophy EMTA$_4$ (**Figure 45)** describing the variety of appearances of theses referred structures observed in GAP healthy cohort subjects. We establish besides the concordance between Scheltens (MTA-scale) and the new new medial temporal lobe atrophy EMTA stages **(Figure 28).**
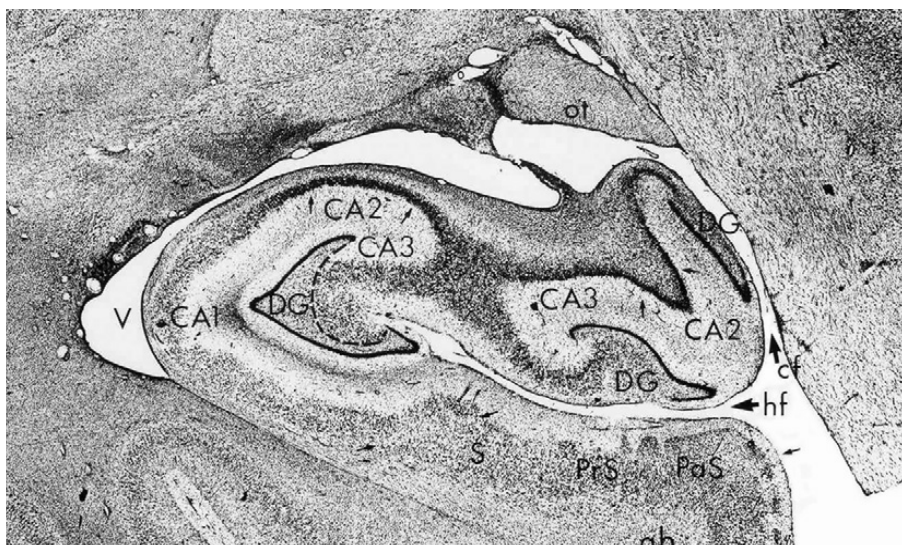
Figure 11- Anatomical landmarks that surrounds the body of the hippocampus (9)
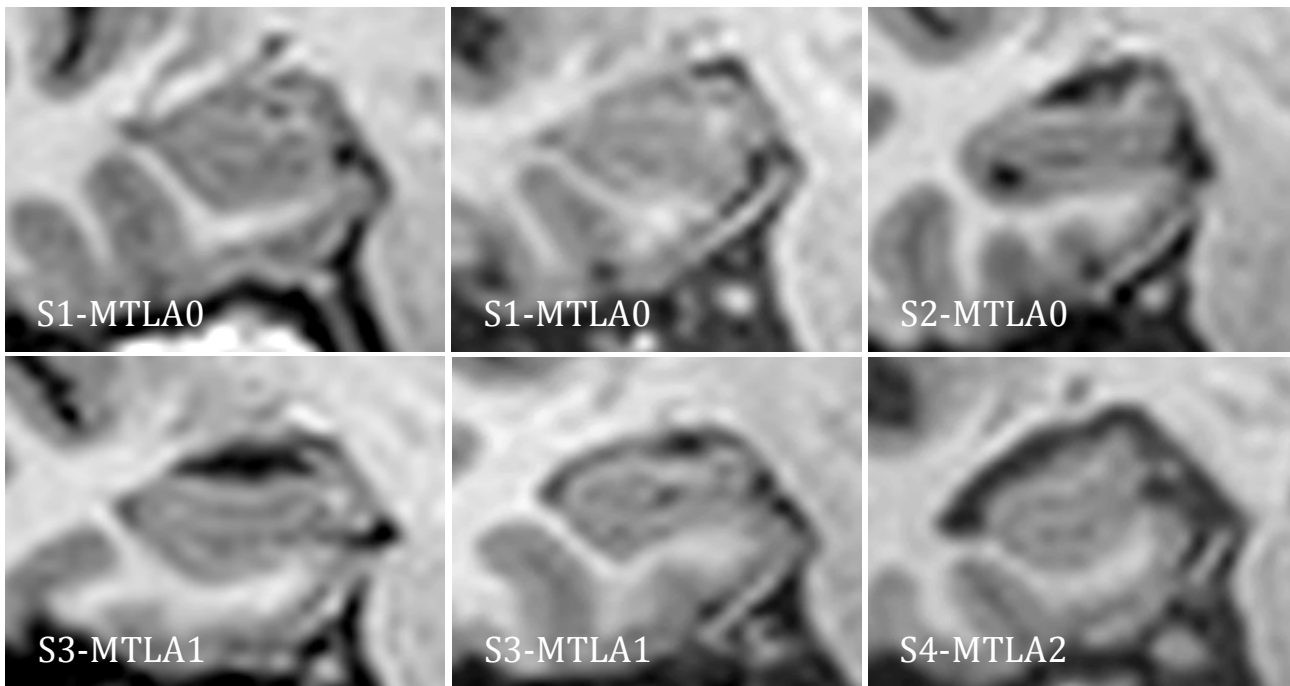
Figure 45- Definition of stages EMTA$_4$

A neuroradiologist (NR, 20 years experienced) firstly rated all the MR images.

After a training of 20 selected cases, a subset of 60 cases was also rated by a neuroradiologist resident (NRr, 2 years experienced). Both ratters were blinded to the subjects' age, sex and diagnosis.

Intra-ratter reliability (NR, 20 years experience) was determined for the same subset of 60 cases out of the 360 subjects included in the data set, express a weighted kappa (quadratic weights) of 0.72 for left and 0,80 right scores. Inter-ratter reliability between NR and NRr registered a weighted kappa (quadratic weights) of 0.76 for left and 0,82 right scores.

5- DISCUSSION.

In the present study we developed and validated it through VBM studies the new EMTA$_4$ that has the capability to measure the low-grade atrophy changes that occurs before it becomes detectable with MTA.

The S1 EMTA$_4$ (former S1 and S2 EMTA$_6$ collapsed) as well as S2 EMTA$_4$ (former S3 EMTA$_6$) corresponds to MTA 0 stages. S3 EMTA$_4$ is equivalent to MTA 1 (S3 EMTA$_4$ has two possible morphological patterns that correspond to former S4 & S5 EMTA$_6$). S4 EMTA$_4$ matches the early MTA 2 pattern.

Although MTA 0 and MTA 1 have been considered non-relevant stages by the original proposal by Scheltens and colleagues as far as they promoted an age-adjusted cut-off of MTA score ≥2 in either of the two hemispheres to be considered abnormal below the age of 75 years (5) and others authors (11, 14) proposed a cut-off of ≥1.5 based on the average score of both hemispheres between 45-65 years (at the PcAD age spectrum), we have found a progressive cortical thinning (PCTh) of the hippocampus from S1 to S3 EMTA$_4$ (MTA 0 and MTA 1 stages) **(Figures 41 and 42)** accompanied also by a progressive decrease in CSF of Aβ1-42 levels **Tables 41 and 43** for RT and LT.

While Scheltens and colleagues (5) proposed a cut-off of MTA score ≥2 in either of the two hemispheres as abnormal below the age of 75 years, we have demonstrate incipient hippocampus volume atrophy (HVa) at S4 EMTA$_4$ (early MTA2) mean aged 68,1 years RT & 61,8 years LT **Tables 41,42** and **(Figure-43)** accompanied by low performance normal scores in verbal memory test (VMT) (related subjects of the same age and educational level) for LT **Table-44** and statistical significant differences in CSF Aβ1-42/tau or CSF Aβ1-42/p-tau biomarkers between S1 vs S4 (MTA0 vs early MTA2) for RT **Table 40**.

The solid validation of the EMTA$_4$, is as good as the one obtained formerly by Sheltens et al (5) at the MTA original study, or in more recent studies by Wahlund et al. (applying the MTA to study AD at dementia stage, cognitively normal subjects (CN) and subjects demented diagnosed of other types of dementia) (21), Westman et al. (applying the MTA to study AD at dementia stage, CN and AD at mild cognitive impairment (MCI) subjects) (22) or Cavallin et al. (applying MTA to a cohort of elderly healthy people mean aged ≥ 60 years old)(13).

We also discuss our work with three relevant studies: Wang et al.(23), Fortea et al. (24) and finally Jack et al. (25) corresponding to longitudinal studies of memory and ageing (KADRC-Washington-USCM study(23), ADNI(24) and MACSA-Mayo study(25)) based on volunteers as the GAP cohort. Therefore there are differences between these four studies related to the methods: 1-their mean age (71years(23), 73,4years(24), 72years(25) and 56,6years GAP) and 2-the criteria used to entitle the volunteers as CN; in the Wang et al have a CDR of 0, and in the Fortea et al. (24) have a MMSE of 29,1 while in our study we included n=199 subjects with CDR score ≤ 0.5 and also n=15 with MMSE < 26 but CDR score > 0.5 and 3-the number of volunteers enrolled varying between n=100 (23) and n=1246(25) passing through n=145(24) and n= 214 our series.

In the one hand the main differences reflected between our study and Wang et al.(23), Fortea et al. (24) and finally Jack et al. (25) are concentrated on: 1- (23) they found that elevated CSF tau was associated with AD signature PCTh but not HVa but in our work we found both phenomena associated, 2-(23) these authors found that reduced CSF Aβ1-42 was related to poorer performance on episodic memory but in our study was related with poorer performance in VMT, 3-(25) at this work found memory worsened from age 30years through the 90s while we have found only VMT worsened for S4 mean aged 68,1 years RT & 61,8 years LT (Tables 6,8), 4-(25) these authors found HVa worsened gradually from age 30 years to the mid-60s and more steeply beyond that age while we demonstrate incipient HVa at S4 EMTA$_4$.

On the other hand the main coincidences between our study and Wang et al. (23) **(Figure46)**, Fortea et al. (24) **(Figure47)** and finally Jack et al. (25) **(Figure48)** are concentrated on: 1- PCTh (23, 24) in relation to AD signature cortical as in our work, 2-(24) found data that suggest interactions between biomarkers in AD result in a 2-phase phenomenon of PCTh associated with low CSF Aβ, followed by HVa once CSF p-tau becomes abnormal like we found in our series and 3- (24, 25) in this works and in our series HVa is the last phenomena appearing in the aging process.

One limitation of the present study is that we have included n=199 subjects with CDR score ≤ 0.5 and also n=15 with MMSE < 26 but CDR score > 0.5, so our results are influence by this circumstance compared with Wang et al. (23) that included in their work only CDR 0 subjects or Fortea et al. (24) which included MMSE 29,1 subjects. Other limitation of our study is related with the sample size of n=357 for the VBM and

neurophysiological analysis which is limited to n=214 when correlate VBM with CSF biomarkers. Finally another limitation of the present approach is that we have investigated the relationship between early morphological MRI changes and CSF and neuropsychological biomarkers cross-sectionally, and so we are unable to investigate if these changes are related clinical outcomes. However, a strong aspect of our approach is that we used a combination of CSF and neuropsycological biomarkers for a limited but notorious n=214 volunteers, more than the sample of Wang et al (23) n=100 and Fortea et al (24) n=145. Currently, longitudinal follow-up data of the GAP study is being collected. With this data we can further investigate if EMTA$_4$ may have use as a biomarker for early diagnosis of the disease.
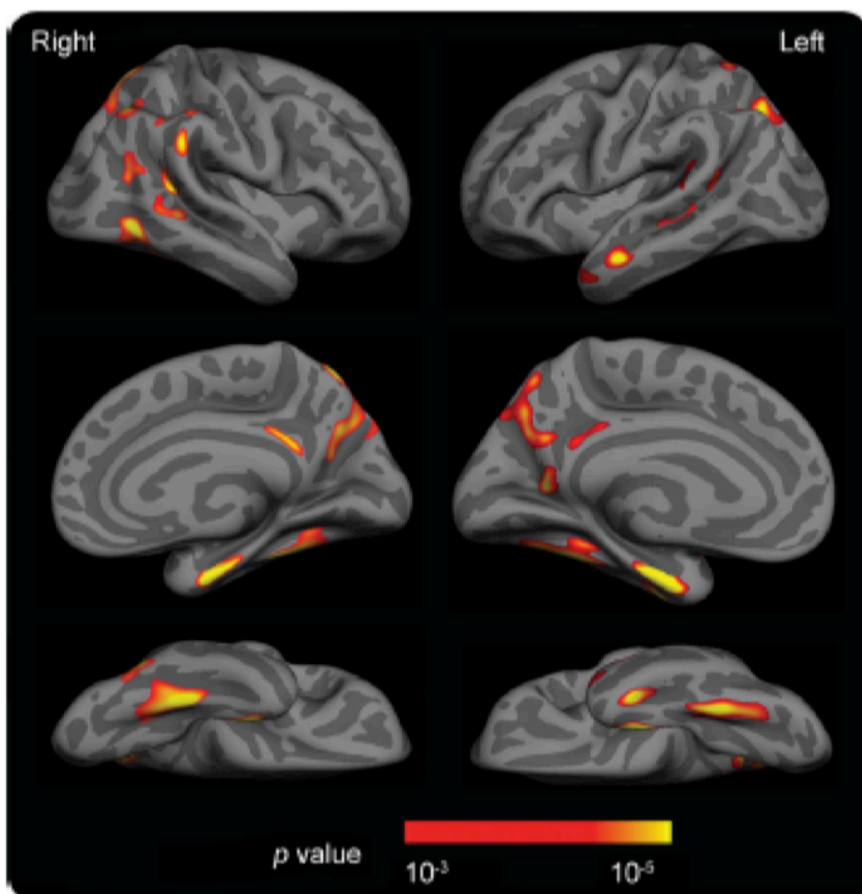
Figure 46- Surface maps of cortical thickness were compared between cognitively normal (CN) individuals (n=100) who were negative for CSF Aβ_{1-42} (>500pg/ml) and CSF Tau (<500pg/ml) and individuals with Alzheimer disease (AD) (n=20) who were positive for either CSF Aβ_{1-42} (≤500pg/ml) or amyloid imaging with Pittsburgh compound B (mean cortical binding potential ≥0.18) using a general linear model. A group difference map (AD<CN) was thresholded at a vertex-level $p < 0.001$ and a cluster size >100mm^2 after adjustment for age,

sex, presence of APOE ε4 allele, and scanner type (3T Trio vs. 1.5T Vision). The map is displayed on the semi-inflated cortical surface of Free Surfer average brain with light grey regions representing gyri and dark grey regions representing sulci (15).
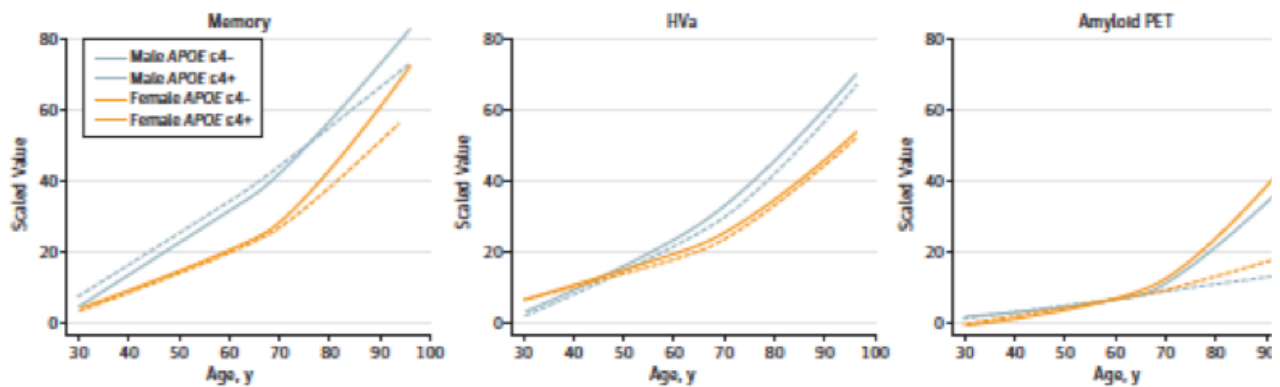
Figure 47- Estimated median regression lines in scaled units vs. age for all demographic groups, with separate panels for memory ,adjusted hippocampal volume (HVa), and amyloid positron emission tomography (PET). Knots were placed at ages 50, 75 and 80 years. Blue lines represent relationships in men, and orange lines represent relationships in women. Solid lines represent APOE ε4 carriers, and dashed lines represent APOE ε4 non-carriers (232).

The intraobserver variability observed applying the EMTA (0,72 weighted kappa values on the left side and 0,80 on the right side) was lower than that observed by Ferreira et al. (0,93 on left side and 0,94 on right side)(14) or Cavallin et al. (0,88 on left side and 0,89 on right side) (13) applying the MTA. The interobserver variability observed applying EMTA (0,76 weighted kappa values on the left side and 0,82 on the right side) was also a little bit lower than that observed for PA atrophy scale (0,85 on the left and right sides)(26) . The explanation for this worse intra e interobserver variability compared with the one obtained with MTA and PA atrophy scale could be related to the proper nature of the EMTA, designed and validated to detect low-grade MTL atrophy changes.

_____
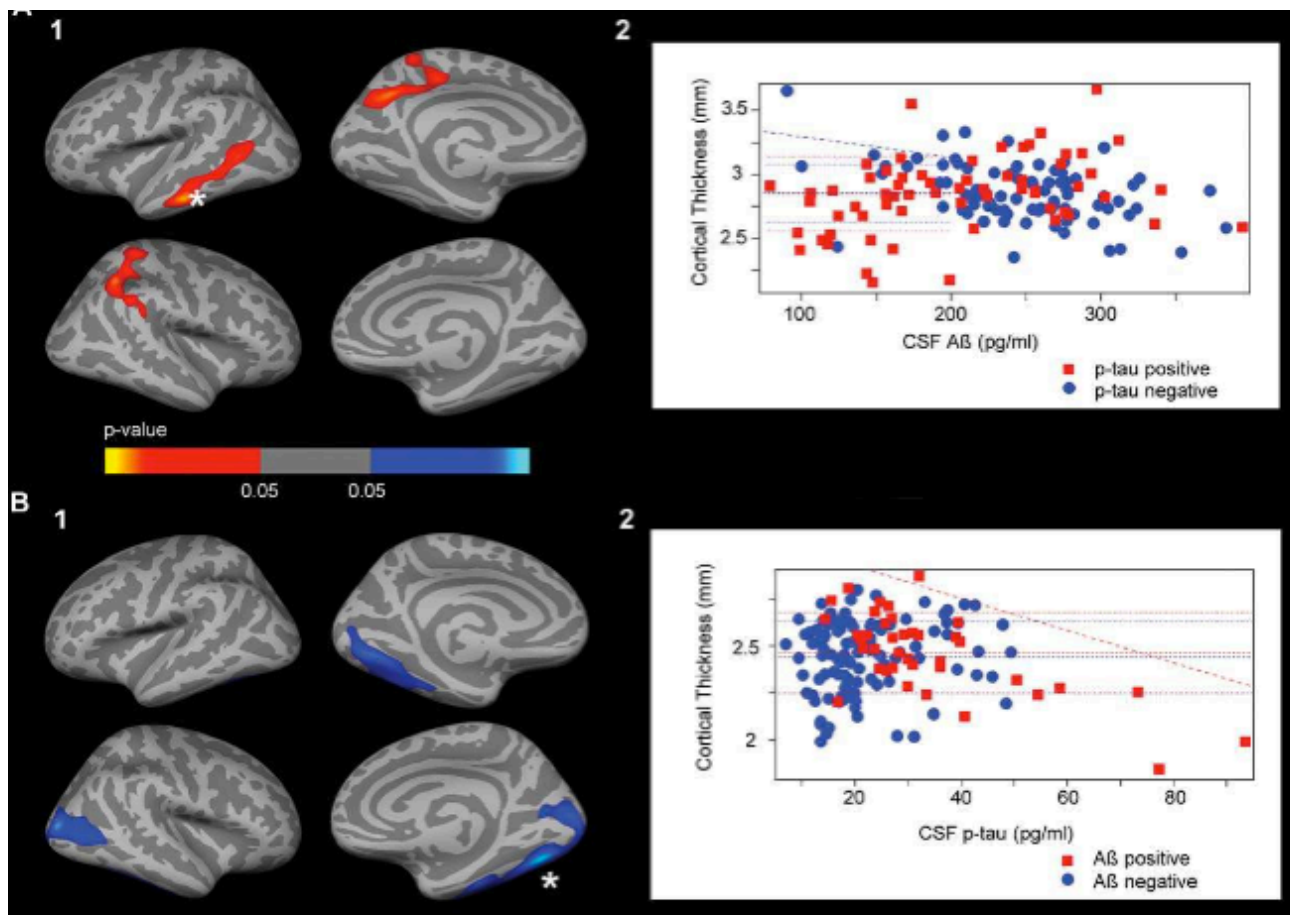
Figure 48-Interaction analyses in Alzheimer´s Disease Neuroimaging Initiative: familywise corrected (p<0.05) cluster in which the correlation between cortical thickness (Cth) and 1 biomarker is modified by the status of the other dichotomized biomarkers. (A1) Areas in which the β amyloid 1_{-42} (AB)-CTh correlation is modified by phospo-tau $_{181p}$ (p-tau) status. (A2) Scatter-plot showing CTh and Aβ values at the maximun significant vertex in the laterotemporal cluster. Ptau-positive subjects are shown in red, and p-tau-negative subjects are shown in blue. (B1) Areas in Ptau-CTh correlation is modified by Aβ status. (B2) Scatter-plot showing CTh and p-tau values at the maximun significant vertex (asteriks) in the fusiform cluster. Aβ positive subjects are shown in red, and Aβ negative subjects are shown in blue. Red-yelow indicates a positive correlation, and blue indicates a negative correlation. CSF= cerebroespinal fluid (233).

173

6- CONCLUSIONS

a) We have made a new scale to measure the medial temporal atrophy (EMTA) through cranial MRI, more sensitive than the more commonly used (MTA)

b) The EMTA was first designed on a visual analysis of the cranial MRI of GAP volunteers based on strict anatomical criteria.

c) The EMTA has been validated by voxel based morphometry studies resulting in 4 stages according to the degree of atrophy: S1 to S4

d) Stages S1 and S2 of the EMTA corresponds to stage 0 of the MTA. The S3 corresponds to MTA 1. The S4 to stage MTA 2 in its initial phase.

e) The EMTA is easy to apply and has a good inter and intra-observer correlation.

f) Individuals stage S4 has a more advanced age than Stage S1 to S3.

g) Individuals stage S4 shown on the right side abnormalities in CSF biomarkers (Aβ1-42/tau o CSF Aβ1-42/p-tau) compared with those in stages S1, S2 and S3.

h) The subjects in S4 shown in left temporal lobe altered cognitive performance test of verbal memory compared with S1 stage subjects.

i) We believe that the EMTA could be considered an early marker of Neurodegeneration in the preclinical phase of Alzheimer´s disease.

7- BIBLIOGRAPHY

1.   Knopman DS, Jack CR, Jr., Wiste HJ, Weigand SD, Vemuri P, Lowe V, et al. Short-term clinical outcomes for stages of NIA-AA preclinical Alzheimer disease. Neurology. 2012;78(20):1576-82.

2.   Vos SJ, Xiong C, Visser PJ, Jasielec MS, Hassenstab J, Grant EA, et al. Preclinical Alzheimer's disease and its outcome: a longitudinal cohort study. The Lancet Neurology. 2013;12(10):957-65.

3.   Dubois B, Feldman HH, Jacova C, Hampel H, Molinuevo JL, Blennow K, et al. Advancing research diagnostic criteria for Alzheimer's disease: the IWG-2 criteria. The Lancet Neurology. 2014;13(6):614-29.

4.   Sperling RA, Aisen PS, Beckett LA, Bennett DA, Craft S, Fagan AM, et al. Toward defining the preclinical stages of Alzheimer's disease: recommendations from the National Institute on Aging-Alzheimer's Association workgroups on diagnostic guidelines for Alzheimer's disease. Alzheimer's & dementia : the journal of the Alzheimer's Association. 2011;7(3):280-92.

5.   Scheltens P, Leys D, Barkhof F, Huglo D, Weinstein HC, Vermersch P, et al. Atrophy of medial temporal lobes on MRI in "probable" Alzheimer's disease and normal ageing: diagnostic value and neuropsychological correlates. Journal of neurology, neurosurgery, and psychiatry. 1992;55(10):967-72.

6.   Dubois B, Feldman HH, Jacova C, Cummings JL, Dekosky ST, Barberger-Gateau P, et al. Revising the definition of Alzheimer's disease: a new lexicon. The Lancet Neurology. 2010;9(11):1118-27.

7.   Hasboun D, Chantome M, Zouaoui A, Sahel M, Deladoeuille M, Sourour N, et al. MR determination of hippocampal volume: comparison of three methods. AJNR American journal of neuroradiology. 1996;17(6):1091-8.

8.   Press GA, Amaral DG, Squire LR. Hippocampal abnormalities in amnesic patients revealed by high-resolution magnetic resonance imaging. Nature. 1989;341(6237):54-7.

9.   Scheltens P, van de Pol L. Impact commentaries. Atrophy of medial temporal lobes on MRI in "probable" Alzheimer's disease and normal ageing: diagnostic value and neuropsychological correlates. Journal of neurology, neurosurgery, and psychiatry. 2012;83(11):1038-40.

10.   Barkhof F, Polvikoski TM, van Straaten EC, Kalaria RN, Sulkava R, Aronen HJ, et al. The significance of medial temporal lobe atrophy: a postmortem MRI study in the very old. Neurology. 2007;69(15):1521-7.

11.   Schoonenboom NS, van der Flier WM, Blankenstein MA, Bouwman FH, Van Kamp GJ, Barkhof F, et al. CSF and MRI markers independently contribute to the diagnosis of Alzheimer's disease. Neurobiology of aging. 2008;29(5):669-75.

12.   Pereira JB, Cavallin L, Spulber G, Aguilar C, Mecocci P, Vellas B, et al. Influence of age, disease onset and ApoE4 on visual medial temporal lobe atrophy cut-offs. J Intern Med. 2014;275(3):317-30.

13.   Cavallin L, Bronge L, Zhang Y, Oksengard AR, Wahlund LO, Fratiglioni L, et al. Comparison between visual assessment of MTA and hippocampal volumes in an elderly, non-demented population. Acta radiologica. 2012;53(5):573-9.

14.   Ferreira D, Cavallin L, Larsson EM, Muehlboeck JS, Mecocci P, Vellas B, et al. Practical cut-offs for visual rating scales of medial temporal, frontal and posterior atrophy in Alzheimer's disease and mild cognitive impairment. J Intern Med. 2015;278(3):277-90.

15.   Jack CR, Jr., Knopman DS, Jagust WJ, Petersen RC, Weiner MW, Aisen PS, et al. Tracking pathophysiological processes in Alzheimer's disease: an updated hypothetical model of dynamic biomarkers. The Lancet Neurology. 2013;12(2):207-16.

16.   Jack CR, Jr., Knopman DS, Weigand SD, Wiste HJ, Vemuri P, Lowe V, et al. An operational approach to National Institute on Aging-Alzheimer's Association criteria for preclinical Alzheimer disease. Annals of neurology. 2012;71(6):765-75.

17.   Bateman R. Alzheimer's disease and other dementias: advances in 2014. The Lancet Neurology. 2015;14(1):4-6.

18.   Dodel R, Rominger A, Bartenstein P, Barkhof F, Blennow K, Forster S, et al. Intravenous immunoglobulin for treatment of mild-to-moderate Alzheimer's disease: a phase 2, randomised, double-blind, placebo-controlled, dose-finding trial. The Lancet Neurology. 2013;12(3):233-43.

19.   Alcolea D, Martinez-Lage P, Sanchez-Juan P, Olazaran J, Antunez C, Izagirre A, et al. Amyloid precursor protein metabolism and inflammation markers in preclinical Alzheimer disease. Neurology. 2015;85(7):626-33.

20.   Pillon B, Dubois B, Bonnet AM, Esteguy M, Guimaraes J, Vigouret JM, et al. Cognitive slowing in Parkinson's disease fails to respond to levodopa treatment: the 15-objects test. Neurology. 1989;39(6):762-8.

21.   Wahlund LO, Julin P, Johansson SE, Scheltens P. Visual rating and volumetry of the medial temporal lobe on magnetic resonance imaging in dementia: a comparative study. Journal of neurology, neurosurgery, and psychiatry. 2000;69(5):630-5.

22.   Westman E, Cavallin L, Muehlboeck JS, Zhang Y, Mecocci P, Vellas B, et al. Sensitivity and specificity of medial temporal lobe visual ratings and multivariate regional MRI classification in Alzheimer's disease. PloS one. 2011;6(7):e22506.

23.   Wang L, Benzinger TL, Hassenstab J, Blazey T, Owen C, Liu J, et al. Spatially distinct atrophy is linked to beta-amyloid and tau in preclinical Alzheimer disease. Neurology. 2015;84(12):1254-60.

24.   Fortea J, Vilaplana E, Alcolea D, Carmona-Iragui M, Sanchez-Saudinos MB, Sala I, et al. Cerebrospinal fluid beta-amyloid and phospho-tau biomarker interactions affecting brain structure in preclinical Alzheimer disease. Annals of neurology. 2014;76(2):223-30.

25.   Jack CR, Jr., Wiste HJ, Weigand SD, Knopman DS, Vemuri P, Mielke MM, et al. Age, Sex, and APOE epsilon4 Effects on Memory, Brain Structure, and beta-Amyloid Across the Adult Life Span. JAMA Neurol. 2015;72(5):511-9.

26.   Moller C, van der Flier WM, Versteeg A, Benedictus MR, Wattjes MP, Koedam EL, et al. Quantitative regional validation of the visual rating scale for posterior cortical atrophy. European radiology. 2014;24(2):397-404.

27.   Jack CR, Jr., Knopman DS, Jagust WJ, Shaw LM, Aisen PS, Weiner MW, et al. Hypothetical model of dynamic biomarkers of the Alzheimer's pathological cascade. The Lancet Neurology. 2010;9(1):119-28.

28.   Burns A, Iliffe S. Alzheimer's disease. BMJ. 2009;338:b158.

29.   Braak H, Braak E. Neuropathological stageing of Alzheimer-related changes. Acta neuropathologica. 1991;82(4):239-59.

30.   Braak H, Braak E. Frequency of stages of Alzheimer-related lesions in different age categories. Neurobiology of aging. 1997;18(4):351-7.

31.   McKhann G, Drachman D, Folstein M, Katzman R, Price D, Stadlan EM. Clinical diagnosis of Alzheimer's disease: report of the NINCDS-ADRDA Work Group under the auspices of Department of Health and Human Services Task Force on Alzheimer's Disease. Neurology. 1984;34(7):939-44.

32.   Dubois B, Feldman HH, Jacova C, Dekosky ST, Barberger-Gateau P, Cummings J, et al. Research criteria for the diagnosis of Alzheimer's disease: revising the NINCDS-ADRDA criteria. The Lancet Neurology. 2007;6(8):734-46.

33.   McKhann GM, Knopman DS, Chertkow H, Hyman BT, Jack CR, Jr., Kawas CH, et al. The diagnosis of dementia due to Alzheimer's disease: recommendations from the National

Institute on Aging-Alzheimer's Association workgroups on diagnostic guidelines for Alzheimer's disease. Alzheimer's & dementia : the journal of the Alzheimer's Association. 2011;7(3):263-9.

34.   Jack CR, Jr., Albert MS, Knopman DS, McKhann GM, Sperling RA, Carrillo MC, et al. Introduction to the recommendations from the National Institute on Aging-Alzheimer's Association workgroups on diagnostic guidelines for Alzheimer's disease. Alzheimer's & dementia : the journal of the Alzheimer's Association. 2011;7(3):257-62.

35.   Norton S, Matthews FE, Barnes DE, Yaffe K, Brayne C. Potential for primary prevention of Alzheimer's disease: an analysis of population-based data. The Lancet Neurology. 2014;13(8):788-94.

36.   Barnes DE, Yaffe K. The projected effect of risk factor reduction on Alzheimer's disease prevalence. The Lancet Neurology. 2011;10(9):819-28.

37.   Biessels GJ. Capitalising on modifiable risk factors for Alzheimer's disease. The Lancet Neurology. 2014;13(8):752-3.

38.   Heneka MT, Carson MJ, El Khoury J, Landreth GE, Brosseron F, Feinstein DL, et al. Neuroinflammation in Alzheimer's disease. The Lancet Neurology. 2015;14(4):388-405.

39.   Braak H, Del Tredici K. The pathological process underlying Alzheimer's disease in individuals under thirty. Acta neuropathologica. 2011;121(2):171-81.

40.   Small SA, Duff K. Linking Abeta and tau in late-onset Alzheimer's disease: a dual pathway hypothesis. Neuron. 2008;60(4):534-42.

41.   Mesulam MM. Neuroplasticity failure in Alzheimer's disease: bridging the gap between plaques and tangles. Neuron. 1999;24(3):521-9.

42.   Duyckaerts C. Tau pathology in children and young adults: can you still be unconditionally baptist? Acta neuropathologica. 2011;121(2):145-7.

43.   Price JL, Morris JC. Tangles and plaques in nondemented aging and "preclinical" Alzheimer's disease. Annals of neurology. 1999;45(3):358-68.

44.   Soldan A, Pettigrew C, Lu Y, Wang MC, Selnes O, Albert M, et al. Relationship of medial temporal lobe atrophy, APOE genotype, and cognitive reserve in preclinical Alzheimer's disease. Hum Brain Mapp. 2015.

45.   Almeida RP, Schultz SA, Austin BP, Boots EA, Dowling NM, Gleason CE, et al. Effect of Cognitive Reserve on Age-Related Changes in Cerebrospinal Fluid Biomarkers of Alzheimer Disease. JAMA Neurol. 2015.

46.   Jindal H, Bhatt B, Sk S, Singh Malik J. Alzheimer disease immunotherapeutics: then and now. Hum Vaccin Immunother. 2014;10(9):2741-3.

47.   Insausti R. Chapter 24. Hippocampal Formation. 2012:896-942.

48.   Insausti R, Amaral DG, Cowan WM. The entorhinal cortex of the monkey: II. Cortical afferents. J Comp Neurol. 1987;264(3):356-95.

49.   Kobayashi Y AD. The hippocampal formation and perirhinal and parahippocampal cortices. In Bloom FE, Bjorklund A, Ho¨kfelt T, editors: The primate nervous system, Amsterdam Elsevier,. 2001:285-401.

50.   Hanke J, Yilmazer-Hanke DM. Pigmentarchitectonic subfields of the entorhinal region as revealed in tangential sections. J Hirnforsch. 1997;38(4):427-32.

51.   M O. Abernathey CD: Atlas of the cerebral sulc. Stuttgart, New York, Thieme Medical Publishers, Inc. 1990.

52.   Heinsen H, Henn R, Eisenmenger W, Gotz M, Bohl J, Bethke B, et al. Quantitative investigations on the human entorhinal area: left-right asymmetry and age-related changes. Anat Embryol (Berl). 1994;190(2):181-94.

53.   Insausti R, Tunon T, Sobreviela T, Insausti AM, Gonzalo LM. The human entorhinal cortex: a cytoarchitectonic analysis. J Comp Neurol. 1995;355(2):171-98.

54.   Ding SL, Van Hoesen GW. Borders, extent, and topography of human perirhinal cortex as revealed using multiple modern neuroanatomical and pathological markers. Hum Brain Mapp. 2010;31(9):1359-79.

55.   Van Hoesen GW. Anatomy of the medial temporal lobe. Magn Reson Imaging. 1995;13(8):1047-55.

56.   Von Economo C. The Cytoarchitectonics of the Human Cerebral Cortex. London and New York, Oxford Univ Press. 1929.

57.   GW VH. The parahippocampal gyrus. New observations regarding its cortical connections in the monkey. Trends Neurosci. 1982;5:345-50.

58.   Broadman K. Vergleichende Lokalisationslehre der Groshirnrinde. Leipzig, Barth. 1909.

59.   Kingler J. Die makroskopische anatomie der Ammonsformation. Denkschr Schweiz Naturforsch Ges 78, Mem. 1948;1:1-80.

60.   Simic G, Bexheti S, Kelovic Z, Kos M, Grbic K, Hof PR, et al. Hemispheric asymmetry, modular variability and age-related changes in the human entorhinal cortex. Neuroscience. 2005;130(4):911-25.

61.   Van Hoesen GW, Hyman BT, Damasio AR. Entorhinal cortex pathology in Alzheimer's disease. Hippocampus. 1991;1(1):1-8.

62.   Braak H. Architectonics of the Human Telencephalic Cortex. New York, Springer-Verlag. 1980.

63.   Retzius G. Menschenhirn. Studien in der Makroskopischen Morphologie. Stockholm,Norstedt & Sohne. 1896.

64.   Duvernoy H. The Human Hippocampus. J F Bergman Verlag Mu¨n- chen 1988:1-166.

65.   Gastaut H. Anatomie du rhinence´phale. In Alajouanine PT, editor Les grandes activite´s dy rhinence´phale, vol 1, Paris, Masson,. 1961:1-56.

66.   Stephan H. Allocortex. In Bargmann W, editor::Handbuch der mikro-skopischen Anatomie des Menschen,vol 4, Berlin,Springer-Verlag. 1975:295-371.

67.   Arantius G. De humano foetu. Ejusdem anatomicorum observa- tionum liber Etc Venice. 1587.

68.   Lewis F. The significance of the term hippocampus. J Comp Neurol. 1923;35:213-30.

69.   Winslow J. "Exposition anatomique de la structure du corps humain.". Paris. 1732.

70.   Garengeot D. "Splanchnologie ou l'anatomie des visceres,". ed 2, Paris, . 1742:250-1.

71.   R LdN. Studies on the structure of the cerebral cortex. II. Continuation of the study of the ammonic system. J Psychol Neurol. 1934;46:113-77.

72.   Gertz SD, Lindenberg R, Piavis GW. Structural variations in the rostral human hippocampus. Johns Hopkins Med J. 1972;130(6):367-76.

73.   Amaral DG, Insausti R, Cowan WM. The commissural connections of the monkey hippocampal formation. J Comp Neurol. 1984;224(3):307-36.

74.   Demeter S, Rosene DL, Van Hoesen GW. Interhemispheric pathways of the hippocampal formation, presubiculum, and entorhinal and posterior parahippocampal cortices in the rhesus monkey: the structure and organization of the hippocampal commissures. J Comp Neurol. 1985;233(1):30-47.

75.   Wilson C. Comparative view of local and interhemispheric limbic pathways in humans: An evoked potential analysis. In EngelJr J, Ojemann GA, Lu¨ders HO, Williamson PD, editors: Fundamental Mechanisms of Human Brain Function, New York, Raven Press. 1987:23-38.

76.   Gloor P, Salanova V, Olivier A, Quesney LF. The human dorsal hippocampal commissure. An anatomically identifiable and functional pathway. Brain : a journal of neurology. 1993;116 (Pt 5):1249-73.

77.   Lim C, Mufson EJ, Kordower JH, Blume HW, Madsen JR, Saper CB. Connections of the hippocampal formation in humans: II. The endfolial fiber pathway. J Comp Neurol. 1997;385(3):352-71.

78.   Seress L. Interspecies comparison of the hippocampal formation shows increased emphasis on the regio superior in the Ammon's horn of the human brain. J Hirnforsch. 1988;29(3):335-40.

79.   West MJ, Gundersen HJ. Unbiased stereological estimation of the number of neurons in the human hippocampus. J Comp Neurol. 1990;296(1):1-22.

80.   Sá MJ. Anatomical asymmetries in the human hippocampal formation. Acta Stereol. 1999;18/2:161–76.

81.   Amaral DG. A Golgi study of cell types in the hilar region of the hippocampus in the rat. J Comp Neurol. 1978;182(4 Pt 2):851-914.

82.   Kondo H, Lavenex P, Amaral DG. Intrinsic connections of the macaque monkey hippocampal formation: II. CA3 connections. J Comp Neurol. 2009;515(3):349-77.

83.   Bakst I, Amaral DG. The distribution of acetylcholinesterase in the hippocampal formation of the monkey. J Comp Neurol. 1984;225(3):344-71.

84.   Cassell M. The numbers of cells in the stratum pyramidale of the rat and human hippocampal formation. PhD, United Kingdom, thesis,University of Bristol. 1980.

85.   Frederickson CJ, Klitenick MA, Manton WI, Kirkpatrick JB. Cytoarchitectonic distribution of zinc in the hippocampus of man and the rat. Brain Res. 1983;273(2):335-9.

86.   Sloviter RS, Sollas AL, Barbaro NM, Laxer KD. Calcium-binding protein (calbindin-D28K) and parvalbumin immunocytochemistry in the normal and epileptic human hippocampus. J Comp Neurol. 1991;308(3):381-96.

87.   Seress L, Gulyas AI, Ferrer I, Tunon T, Soriano E, Freund TF. Distribution, morphological features, and synaptic connections of parvalbumin- and calbindin D28k-immunoreactive neurons in the human hippocampal formation. J Comp Neurol. 1993;337(2):208-30.

88.   Altemus KL, Lavenex P, Ishizuka N, Amaral DG. Morphological characteristics and electrophysiological properties of CA1 pyramidal neurons in macaque monkeys. Neuroscience. 2005;136(3):741-56.

89.   Veazey RB, Amaral DG, Cowan WM. The morphology and connections of the posterior hypothalamus in the cynomolgus monkey (Macaca fascicularis). II. Efferent connections. J Comp Neurol. 1982;207(2):135-56.

90.   Leranth C, Nitsch R. Morphological evidence that hypothalamic substance P-containing afferents are capable of filtering the signal flow in the monkey hippocampal formation. The Journal of neuroscience : the official journal of the Society for Neuroscience. 1994;14(7):4079-94.

91.   Stephan H. Evolutionary trends in limbic structures. Neuroscience and biobehavioral reviews. 1983;7(3):367-74.

92.   Stephan H, Manolescu J. Comparative investigations on hippocampus in insectivores and primates. Z Mikrosk Anat Forsch. 1980;94(6):1025-50.

93.   Rosene DL VHG. The hippocampal formation of the primate brain. A review of some comparative aspects of cytoarchitecture connections. n Jones EG, Peters A, editors: Cere- bral Cortex, vol 6, New York, Plenum Press,. 1987:345-456.

94.   Braak H. [Pigmentarchitecture of the human cortex cerebri. I. Regio entorhinalis]. Z Zellforsch Mikrosk Anat. 1972;127(3):407-38.

95.   Braak H. On the structure of the human archicortex. I. The cornu ammonis. A Golgi and pigmentarchitectonic study. Cell Tissue Res. 1974;152(3):349-83.

96.   Olbrich HG, Braak H. Ratio of pyramidal cells versus non-pyramidal cells in sector CA1 of the human Ammon's horn. Anat Embryol (Berl). 1985;173(1):105-10.

97.   West MJ, Coleman PD, Flood DG, Troncoso JC. Differences in the pattern of hippocampal neuronal loss in normal ageing and Alzheimer's disease. Lancet. 1994;344(8925):769-72.

98.   Simic G, Kostovic I, Winblad B, Bogdanovic N. Volume and number of neurons of the human hippocampal formation in normal aging and Alzheimer's disease. J Comp Neurol. 1997;379(4):482-94.

99.   Braak H. [Pigmentarchitecture of the human cortex cerebri. II. Subiculum]. Z Zellforsch Mikrosk Anat. 1972;131(2):235-54.

100.   Amaral DG, Insausti R, Cowan WM. The entorhinal cortex of the monkey: I. Cytoarchitectonic organization. J Comp Neurol. 1987;264(3):326-55.

101.   sog RMD. Riechrinde beim Menschem und beim Aften. II. Teil des Allocortex bei Tier und Mensch. J Psychol Neurol. 1927;34:261-401.

102.   Krimer LS, Hyde TM, Herman MM, Saunders RC. The entorhinal cortex: an examination of cyto- and myeloarchitectonic organization in humans. Cerebral cortex. 1997;7(8):722-31.

103.   Ramón y Cajal S. Sobre un ganglio especial de la corteza esfeno-occipital,. Trab Lab Invest Biol Univ Madrid 1 189–206. 1901-1902.

104.   Hammarberg C. Studien uber Klinik und Pathologie der Idiotie nebst Untersuchungen uber die normale Anatomie der Hirn- rinde.". Berling, Upsala. 1895.

105.   Hevner RF, Wong-Riley MT. Entorhinal cortex of the human, monkey, and rat: metabolic map as revealed by cytochrome oxidase. J Comp Neurol. 1992;326(3):451-69.

106.   Beall MJ, Lewis DA. Heterogeneity of layer II neurons in human entorhinal cortex. J Comp Neurol. 1992;321(2):241-66.

107.   Solodkin A, Van Hoesen GW. Entorhinal cortex modules of the human brain. J Comp Neurol. 1996;365(4):610-7.

108.   Goldenberg TM, Bakay RA, Ribak CE. Electron microscopy of cell islands in layer II of the primate entorhinal cortex. J Comp Neurol. 1995;355(1):51-66.

109.   Mikkonen M. Morphology of spiny neurons in the human entorhinal cortex: intra-cellular filling with Lucifer Yellow. Neuroscience 2000;96:515-22.

110.   Hyman BT, Van Hoesen GW, Damasio AR, Barnes CL. Alzheimer's disease: cell-specific pathology isolates the hippocampal formation. Science. 1984;225(4667):1168-70.

111.   West MJ, Slomianka L. Total number of neurons in the layers of the human entorhinal cortex. Hippocampus. 1998;8(1):69-82.

112.   Witter MP, Amaral DG. Entorhinal cortex of the monkey: V. Projections to the dentate gyrus, hippocampus, and subicular complex. J Comp Neurol. 1991;307(3):437-59.

113.   West MJ. Regionally specific loss of neurons in the aging human hippocampus. Neurobiology of aging. 1993;14(4):287-93.

114.   Price JL, Ko AI, Wade MJ, Tsou SK, McKeel DW, Morris JC. Neuron number in the entorhinal cortex and CA1 in preclinical Alzheimer disease. Archives of neurology. 2001;58(9):1395-402.

115.   Insausti R, Insausti AM, Sobreviela MT, Salinas A, Martinez-Penuela JM. Human medial temporal lobe in aging: anatomical basis of memory preservation. Microsc Res Tech. 1998;43(1):8-15.

116.   Tomlinson B. Ageing and the dementias. In Adams JH, Corsellis JAN, Duchen LW, editors: Greenfield's Neuro- pathology, ed 4, New York, Wiley. 1984:951-1025.

117.   Braak H, Braak E. The human entorhinal cortex: normal morphology and lamina-specific pathology in various diseases. Neurosci Res. 1992;15(1-2):6-31.

118.   Corsellis J. The limbic areas in Alzheimer's disease and in other conditions associated with dementia. In Wolstenholme GEW, O'Connor M, editors Alzheimer's Disease and Related Disorders, London Churchill. 1970:37-50.

119.   Ball MJ. Neuronal loss, neurofibrillary tangles and granulovacuolar degeneration in the hippocampus with ageing and dementia. A quantitative study. Acta neuropathologica. 1977;37(2):111-8.

120. Ball M. Granulovacuolar degeneration. In Reisberg B, editor: Alz- heimer 's Disease, New York, Free Press,. 1983:62-8.

121. Stoub TR. Hippocampal disconnection contributes to memory dysfunction in individuals at risk for Alzheimer's disease. PNAS. 2006;123:10041-5.

122. Frisoni GB, Fox NC, Jack CR, Jr., Scheltens P, Thompson PM. The clinical use of structural MRI in Alzheimer disease. Nat Rev Neurol. 2010;6(2):67-77.

123. Konrad C. Defining the human hippocampus in cerebral magnetic resonance images, An overview of current segmentation protocols. Neuro Image 2009;47:1185-95.

124. Amunts K, Kedo O, Kindler M, Pieperhoff P, Mohlberg H, Shah NJ, et al. Cytoarchitectonic mapping of the human amygdala, hippocampal region and entorhinal cortex: intersubject variability and probability maps. Anat Embryol (Berl). 2005;210(5-6):343-52.

125. Desikan RS, Cabral HJ, Hess CP, Dillon WP, Glastonbury CM, Weiner MW, et al. Automated MRI measures identify individuals with mild cognitive impairment and Alzheimer's disease. Brain : a journal of neurology. 2009;132(Pt 8):2048-57.

126. Fjell AM, Walhovd KB, Fennema-Notestine C, McEvoy LK, Hagler DJ, Holland D, et al. CSF biomarkers in prediction of cerebral and clinical change in mild cognitive impairment and Alzheimer's disease. The Journal of neuroscience : the official journal of the Society for Neuroscience. 2010;30(6):2088-101.

127. Shiino A, Watanabe T, Maeda K, Kotani E, Akiguchi I, Matsuda M. Four subgroups of Alzheimer's disease based on patterns of atrophy using VBM and a unique pattern for early onset disease. NeuroImage. 2006;33(1):17-26.

128. Karas GB, Burton EJ, Rombouts SA, van Schijndel RA, O'Brien JT, Scheltens P, et al. A comprehensive study of gray matter loss in patients with Alzheimer's disease using optimized voxel-based morphometry. NeuroImage. 2003;18(4):895-907.

129. Whitwell JL, Przybelski SA, Weigand SD, Knopman DS, Boeve BF, Petersen RC, et al. 3D maps from multiple MRI illustrate changing atrophy patterns as subjects progress from mild cognitive impairment to Alzheimer's disease. Brain : a journal of neurology. 2007;130(Pt 7):1777-86.

130. Desikan RS, Cabral HJ, Fischl B, Guttmann CR, Blacker D, Hyman BT, et al. Temporoparietal MR imaging measures of atrophy in subjects with mild cognitive impairment that predict subsequent diagnosis of Alzheimer disease. AJNR American journal of neuroradiology. 2009;30(3):532-8.

131. Weiner MW. Expanding ventricles may detect preclinical Alzheimer disease. Neurology. 2008;70(11):824-5.

132. Stoub TR, Detoledo-Morrell L, Dickerson BC. Parahippocampal white matter volume predicts Alzheimer's disease risk in cognitively normal old adults. Neurobiology of aging. 2014;35(8):1855-61.

133. Franko E, Joly O, Alzheimer's Disease Neuroimaging I. Evaluating Alzheimer's disease progression using rate of regional hippocampal atrophy. PloS one. 2013;8(8):e71354.

134. Cabeza R, Ciaramelli E, Olson IR, Moscovitch M. The parietal cortex and episodic memory: an attentional account. Nature reviews Neuroscience. 2008;9(8):613-25.

135. Ross SJ, Graham N, Stuart-Green L, Prins M, Xuereb J, Patterson K, et al. Progressive biparietal atrophy: an atypical presentation of Alzheimer's disease. Journal of neurology, neurosurgery, and psychiatry. 1996;61(4):388-95.

136. Jacobs HI, Van Boxtel MP, Uylings HB, Gronenschild EH, Verhey FR, Jolles J. Atrophy of the parietal lobe in preclinical dementia. Brain and cognition. 2011;75(2):154-63.

137. Karas G, Scheltens P, Rombouts S, van Schijndel R, Klein M, Jones B, et al. Precuneus atrophy in early-onset Alzheimer's disease: a morphometric structural MRI study. Neuroradiology. 2007;49(12):967-76.

138.   Ishii K, Kawachi T, Sasaki H, Kono AK, Fukuda T, Kojima Y, et al. Voxel-based morphometric comparison between early- and late-onset mild Alzheimer's disease and assessment of diagnostic performance of z score images. AJNR American journal of neuroradiology. 2005;26(2):333-40.

139.   Shibuya Y, Kawakatsu S, Hayashi H, Kobayashi R, Suzuki A, Sato C, et al. Comparison of entorhinal cortex atrophy between early-onset and late-onset Alzheimer's disease using the VSRAD, a specific and sensitive voxel-based morphometry. International journal of geriatric psychiatry. 2013;28(4):372-6.

140.   Moller C, Vrenken H, Jiskoot L, Versteeg A, Barkhof F, Scheltens P, et al. Different patterns of gray matter atrophy in early- and late-onset Alzheimer's disease. Neurobiology of aging. 2013;34(8):2014-22.

141.   Okonkwo OC, Xu G, Dowling NM, Bendlin BB, Larue A, Hermann BP, et al. Family history of Alzheimer disease predicts hippocampal atrophy in healthy middle-aged adults. Neurology. 2012;78(22):1769-76.

142.   Schott JM, Fox NC, Frost C, Scahill RI, Janssen JC, Chan D, et al. Assessing the onset of structural change in familial Alzheimer's disease. Annals of neurology. 2003;53(2):181-8.

143.   Duara R, Loewenstein DA, Shen Q, Barker W, Varon D, Greig MT, et al. The utility of age-specific cut-offs for visual rating of medial temporal atrophy in classifying Alzheimer's disease, MCI and cognitively normal elderly subjects. Frontiers in aging neuroscience. 2013;5:47.

144.   Kim GH, Kim JE, Choi KG, Lim SM, Lee JM, Na DL, et al. T1-weighted axial visual rating scale for an assessment of medial temporal atrophy in Alzheimer's disease. Journal of Alzheimer's disease : JAD. 2014;41(1):169-78.

145.   Lehmann M, Koedam EL, Barnes J, Bartlett JW, Ryan NS, Pijnenburg YA, et al. Posterior cerebral atrophy in the absence of medial temporal lobe atrophy in pathologically-confirmed Alzheimer's disease. Neurobiology of aging. 2012;33(3):627 e1- e12.

146.   Clerx L, Visser PJ, Verhey F, Aalten P. New MRI markers for Alzheimer's disease: a meta-analysis of diffusion tensor imaging and a comparison with medial temporal lobe measurements. Journal of Alzheimer's disease : JAD. 2012;29(2):405-29.

147.   Wang L, Goldstein FC, Veledar E, Levey AI, Lah JJ, Meltzer CC, et al. Alterations in cortical thickness and white matter integrity in mild cognitive impairment measured by whole-brain cortical thickness mapping and diffusion tensor imaging. AJNR American journal of neuroradiology. 2009;30(5):893-9.

148.   Firbank MJ, Blamire AM, Krishnan MS, Teodorczuk A, English P, Gholkar A, et al. Atrophy is associated with posterior cingulate white matter disruption in dementia with Lewy bodies and Alzheimer's disease. NeuroImage. 2007;36(1):1-7.

149.   Canu E, Frisoni GB, Agosta F, Pievani M, Bonetti M, Filippi M. Early and late onset Alzheimer's disease patients have distinct patterns of white matter damage. Neurobiology of aging. 2012;33(6):1023-33.

150.   He Y, Chen ZJ, Evans AC. Small-world anatomical networks in the human brain revealed by cortical thickness from MRI. Cerebral cortex. 2007;17(10):2407-19.

151.   Damoiseaux JS, Beckmann CF, Arigita EJ, Barkhof F, Scheltens P, Stam CJ, et al. Reduced resting-state brain activity in the "default network" in normal aging. Cerebral cortex. 2008;18(8):1856-64.

152.   O'Sullivan M, Jones DK, Summers PE, Morris RG, Williams SC, Markus HS. Evidence for cortical "disconnection" as a mechanism of age-related cognitive decline. Neurology. 2001;57(4):632-8.

153.   Davis SW, Dennis NA, Daselaar SM, Fleck MS, Cabeza R. Que PASA? The posterior-anterior shift in aging. Cerebral cortex. 2008;18(5):1201-9.

154.   Sorg C, Riedl V, Muhlau M, Calhoun VD, Eichele T, Laer L, et al. Selective changes of resting-state networks in individuals at risk for Alzheimer's disease. Proceedings of the National Academy of Sciences of the United States of America. 2007;104(47):18760-5.

155.   Binnewijzend MA, Schoonheim MM, Sanz-Arigita E, Wink AM, van der Flier WM, Tolboom N, et al. Resting-state fMRI changes in Alzheimer's disease and mild cognitive impairment. Neurobiology of aging. 2012;33(9):2018-28.

156.   Buckner RL, Snyder AZ, Shannon BJ, LaRossa G, Sachs R, Fotenos AF, et al. Molecular, structural, and functional characterization of Alzheimer's disease: evidence for a relationship between default activity, amyloid, and memory. The Journal of neuroscience : the official journal of the Society for Neuroscience. 2005;25(34):7709-17.

157.   Ossenkoppele R, Tolboom N, Foster-Dingley JC, Adriaanse SF, Boellaard R, Yaqub M, et al. Longitudinal imaging of Alzheimer pathology using [11C]PIB, [18F]FDDNP and [18F]FDG PET. European journal of nuclear medicine and molecular imaging. 2012;39(6):990-1000.

158.   Lee YC, Liu RS, Liao YC, Sun CM, Wang PS, Wang PN, et al. Statistical parametric mapping of brain SPECT perfusion abnormalities in patients with Alzheimer's disease. European neurology. 2003;49(3):142-5.

159.   Alsop DC, Detre JA, Grossman M. Assessment of cerebral blood flow in Alzheimer's disease by spin-labeled magnetic resonance imaging. Annals of neurology. 2000;47(1):93-100.

160.   Tosun D, Joshi S, Weiner MW, the Alzheimer's Disease Neuroimaging I. Multimodal MRI-based Imputation of the Abeta+ in Early Mild Cognitive Impairment. Annals of clinical and translational neurology. 2014;1(3):160-70.

161.   Koedam EL, Lauffer V, van der Vlies AE, van der Flier WM, Scheltens P, Pijnenburg YA. Early-versus late-onset Alzheimer's disease: more than age alone. Journal of Alzheimer's disease : JAD. 2010;19(4):1401-8.

162.   Ossenkoppele R, Zwan MD, Tolboom N, van Assema DM, Adriaanse SF, Kloet RW, et al. Amyloid burden and metabolic function in early-onset Alzheimer's disease: parietal lobe involvement. Brain : a journal of neurology. 2012;135(Pt 7):2115-25.

163.   Sanz-Arigita E. REDES EN RIESGO: Cambios en la red de memoria en sujetos de alto riesgo de la enfermedad de Alzheimer. 2011:21.

164.   Damoiseaux JS, Greicius MD. Greater than the sum of its parts: a review of studies combining structural connectivity and resting-state functional connectivity. Brain structure & function. 2009;213(6):525-33.

165.   Johnson NA. Pattern of cerebral hypoperfusion in Alzheimer's disease and mild cognitive impairment measured with arterial spin-labeling MR imaging: Initial experience. International Congress Series. 2006;1290:108-22.

166.   Rosset A, Spadola L, Ratib O. OsiriX: an open-source software for navigating in multidimensional DICOM images. J Digit Imaging. 2004;17(3):205-16.

167.   Patenaude B, Smith SM, Kennedy DN, Jenkinson M. A Bayesian model of shape and appearance for subcortical brain segmentation. NeuroImage. 2011;56(3):907-22.

168.   Mak E, Bergsland N, Dwyer MG, Zivadinov R, Kandiah N. Subcortical atrophy is associated with cognitive impairment in mild Parkinson disease: a combined investigation of volumetric changes, cortical thickness, and vertex-based shape analysis. AJNR American journal of neuroradiology. 2014;35(12):2257-64.

169.   Thordardottir S, Stahlbom AK, Ferreira D, Almkvist O, Westman E, Zetterberg H, et al. Preclinical cerebrospinal fluid and volumetric magnetic resonance imaging biomarkers in Swedish familial Alzheimer's disease. Journal of Alzheimer's disease : JAD. 2015;43(4):1393-402.

170.   Greenblatt EE, Winkler T, Harris RS, Kelly VJ, Kone M, Venegas J. Analysis of three-dimensional aerosol deposition in pharmacologically relevant terms: beyond black or white ROIs. J Aerosol Med Pulm Drug Deliv. 2015;28(2):116-29.

171.   Ashburner J. A fast diffeomorphic image registration algorithm. NeuroImage. 2007;38(1):95-113.

172.   Fazekas F, Chawluk JB, Alavi A, Hurtig HI, Zimmerman RA. MR signal abnormalities at 1.5 T in Alzheimer's dementia and normal aging. AJR Am J Roentgenol. 1987;149(2):351-6.

173.   Enzinger C, Fazekas F, Matthews PM, Ropele S, Schmidt H, Smith S, et al. Risk factors for progression of brain atrophy in aging: six-year follow-up of normal subjects. Neurology. 2005;64(10):1704-11.

174.   Debette S, Markus HS. The clinical importance of white matter hyperintensities on brain magnetic resonance imaging: systematic review and meta-analysis. BMJ. 2010;341:c3666.

175.   Field A, editor. Discovering Statistics Using IBM SPSS Statistics. SAGE ed2013.

176.   Reuter M, Fischl B. Avoiding asymmetry-induced bias in longitudinal image processing. NeuroImage. 2011;57(1):19-21.

177.   Segonne F, Dale AM, Busa E, Glessner M, Salat D, Hahn HK, et al. A hybrid approach to the skull stripping problem in MRI. NeuroImage. 2004;22(3):1060-75.

178.   Fischl B, Salat DH, Busa E, Albert M, Dieterich M, Haselgrove C, et al. Whole brain segmentation: automated labeling of neuroanatomical structures in the human brain. Neuron. 2002;33(3):341-55.

179.   Fischl B, Salat DH, van der Kouwe AJ, Makris N, Segonne F, Quinn BT, et al. Sequence-independent segmentation of magnetic resonance images. NeuroImage. 2004;23 Suppl 1:S69-84.

180.   Sled JG, Zijdenbos AP, Evans AC. A nonparametric method for automatic correction of intensity nonuniformity in MRI data. IEEE Trans Med Imaging. 1998;17(1):87-97.

181.   Fischl B, Liu A, Dale AM. Automated manifold surgery: constructing geometrically accurate and topologically correct models of the human cerebral cortex. IEEE Trans Med Imaging. 2001;20(1):70-80.

182.   Segonne F, Pacheco J, Fischl B. Geometrically accurate topology-correction of cortical surfaces using nonseparating loops. IEEE Trans Med Imaging. 2007;26(4):518-29.

183.   Dale AM, Fischl B, Sereno MI. Cortical surface-based analysis. I. Segmentation and surface reconstruction. NeuroImage. 1999;9(2):179-94.

184.   Dale AM, Sereno MI. Improved Localizadon of Cortical Activity by Combining EEG and MEG with MRI Cortical Surface Reconstruction: A Linear Approach. J Cogn Neurosci. 1993;5(2):162-76.

185.   Fischl B, Dale AM. Measuring the thickness of the human cerebral cortex from magnetic resonance images. Proceedings of the National Academy of Sciences of the United States of America. 2000;97(20):11050-5.

186.   Romano A, Cornia R, Moraschi M, Bozzao A, Chiacchiararelli L, Coppola V, et al. Age-Related Cortical Thickness Reduction in Non-Demented Down's Syndrome Subjects. J Neuroimaging. 2015.

187.   Andreasen N, Gottfries J, Vanmechelen E, Vanderstichele H, Davidson P, Blennow K, et al. Evaluation of CSF biomarkers for axonal and neuronal degeneration, gliosis, and beta-amyloid metabolism in Alzheimer's disease. Journal of neurology, neurosurgery, and psychiatry. 2001;71(4):557-8.

188.   Sunderland T, Linker G, Mirza N, Putnam KT, Friedman DL, Kimmel LH, et al. Decreased beta-amyloid1-42 and increased tau levels in cerebrospinal fluid of patients with Alzheimer disease. JAMA : the journal of the American Medical Association. 2003;289(16):2094-103.

189.   Hansson O, Zetterberg H, Buchhave P, Londos E, Blennow K, Minthon L. Association between CSF biomarkers and incipient Alzheimer's disease in patients with mild cognitive impairment: a follow-up study. The Lancet Neurology. 2006;5(3):228-34.

190.   Tabaraud F, Leman JP, Milor AM, Roussie JM, Barriere G, Tartary M, et al. Alzheimer CSF biomarkers in routine clinical setting. Acta Neurol Scand. 2012;125(6):416-23.

191.   Buchhave P, Minthon L, Zetterberg H, Wallin AK, Blennow K, Hansson O. Cerebrospinal fluid levels of beta-amyloid 1-42, but not of tau, are fully changed already 5 to 10 years before the onset of Alzheimer dementia. Archives of general psychiatry. 2012;69(1):98-106.

192.   Blazquez L, De Juan D, Ruiz-Martinez J, Emparanza JI, Saenz A, Otaegui D, et al. Genes related to iron metabolism and susceptibility to Alzheimer's disease in Basque population. Neurobiology of aging. 2007;28(12):1941-3.

193.   Benedet MyA, MA. . Test de Aprendizaje Verbal España-Complutense (TAVEC). 1998.

194.   A R. Test de copia y de reproducción de memoria de figuras geométricas complejas. 2009.

195.   Pena-Casanova J, Gramunt-Fombuena N, Quinones-Ubeda S, Sanchez-Benavides G, Aguilar M, Badenes D, et al. Spanish Multicenter Normative Studies (NEURONORMA Project): norms for the Rey-Osterrieth complex figure (copy and memory), and free and cued selective reminding test. Arch Clin Neuropsychol. 2009;24(4):371-93.

196.   Palomo R, Casals-Coll M, Sanchez-Benavides G, Quintana M, Manero RM, Rognoni T, et al. Spanish normative studies in young adults (NEURONORMA young adults project): norms for the Rey-Osterrieth Complex Figure (copy and memory) and Free and Cued Selective Reminding Test. Neurologia. 2013;28(4):226-35.

197.   Wechsler D. WAIS-III. Escala de inteligencia de Wechsler para adultos-III (2ª ed.). . 2001.

198.   Goodglass H. Evaluación de la afasia y de trastornos relacionados. 2005.

199.   Pena-Casanova J, Quinones-Ubeda S, Gramunt-Fombuena N, Aguilar M, Casas L, Molinuevo JL, et al. Spanish Multicenter Normative Studies (NEURONORMA Project): norms for Boston naming test and token test. Arch Clin Neuropsychol. 2009;24(4):343-54.

200.   Aranciva F, Casals-Coll M, Sanchez-Benavides G, Quintana M, Manero RM, Rognoni T, et al. Spanish normative studies in a young adult population (NEURONORMA young adults Project): norms for the Boston Naming Test and the Token Test. Neurologia. 2012;27(7):394-9.

201.   Benton A. Contributions to neuropsychological assessment: A clinical manual. 1983.

202.   Pena-Casanova J, Quintana-Aparicio M, Quinones-Ubeda S, Aguilar M, Molinuevo JL, Serradell M, et al. Spanish Multicenter Normative Studies (NEURONORMA Project): norms for the visual object and space perception battery-abbreviated, and judgment of line orientation. Arch Clin Neuropsychol. 2009;24(4):355-70.

203.   Calvo L, Casals-Coll M, Sanchez-Benavides G, Quintana M, Manero RM, Rognoni T, et al. Spanish normative studies in young adults (NEURONORMA young adults project): norms for the Visual Object and Space Perception Battery and Judgment of Line Orientation tests. Neurologia. 2013;28(3):153-9.

204.   Benton AL. Multilingual Aphasia Examination. 1989.

205.   Pena-Casanova J, Quinones-Ubeda S, Gramunt-Fombuena N, Quintana-Aparicio M, Aguilar M, Badenes D, et al. Spanish Multicenter Normative Studies (NEURONORMA Project): norms for verbal fluency tests. Arch Clin Neuropsychol. 2009;24(4):395-411.

206.   Casals-Coll M, Sanchez-Benavides G, Quintana M, Manero RM, Rognoni T, Calvo L, et al. Spanish normative studies in young adults (NEURONORMA young adults project): norms for verbal fluency tests. Neurologia. 2013;28(1):33-40.

207.   Wechsler D. WAIS-III. Escala de inteligencia de Wechsler para adultos-III 2001.

_____

208.   Pena-Casanova J, Quinones-Ubeda S, Quintana-Aparicio M, Aguilar M, Badenes D, Molinuevo JL, et al. Spanish Multicenter Normative Studies (NEURONORMA Project): norms for verbal span, visuospatial span, letter and number sequencing, trail making test, and symbol digit modalities test. Arch Clin Neuropsychol. 2009;24(4):321-41.

209.   Tamayo F, Casals-Coll M, Sanchez-Benavides G, Quintana M, Manero RM, Rognoni T, et al. [Spanish normative studies in a young adult population (NEURONORMA young adults Project): norms for the verbal span, visuospatial span, Letter-Number Sequencing, Trail Making Test and Symbol Digit Modalities Test]. Neurologia. 2012;27(6):319-29.

210.   Golden CJ. Stroop, test de colores y palabras 2007.

211.   Pena-Casanova J, Quinones-Ubeda S, Gramunt-Fombuena N, Quintana M, Aguilar M, Molinuevo JL, et al. Spanish Multicenter Normative Studies (NEURONORMA Project): norms for the Stroop color-word interference test and the Tower of London-Drexel. Arch Clin Neuropsychol. 2009;24(4):413-29.

212.   Rognoni T, Casals-Coll M, Sanchez-Benavides G, Quintana M, Manero RM, Calvo L, et al. Spanish normative studies in young adults (NEURONORMA young adults project): norms for Stroop Color-Word Interference and Tower of London-Drexel University tests. Neurologia. 2013;28(2):73-80.

213.   Wilson BA. BADS: Behavioural Assessment of the Dysexecutive Syndrome, Manual. 1996.

214.   Tsoi KK, Chan JY, Hirai HW, Wong SY, Kwok TC. Cognitive Tests to Detect Dementia: A Systematic Review and Meta-analysis. JAMA Intern Med. 2015.

215.   Ferrero-Arias J, Turrion-Rojo MA. Standardization of the Test Your Memory and evaluation of their concordance with the outcome of the psychometric examination. Neurologia. 2015.